# ***DRAFT***DRAFT***DRAFT***
# Benchmarking Geant4 Hadronic Cascade Models with Data from the GLAST-GSI and GLAST-CERN beam tests.

Johan Bregeon, C.E.N.B.G.

August 2005

**Abstract**

Hadronic background rejection is an issue for GLAST as the final expected rejection rate is to be $10^6$ to 1. Most hadronic events will be rejected by the ACD that vetoes charged particles, but more evolved trigger and analysis algorithms are required to reach such a rejection factor. Monte-Carlo simulations play a key role in the development and tuning of hadronic background rejection algorithms and until now, most of them are based on the Geant4 tool kit using the LHEP model (from the GHEISHA code) for hadronic cascade simulations. Actually more hadronic cascade models are available in Geant4, such as the Bertini intra-nuclear cascade model and the Binary Cascade model under 10GeV, and a few QGS ( Quark Gluon String ) based models over 20GeV. These models propose very different distributions as far as nuclear reaction products are concerned. Benchmarking these models using beam test data should help us to determine, first, if the default LHEP model reproduces well our variables and second, if one model is better than the others.

During the GLAST-GSI beam test, we had 1.7GeV proton and 3.4GeV deuteron beams on the Engineering Model, that we use to benchmark hadronic cascade models at low energy. The high energy part is covered by data from the GLAST-CERN beam test where we had 10GeV/c and 20GeV/c hadrons on a GLAST like CsI calorimeter. Benchmarking simulations is done by comparing data and simulations for some basic variables such as the energy deposit and the number of logs hit per layer and for the whole calorimeter, but also for more evolved variables, e.g. maximum energy deposit in a layer etc... We will be sensitive mostly to the global shape of the distributions that can give us hints that the topology of hadronic cascades is well reproduced, or not, by simulations.

This study concludes that at low energy, i.e. under 10GeV, all the simulations painfully reproduce the calorimeter energy sum under 200MeV. However the Bertini model has to be put forward as it proposes distributions significantly closer to the data. The Bertini intra-nuclear cascade model should be used instead of LHEP to generate event sets dedicated to hadronic background rejection. At high energy, i.e. over 10GeV, the LHEP model gives good results and the only small discrepancy pointed out concerns the energy deposit dispersion. Actually this small discrepancy a priori cannot have bad consequences for background rejection algorithms. So the LHEP model should still be used over 10GeV to generate hadronic cascades.

# Contents

# Introduction

This note presents results from a study aiming at benchmarking Geant4 hadronic cascade simulations in a GLAST like calorimeter by comparing some pertinent output variables with real data from the GLAST-GSI and GLAST-CERN beam tests lead in 2003.

The first part briefly recalls the issue of hadronic background rejection for GLAST and the key role played by Monte-Carlo simulations in the development and tuning of rejection algorithms.

A review of the different hadronic cascade models available in Geant4 [7][26] is then proposed, trying to point out the main differences between their nuclear reaction product properties.

The third part refers to the GLAST-GSI beam test and details the experimental setup and the data analysis that leads to two clean sets of 1.7GeV protons and 3.4GeV deuterons data. Both data sets are used to benchmark the results of low energy Geant4 Monte-Carlo simulations.

The fourth part deals with the GLAST-CERN beam test during which we had 10GeV/c and 20GeV/c mixed hadrons and electrons beam hit a GLAST like CsI calorimeter. These data are used to compare hadronic cascades and electromagnetic showers and to validate Geant4 high energy hadronic cascade simulations from a GLAST oriented point of view.

# 1 Hadronic background rejection

## 1.1 GLAST Hadronic background rejection

When in space, most of GLAST triggers will be due to cosmic rays, so that hadronic background rejection is a key step to the mission success [21] [16]. The required rejection rate is $10^5$ to 1 according to the specifications, but actually, the ultimate goal is nothing else than $10^6$ to 1, the rate reached for EGRET. The ACD *Anti Coincidence Detector* veto that detects charged particles will reject most of hadronic events. Coupling the ACD, calorimeter and tracker information together in an on-board filter will enhanced the rate of real gamma events sent to the ground. The emission band width is limited to about $40Hz$, and only half of these events are gamma rays. Consequently, the ground analysis also needs for powerful and efficient algorithms to discriminate gamma and hadronic events.

As far as the on-board filter and the ground analysis are concerned, all the hadronic rejection algorithms are developed and tuned relying on `GlastRelease` which is the official GLAST Monte-Carlo simulation. `GlastRelease` is based on the GEANT4 simulation tool kit that uses the LHEP (GHEISHA) model for hadronic cascade simulations. Besides, cosmic rays cover a wide range of energy from a couple hundreds of $MeV$ to tens of $GeV$ and hadronic cascade are completely different kind of events when they are peripheral or central reactions.

Hadronic cascade simulation on such a wide range is challenging so that we really need to check how well they can reproduce real data. A common goal of both the GLAST GSI and CERN beam test was to measure some real hadronic cascades in GLAST like calorimeters to benchmark the LHEP model used in GEANT4 for the variables we are interested in. The aim is really to make the most straight forward comparison between data and simulation, to determine which hadronic model we should use in GEANT4 for GLAST hadronic studies purpose.

## 1.2 Variables of interest

### 1.2.1 First order

For our GLAST like calorimeters, energy deposits from each side of each CDE are the only data we have, but there are many ways to combine them. Our goal is to characterize hadronic cascades and to check if the simulated one present the same features. Let's first have a look to some typical hadronic and electromagnetic cascades from the CERN beam test. Figure 1.1 show the mean energy deposit per CDE, and the number of time each CDE has been hit (i.e. received more than $50MeV$) for electromagnetic and hadronic cascades for $20GeV/c$ incident particles. A primary feature of electromagnetic showers, obvious on the left side of figure 1.1, is the energy deposit longitudinal profile that is very well described by a $\Gamma$ function. As opposed to this, hadronic cascades do not show any particular feature, one can just expect a strong energy deposit when a strong nuclear reaction occurs in a layer (e.g. central collision). Consequently, the first variable we want to test is certainly the energy deposit per layer. The cascade spatial development in the

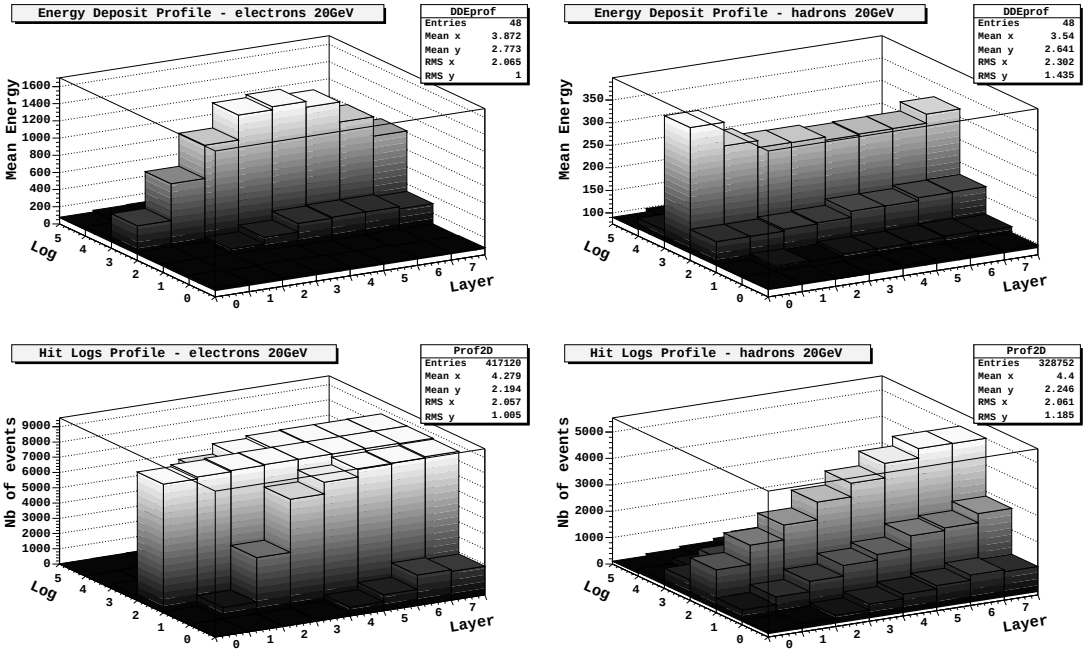


Figure 1.1: Mean energy deposit profile and number of hits for each CDE in CERN GLAST-like calorimeter : on the left, for $20GeV/c$ incident electrons and on the right for $20GeV/c$ pions - 10000 events from beam data.

calorimeter presents the same kind of features. Whereas electromagnetic showers develop early and progressively in the calorimeter, hadronic cascades have not such a common feature as the number of hits per logs on the right side of figure 1.1 shows. To characterize the cascade spatial development, the second variable is to be the number of logs hit per layer. From a global point of view, electromagnetic showers have strong common features with little dispersion compared to hadronic cascades.

To complete the first two variables and test for layer correlations, we are also going to test the total energy deposit and the total number of logs hit in the whole calorimeter.

### 1.2.2 Reconstruction : Longitudinal profile fitting

As it's already been said, the longitudinal profile of energy deposit for electromagnetic showers is reasonably well described by a $\Gamma$ function between $1GeV$ and $100GeV$ (see [19]). One of the GLAST energy reconstruction methods consists in fitting the energy deposit profile sampled by the calorimeter with an appropriate function to get the energy of the incident photon as shown on figure 1.2. As only electromagnetic showers show this feature, one can expect the $\chi^2$ of the fit to be a very interesting variable to discriminate hadronic and electromagnetic cascades. However, the profile fitting only works above a few $GeV$ so that we will test it only for the CERN beam test data at $10GeV/c$ and $20GeV/c$.

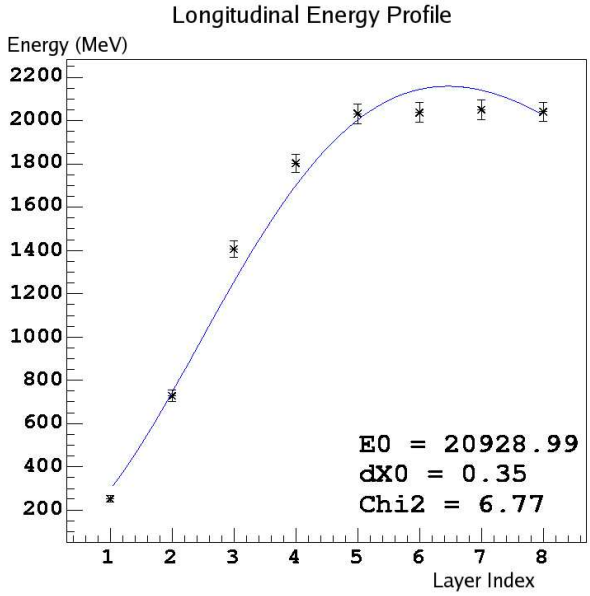


Figure 1.2: Energy deposit longitudinal profile fitted by a $\Gamma$ function on one event $e^-$ $20GeV$. Error bars correspond to the stochastic error on the energy deposit, thus are in $\sqrt{\Delta E_i}$.

I coded the profile fitting method for the energy deposit sampled in the 8 layers of the calorimeter, the same way it's done in the `CalRecon` package of GlastRelease. Let the equation (1.1) define the energy deposit sampled in the $i^{th}$ layer of the calorimeter :

$$\Delta E_i = -E_0 * \left( \Gamma(\alpha, \frac{(i + dX_0) * B_{X_0}}{\lambda}) - \Gamma(\alpha, \frac{(i + dX_0) * B_{X_0} + 1}{\lambda}) \right) \qquad (1.1)$$

where • $E_0$ is the incident particle energy in MeV.
- $\Gamma$ is the generalized gamma function.
- $\alpha = 2.65 * e^{0.15 * log(E_0/1000.)}$ parametrized in [23]
- $\lambda = 2.29 * e^{-0.031 * log(E_0/1000.)}$ parametrized in [23]
- $B_{X_0} = \frac{18.5\ cm}{19.9\ cm}$ is a constant to switch to unit of CsI log thickness from the radiation length in CsI

The fit has two free parameters : $E_0$, the energy we are looking for and $dX_0$, that refers to the starting point of the shower. The parameters $\alpha$ and $\lambda$ are linked to the CsI intrinsic properties and the geometry of the calorimeter [19]. To compute the $\chi^2$, the error chosen on the mean energy deposit per layer $\Delta E_i$ is $\sqrt{\Delta E_i}$ that corresponds to the stochastic error on the energy deposit.

So, the fit outputs are $E_0$, $dX_0$ and the $\chi^2$, three new and useful variables proposing a different way to compare data and simulations of hadronic cascades.

### 1.2.3 Hadronic oriented variables

The main feature of hadronic cascades is that they are very different one from each other. A peripheral nuclear reaction will have very different energy deposits from a central one. For instance, a peripheral reaction is probably to have a quite smooth energy profile with slowly increasing energies, whereas a central reaction will cause just a very high energy deposit in the layer where it takes place. Moreover, the same kind of nuclear reactions can engender very different energy profiles depending on the layer where they occur.

These statements lead us to test three more variables that try to characterize these features of hadronic cascades. The raw RMS of layer energy deposits (the energy profile RMS) helps us to test that the simulation reproduces the great diversity of hadronic cascades. Then, we will have a look to the maximum energy deposit in a layer along the longitudinal profile (the energy profile maximum) that is linked to the power and the development of hadronic cascades in the calorimeter. In association, the layer number of the energy profile maximum is also to be tested.

All the variables introduced here constitute the basis of the benchmark :

- energy deposit per layer : $E_{Layer}$
- number of logs hit per layer : multiplicity per layer $M_{Layer}$.
- total energy deposit in the whole calorimeter : $E_{Sum}$.
- sum of logs hit in the whole calorimeter : total multiplicity $M_{Sum}$.
- profile fitting variables : reconstructed energy and starting point, $\chi^2$.
- energy profiles RMS.
- energy profiles maximum $E_{Max}$ and corresponding layer index $J_{Emax}$.

Of course, along the analysis we might be willing to check some other variables to improve our understanding of some unexpected features.

# 2 Hadronic cascade simulations in GEANT4

## 2.1 Overview

Before entering the cascade simulation itself, the first step is to get the inelastic scattering cross section of protons on CsI. For this purpose, GEANT4 uses a re-engineered piece of code inherited from GHEISHA, that is able to compute the cross sections by interpolating on tabulated data. The inelastic scattering cross section of 1.7GeV protons on CsI processed by GEANT4 is 1308mb what is compatible with the literature [25].

Different hadronic cascade models are proposed by the GEANT4 tool-kit [8], however, all of them are more or less based on the intranuclear cascade scheme introduced by Serber [22] in 1947 and presented on figure 2.1. Serber early noticed that for high energy hadron-nucleus interactions, the de Broglie wave length of the incident particle is small in front of the characteristic length of nucleons within the nucleus. The consequence is that hadron-nucleus interactions can be described as multiple interactions of the incident particle with the individual nucleons of the nucleus. This assumption gives a low energy limit around $200MeV$ hadrons for all intranuclear cascade models.

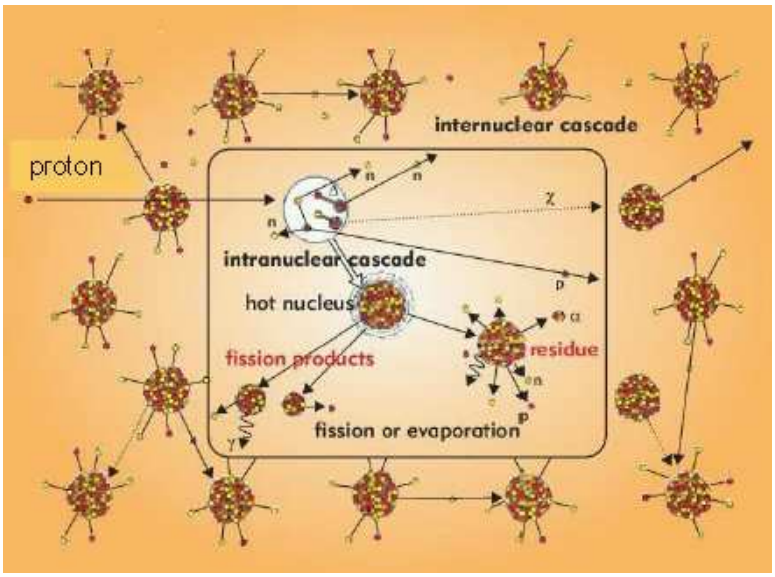


Figure 2.1: The intra-nuclear cascade model : the incident proton interacts with the nucleons inside the nucleus. Any particle, primary or secondary, that can escape from the first nucleus is also allowed to interact with other nucleus to generate an internuclear cascade.

Hadronic cascades can be well described in three steps :

- intranuclear cascade : the bullet interacts individually with the nucleons within the nucleus, generating secondary particles (protons, neutrons, pions, deuterons

etc...) that are also able to interact with other nucleons within the same nucleus or with an other nucleus then creating an inter-nuclear cascade.

- pre-equilibrium : the target nucleus, excited by the intranuclear cascade, is far from the thermodynamical equilibrium and part of the nucleons, called excitons, have a high kinetic energy. The nucleus thermalizes emitting excitons and light nuclei, till alpha particles.

- break up/evaporation : the thermalized nucleus still have a high residual excitation energy that can be dissipated by a change of state and $\gamma$ emission or by evaporation of one or more nucleons. If the residual energy is high enough, heavy nuclei can even break up. The work of Weisskopf and Ewing are the reference for these processes [24].

Now let's have a quick tour of the main hadronic cascade models available in GEANT4 in the energy range $100MeV$ to $100GeV$. In order to check for the main characteristics of each model, we will rely on a few features of nuclear reaction products :

- Multiplicity : Number of secondary particles.

- Charge : Charge distribution of secondary particles..

- Px : Momentum distribution of secondary particles along the beam axis.

- Angle :Angular distribution of secondaries with respect to the beam axis, 0° is forward, 180° is backward.

The following plots have been obtained with GEANT4, simulating a $1.7GeV$ proton beam at normal incidence on a GLAST like calorimeter. All the hadronic models accept many different hadrons as input, but none is able to simulate hadronic cascades generated by deuterons or other light nuclei.

## 2.2 LHEP model

LHEP is GEANT4 default model when one just turns on hadronic processes. It's based on GHEISHA, a hadronic cascade code developed by H. Fesefeldt [5][28] since 1978. LHEP modeling parametrizes the final states of hadronic interactions from fits on real data but the great number of free parameters with hazardous physical interpretation entails that it can only be used as an hadronic event generator. The implementation of GHEISHA in GEANT4 actually separates in two branches : LEP from 100MeV to 20GeV and HEP from 20GeV up to 10TeV. This wide energy range is a real advantage of the LHEP code that is known to reproduce average quantities well in short computation time.

The charge distribution on figure 2.2 shows up that nuclear reaction products are only light ions, heavy ions one can see are only target nucleus of the material. This feature is not physical as one would expect to see quasi-target nucleus but let's wait and see if this has a strong effect on our variables. Besides, the same features can be observed with $20GeV$ incident protons.

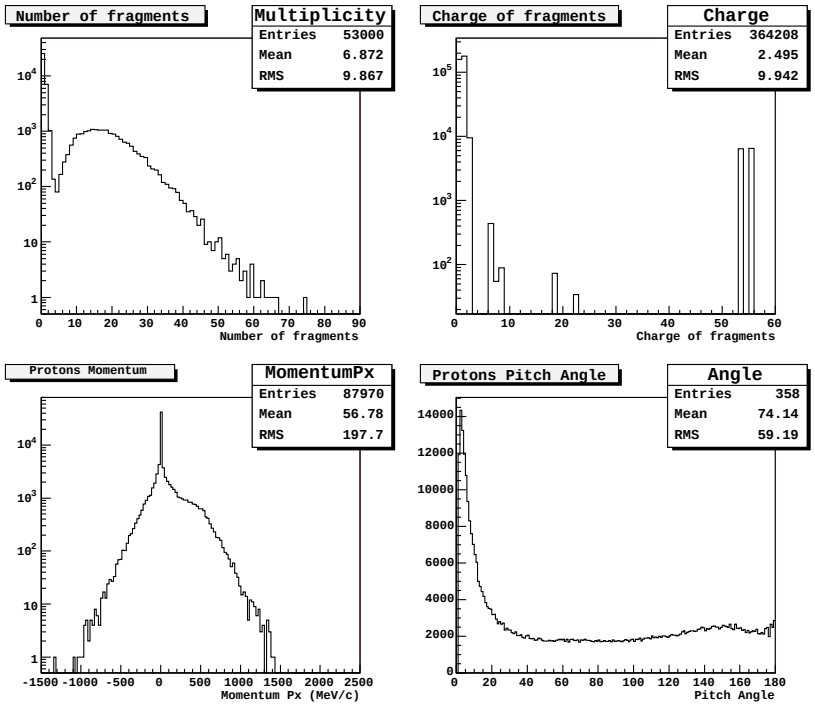


Figure 2.2: Main features of nuclear products for the LHEP model : number of secondaries, charge distribution, momentum along the beam axis and angle with respect to this axis. Simulation of 1.7GeV protons on a GLAST like CsI calorimeter, features are equivalent at higher energies.

### 2.2.1 LHEP-GN model

The LHEP model can be enhanced at low energy (under $3GeV$) by taking into account gamma-nuclear and electro-nuclear interactions. The main effect is an increase of the number of secondaries emitted backward. However, the consequences on our variables are so small that we will not present the results obtained with this model.

## 2.3 Bertini intra-nuclear cascade model : BERT model

The Bertini intra-nuclear cascade model is probably one of the oldest as the first results were published by H.W. Bertini in 1963 [2] at low energy and then in 1969 [3] and 1971 [4] for energies from $300MeV$ à $3000MeV$. Bertini's original idea was to model the nucleus by a central spheres and two shells, each region with each its own nuclear density. The implementation of this model in GEANT4 is valid for proton, neutron and pion bullets with kinetic energy ranging from $100MeV$ up to $10GeV$. The code takes into account the Bertini intra-nuclear cascade model with excitons [10] [11] , a precompound model, a simple nucleus explosion model, a fission model and an evaporation model.

The charge distribution of secondaries shown on figure 2.3 really looks great with nice distributions of quasi-target nucleus with less and less charge starting from Cs and I. Quasi-targets are created by very peripheral nuclear reactions when the incident particle just knock a couple of nucleons out of the nucleus.

## 2.4 Binary cascade : BIC model

The binary cascade model develops an original approach as it propagates primary and secondary particles in a 3D nucleus [6]. Moreover, for the disintegration, the model takes into account the resonances using tabulated cross sections when they exist. Pre-equilibrium and des-excitation problems are not treated by the model itself but by general GEANT4 modules. Actually, the binary cascade model is really part of GEANT4 and evolves quickly and constantly trying to answer the willing of the LHC detectors teams. This model covers the same energy range as the Bertini model, from $100MeV$ to $10GeV$. It's tuned to compute the best cross sections within hadronic interaction as it's mainly used for spallation problem calculations, but the drawback is that computation times are are known to be long.

Figure 2.4 presents quite a nice distribution of charge with quasi-target nucleus, about the same as for the Bertini model, but one can also notice that there are less particles at high angles.

## 2.5 High energy models : QGS models

At high energy, three more models are available : QGSP, QGSC and FTFP. These theory driven models use quark gluon string models for the punch-through interactions of the projectile with a nucleus. They are valid for incident hadrons from $10GeV$ up to $10TeV$ so, I tested them against $20GeV$ hadrons from the GLAST

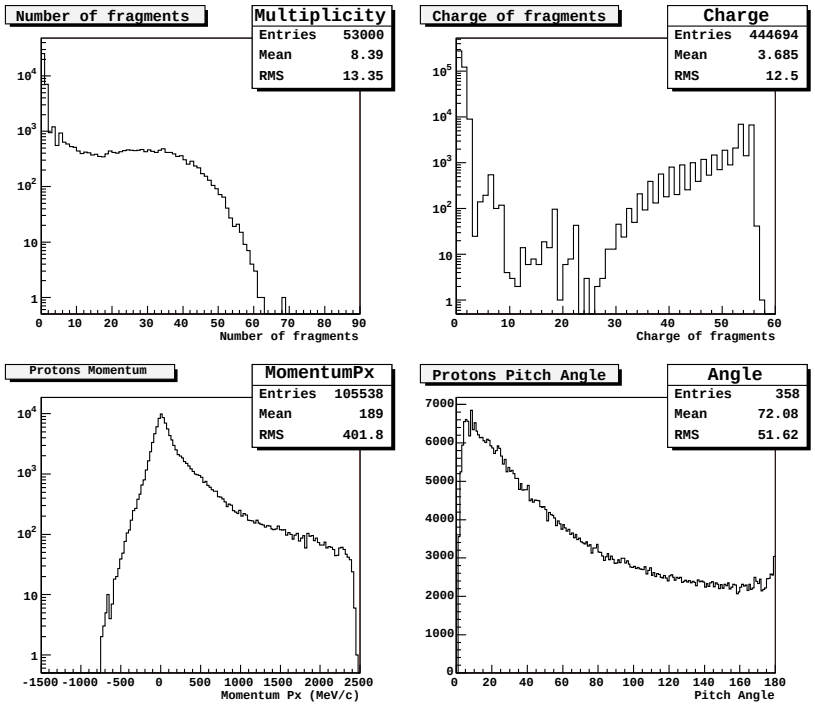


Figure 2.3: Main features of nuclear products for the BERT model : number of secondaries, charge distribution, momentum along the beam axis and angle with respect to this axis. Simulation of 1.7GeV protons on a GLAST like CsI calorimeter. Charge distribution shows up with nice quasi-target nucleus.

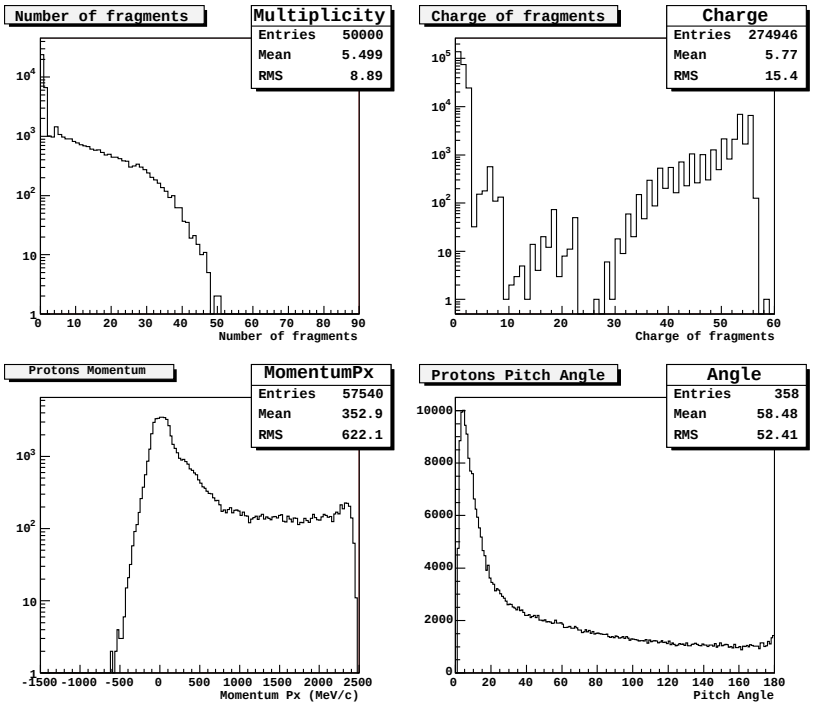


Figure 2.4: Main features of nuclear products for the BIC model : number of secondaries, charge distribution, momentum along the beam axis and angle with respect to this axis. Simulation of 1.7GeV protons on a GLAST like CsI calorimeter. Charge distribution shows up with nice quasi-target nucleus but few particles at high angles.

CERN beam test. As far as our variables are concerned, the results from these parton string models for $20GeV$ protons are comparable within a few percents to the LHEP simulations. Consequently, I will not describe these models in details and the results will be presented in appendix A.1 only.

# 3 GLAST GSI beam test

## 3.1 Experimental setup

### 3.1.1 FRS line

The GSI [27] beam test was performed on the FRS * line. For proton and light ion runs, we had a $^{12}C$ primary beam, accelerated to 1.7GeV in the SIS (the ion synchrotron), at the entry window of the FRS, see figure 3.1. The carbon ions hit a target generating nuclear reactions, then the secondaries follow the path through the fragment separator : only particles with the selected properties will go out of the line and enter the calorimeter. The FRS line is equipped with scintillators for triggering

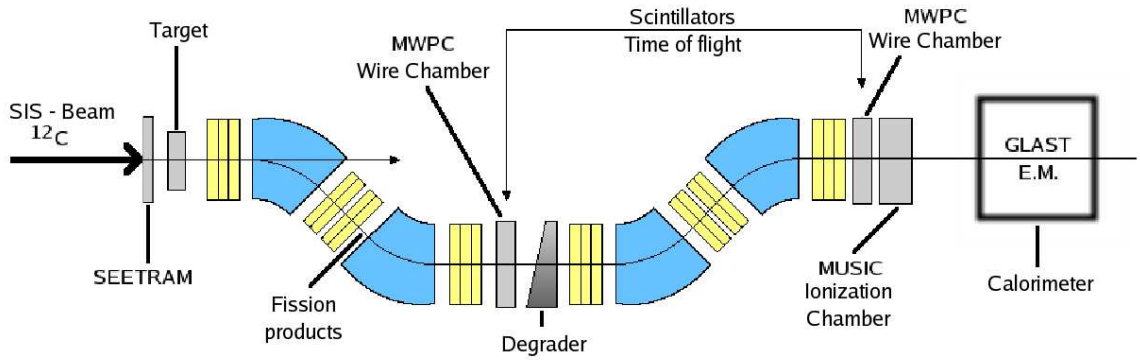


Figure 3.1: The FRS `Fragment Separator` : Primary ions from the SIS hit the target, nuclear reaction products will go through the whole FRS magnet optical path only if they have the selected properties (energy, charge to mass ratio).

and time of flight measurements, multi-wire proportional chambers for tracking and ionization chamber for energy loss. However, these detectors are designed to work with heavy ions so that they are useless for proton and deuteron analysis. For the trigger we had to add our own thick plastic scintillator to enhance the triggering efficiency.

### 3.1.2 E.M. GLAST like calorimeter

During this beam test, the N.R.L.† provided us with the Engineering Model 1 (EM). The EM has nearly all the features of a flight tower calorimeter [12] [13] as it is equipped with flight CDEs, a flight carbon structure and flight like electronic circuits. We had no tracker in order to have a minimum of material in front of the calorimeter. As shown on picture 3.2, the EM was placed a mobile table, it could move in the plane orthogonal to the beam axis, and a rotating system enabled the EM to face the sky to collect cosmic muons.

*Fragment Separator
†Naval Research Laboratory

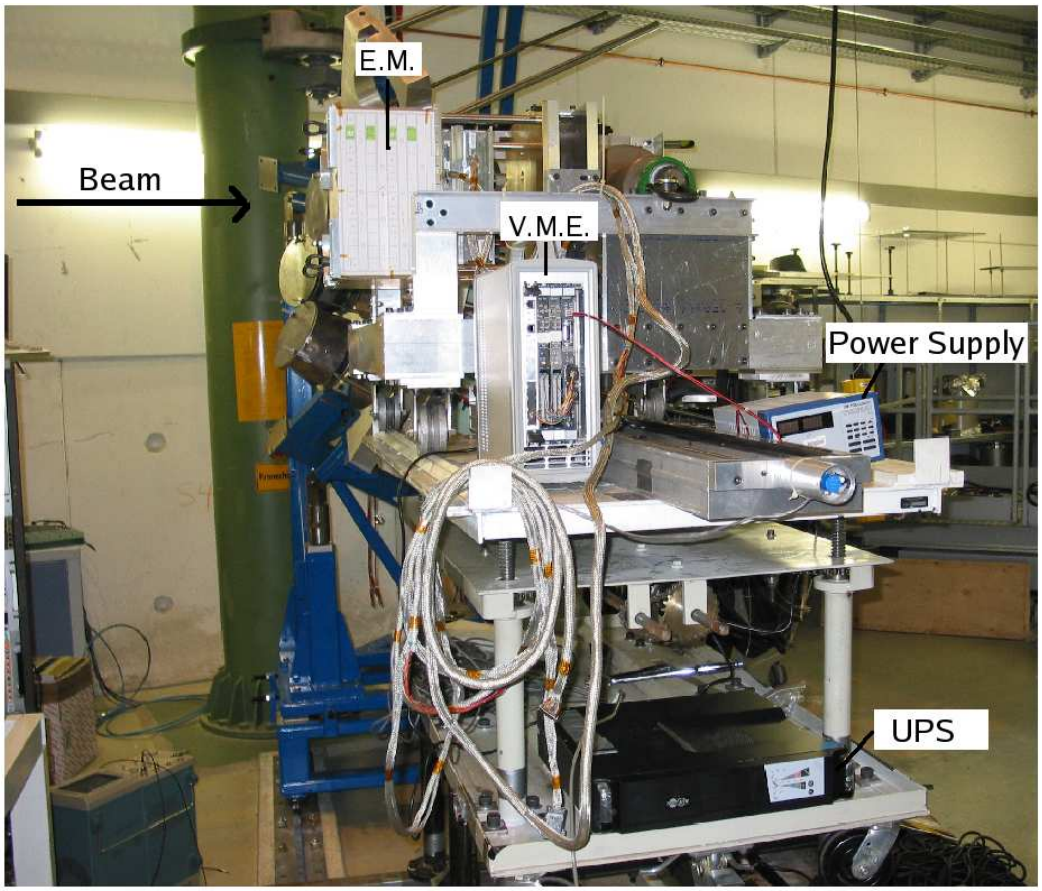


Figure 3.2: The E.M. in place on his moving table, facing the FRS beam.

## 3.2 Data analysis

### 3.2.1 FRS settings

I will briefly describe here how we used the FRS for particle selection, more details can be found in [9]. Let a particle of charge q, with a momentum p(GeV/c) moving in a magnetic field B, the gyration radius $\rho$ is given by :

$$B\rho = \frac{p(GeV)}{0.3q} \tag{3.1}$$

The optical path of the FRS line gives the limits of the radius $\rho$ in each of both turns so that equation 3.1 shows that setting the magnetic field B is selecting the particles with a defined ratio $\frac{p}{q} \sim \frac{A}{Z}$. Moreover, between the two sets of bending magnets, an achromatic degrader is responsible for an energy loss that is different for each isotope as it goes like $\frac{Z^2}{A}$. Consequently, the isotopes will be spatially separated in the final focal plane. By setting the two sets of bending magnets, one is able to select particles with defined $\frac{A}{Z}$ and $\frac{p}{q}$ ratios at the center of the final focal plane. For instance, during the light ion runs, we wanted to select particles with $\frac{A}{Z} = 2$ in order to have $\alpha$ particles and we also had deuterons.

For protons runs, FRS settings were somewhat special as protons are the only particles for which $A = Z = 1$. The selection is, a priori, very strong, however relativistic protons can easily generate nuclear reactions within the line, and part of nuclear products may get out so that we don't know how much pure is the proton beam.

### 3.2.2 E.M. energy calibration

The EM energy calibration has been done by S. Checktman using cosmic muons and charge injection runs. Charge injection consists in applying a define and well known set of voltages on each channel in order to quantify the electronic gain response function. For perfect electronic circuits, the response is linear, but GLAST electronic shows up non-linearities that rise to more than 10% for low voltages and high gains. So the response functions are used to inter-calibrate channels on a same diode taking account for non-linearities.

The equation 3.2 define the energy calibration for LEX8 directly from cosmic muon data.

$$LEX8(MeV) = (LEX8(bin) - Ped(bin)) \times Gain \tag{3.2}$$

where • $LEX8(MeV)$ is the measured energy in LEX8 in MEV.
- $LEX8(bin)$ is number of bins read by the ADC for LEX8.
- $Ped(bin)$ is the pedestal calculated for LEX8 in bins.
- $Gain$ is the conversion factor in ADC bins per MeV for LEX8,

determined from the ionization energy deposit of cosmic muons in the CsI log.

Pedestal are calculated by fitting a Gaussian on the peak seen in ADC channels for logs not hit by any particle. To define the right conversion factor from ADC

bins to MeV, we use cosmic muons that are merely minimum ionizing particle so that the energy deposit distribution follows a Landau with a most probable value around 11.2MeV for 19.9mm of CsI. As cosmic muons have an angular distribution, a selection is done on good trajectories, using crossing logs, to reduce the broadening of the Landau distribution. The energy calibration of other gains is done with respect to LEX8. The method can be summarized as follow :

- LEX8 : direct calibration from cosmic muons.
- HEX8 : HEX8 has a special muon mode $HEX8_{\mu}$ which gain is multiply by 10. First, the muon gain mode is inter-calibrated with LEX8 using cosmic muon data. Second, charge injection calibration of $HEX8_{\mu}$ over HEX8 is achieved.
- LEX1 : charge injection calibration over LEX8
- HEX1 : charge injection calibration over HEX8

With this energy calibration method, all channels have been calibrated. Besides, 1.7GeV protons of the FRS beam can also be used to check this calibration as they are also minimum ionizing particle when they do not generate hadronic cascades. All the logs have not seen the primary protons, that's why we could not use them for the whole calibration.

To check the calibration, we superpose a GEANT4 simulation of the energy deposit of 1.7GeV protons in our calorimeter to the beam data, and this reveals a 4% discrepancy on the most probable value of Landau distributions. For consistency, I correct for this systematic error by applying the appropriate correction factor on all channels. Eventually, the agreement is almost perfect between data and simulation as shown on figure 3.3 for the first four layers. Moreover, 1.7GeV protons and 3.4GeV deuterons data do not show energy deposit per log greater than 1GeV, so that for the analysis, we will only use the first two gains : LEX8 up till 100MeV and LEX1 over 100MeV. We also set a threshold of 5MeV per log : above 5MeV, the log is said to be hit and it's energy is summed in the energy deposit per layer.

Last but not least, one must keep in mind that this calibration is not valid for heavy ions because of scintillation quenching [17][18] which was the main goal of the GSI beam test [15]. For instance, energy deposits of secondary ions from nuclear reactions are obviously badly measured and this possibly sets a limit on the expected agreement between data and simulations.

### 3.2.3 Cuts

Among the many runs taken during the GSI beam test, two are of interest for our analysis. The first one is run 165 with 1.7GeV protons, the second is run 178 that contains 3.4GeV deuterons. As already explained, the FRS line is not suited for such light ions, so that we can only rely on the calorimeter for the particle identification. A set of cuts is applied to both runs in order to make a strong selection and keep only good proton events from run 165 and deuteron events from run 178, as shown on figure 3.4. The first two cuts select events for which the energy deposit in the entry log of the first layer is between 8MeV and 20MeV, this entry log being the only

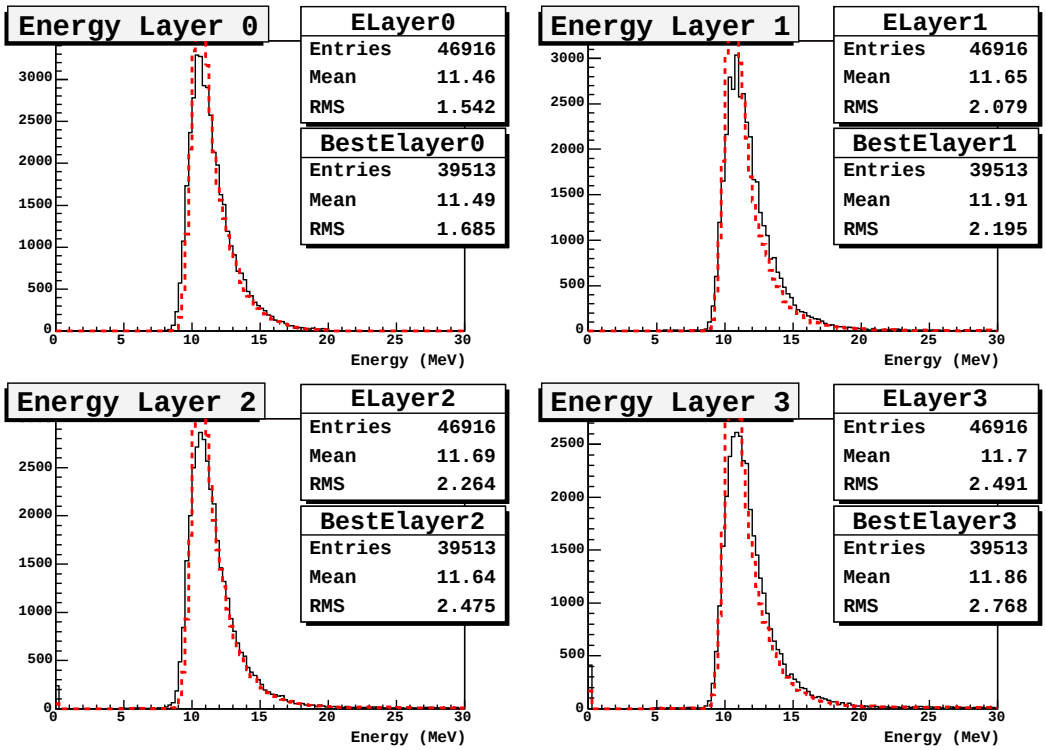


Figure 3.3: Checking the energy calibration for the first four layers of the calorimeter after the correction for a 4% systematic error. Data are in continuous line and simulation in dashed line. The great agreement shown here is used as a reference for the following comparisons between data and simulations on hadronic cascades.

one in the first layer to be hit. The third cut ensures that at least one log is hit in the second layer in order to avoid events going through the gaps between logs.

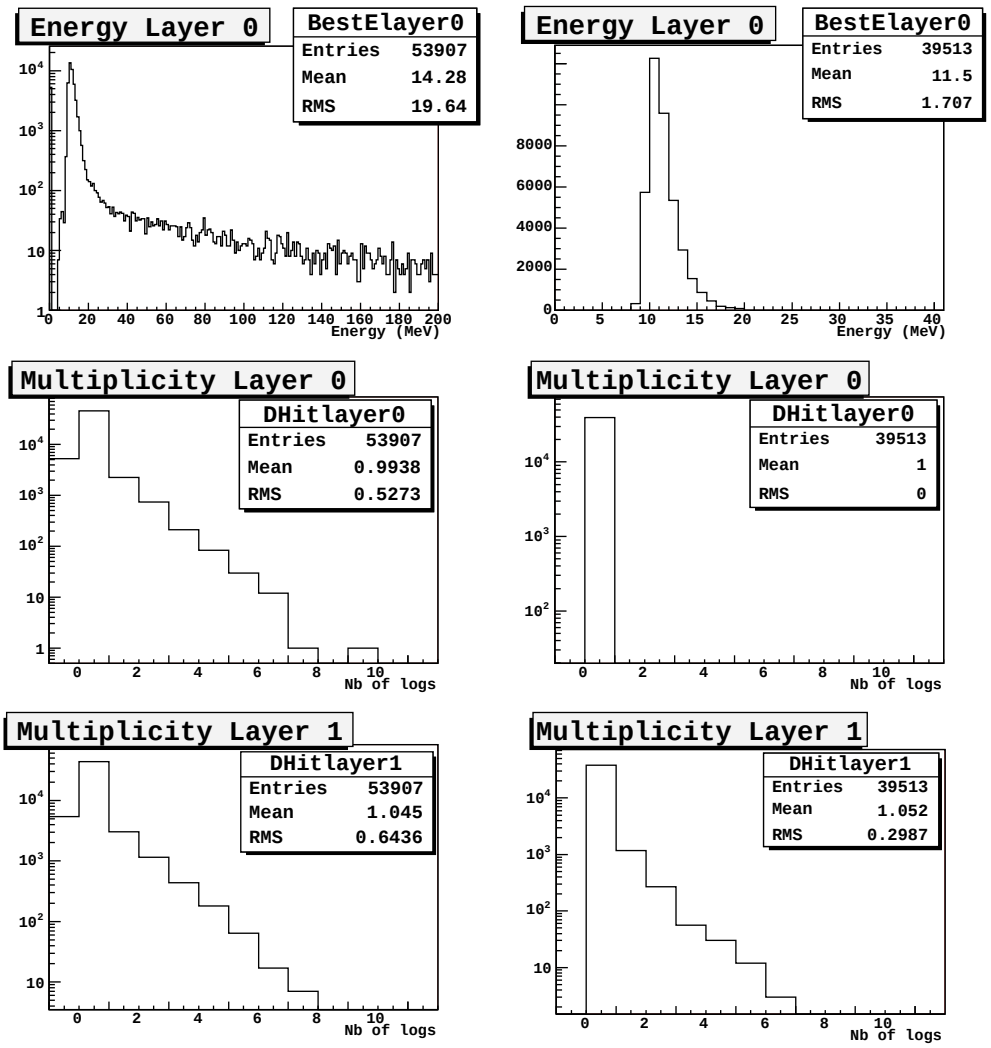


Figure 3.4: Set of cuts on the first two layers to select MIPS : before cuts on the left and after cuts on the right. The upper plot shows the cut on the energy deposit in the entry log of the first layer, the middle one shows that only one log is hit in the first layer and the lower one shows that at least one log is hit in the second layer to avoid gaps. Beam test data 1.7GeV protons

One has certainly noticed on figure 3.4 that the cuts are strong and get rid of a quarter of all events. In addition to this, simulations show that the events removed by the cuts are mainly hadronic cascades ! Actually, nuclear reactions generate back-splash, i.e. particles emitted backward, and back-splash effects are quite strong at a few GeV. For instance, we know from simulations that half of the reactions that took place in the second layer are responsible for energy deposits greater than 20MeV in the first layer, these reactions are cut. The consequence is that one can expect the cuts to remove particularly nuclear reactions with strong back-splash. To check if it

is not a too important bias for our analysis one can have a look to the total energy deposit in the whole calorimeter as show on figure 3.5. Energy distributions before and after the cuts are presented. The conclusion is that the cuts do not change the shape of this distribution dramatically.

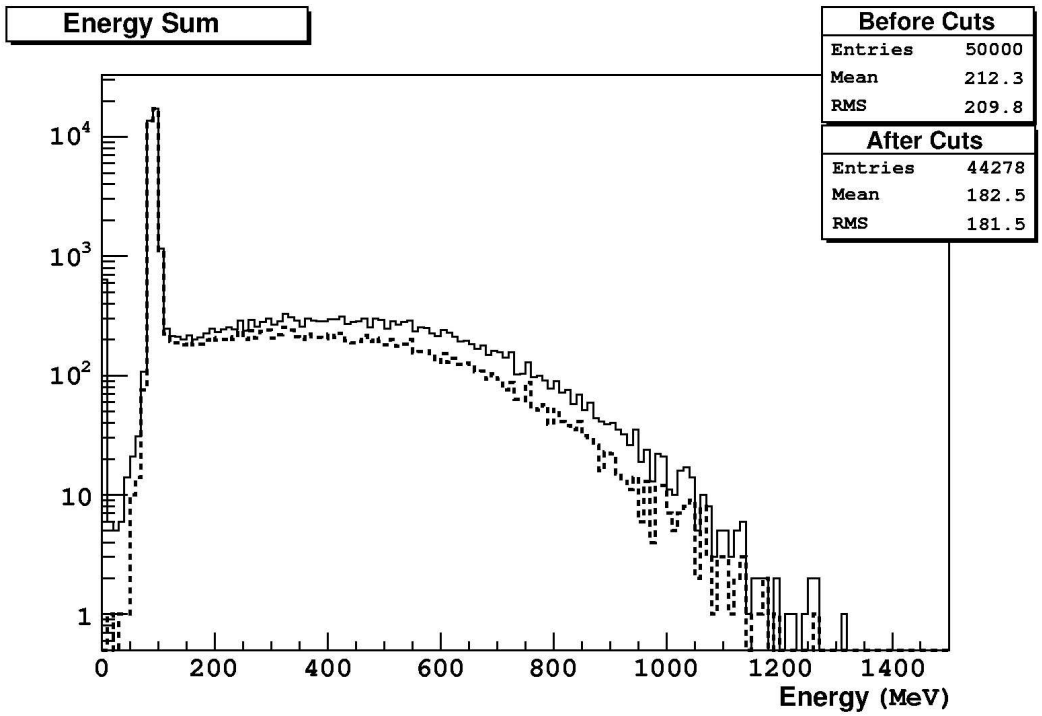


Figure 3.5: Simulation (BERT model) : cuts impact on the total energy deposit in the whole calorimeter. Histogram in plain line before the cuts, and in dashed line after the cuts. The shape of the original distribution is preserved by the cuts.

## 3.3 Simulation and results for 1.7GeV protons

### 3.3.1 1.7GeV protons simulation

Simulations have been set up using the GEANT4 tool kit version v6.2p02.The geometry takes into account 8 crossed layers of 12 CsI logs, a carbon structure and the aluminum cover plate. The FRS detectors have also been considered as they are a possible cause of energy loss or nuclear reactions. We do not have much information about the beam profile, but energy distributions in the different logs of the first layer led us to use a 3D Gaussian beam extending over 3 logs. Eventually, it's interesting to notice that a much simpler geometry with CsI logs and a punctual beam only, gives the same results.

Using this setup, 53000 protons are generated at normal incidence with 1.7GeV kinetic energy. The same cuts are applied on this simulated run as on the beam data in order to have consistent comparisons.

### 3.3.2 Data and simulation comparisons

For all the comparisons, histograms from the simulations are normalized to histograms from the data using the number of events. The norm factor is usually around 1. as the number of event simulated is somewhat equal to that of real events. The issue is to compare the shape of the distributions to make sure that the simulation reproduces well all the different sorts of events. Moreover, table 3.1 reports the values of the first two moments (mean and RMS) of all the simulated and real distributions in order to give more quantitative results. Variable names used in table 3.1 are those reported in section 1.2.3 page 10. For the energy deposit and multiplicity per layer, mean and RMS of the fourth layer are given as representative values for all layers. This table should only be considered as a help to quantify differences between simulated and real distributions, and no conclusions should be drawn without a closer look to histograms themselves.

| **Mean** of distributions for data and LHEP and BERT models | | | | | | | |
|---|---|---|---|---|---|---|---|
| Variables | $E_{layer}$ | $M_{layer}$ | $E_{Sum}$ | $M_{Sum}$ | $E_{Max}$ | $J_{Emax}$ | $RMS$ |
| unit | $MeV$ | logs | $MeV$ | logs | $MeV$ | logs | $MeV$ |
| data | 28 | 1.1 | 201 | 8.9 | 23 | 3.8 | 23 |
| LHEP | 32 | 1.2 | 211 | 9.0 | 25 | 3.7 | 25 |
| $\Delta_{LHEP}$ | 4 | 0.1 | 10 | 0.1 | 2 | -0.1 | 2 |
| BERT | 26 | 1.2 | 182 | 9.0 | 23 | 3.9 | 18 |
| $\Delta_{BERT}$ | -2 | 0.1 | -19 | 0.1 | 22 | 0.1 | -5 |
| **RMS** of distributions for data and LHEP and BERT models | | | | | | | |
| Variables | $E_{layer}$ | $M_{layer}$ | $E_{Sum}$ | $M_{Sum}$ | $E_{Max}$ | $J_{Emax}$ | $RMS$ |
| unit | $MeV$ | logs | $MeV$ | logs | $MeV$ | logs | $MeV$ |
| data | 62 | 0.6 | 220 | 2.5 | 36 | 2.2 | 43 |
| LHEP | 68 | 0.6 | 231 | 2.6 | 40 | 2.2 | 45 |
| $\Delta_{LHEP}$ | -6 | - | 11 | 0.1 | 4 | - | 2 |
| BERT | 49 | 0.6 | 181 | 2.6 | 33 | 2.3 | 32 |
| $\Delta_{BERT}$ | -13 | - | -39 | 0.1 | -3 | 0.1 | -11 |

Table 3.1: $1.7GeV$ protons from GSI data. Differences between the first two moments of both the real and simulated distributions : for a variable $X$, $\Delta_{LHEP} = X_{LHEP} - X_{data}$ et $\Delta_{BERT} = X_{BERT} - X_{data}$

#### Energy deposit and hit multiplicity per layer

Figures 3.6 and 3.7 display the comparisons between data and simulations for energy deposit and multiplicity per layer : plain lines are data, dashed lines are LHEP simulation and dotted lines are BERT simulations. The first bin is hidden for a better look on the distributions and is well reproduced by both simulations within a few percent. The agreement shown between data and both simulations is very good on the overall, despite the lack of a few high energy events for the Bertini model

that entails a 20% difference on the RMS of the energy deposit per layer (only 0.5% of events are concerned anyway).

### Energy sum and total hit multiplicity

Figure 3.8 displays the comparisons between data and simulations for the total energy deposit and the total hit multiplicity. It's striking to see on the energy plot that the simulated energy distributions dramatically lack of events between $100MeV$ and $200MeV$, worst case being for the LHEP model. In details, the bins corresponding to MIPs ($80MeV < E_{Sum} < 100MeV$ and 8 logs hit) are well reproduced by both simulations, within 10%, but for the following bins ($E_{Sum} > 100MeV$ and 9 logs hit) the difference reaches 40%. Between $100MeV$ and $200MeV$, the integrated lack of events is a factor of 5 for the LHEP model and around 20% for the BERT model. This feature might have to be linked to what we said about peripheral nuclear reactions in section 2.3 : the LHEP model does not produce peripheral reactions and these are low energy deposit events. For the total multiplicity, the same feature is present again. If it's less striking, there is a real lack of events with 9 and 10 logs hit. Moreover the simulated distribution are so different from the real ones that here one cannot report to the mean and RMS to get to the right conclusion.

As the LHEP and BERT model have some difficulties here, we should have a look to the Binary Cascade model. As shown on figure 3.9, the BIC model seems to propose a better total energy deposit distribution at low energy at least. But in the mean time, the total multiplicity distribution shows off that these low energy deposits are associated with high multiplicities, a feature not seen in the data. Looking at the correlation between total energy deposit and multiplicity, see figure 3.10, reveals that the BIC model correlation is very different from the one seen in the data. This correlation characterizes the topology of hadronic cascades, their extension in the calorimeter, so that it rules out the BIC model from further studies. The energy-multiplicity correlation is presented on figure 3.11 for the BERT and LHEP models : these two models reproduce well the correlation seen in the data for the most important part of the energy range, i.e. from 0 to $800MeV$ where almost all events are.

### Energy profile maximum and RMS, index of the layer with the maximum energy deposit

The first comparisons revealed discrepancies between data and simulations, we need to look at more variables to understand them better. Figure 3.12 displays the distributions for the energy profile maximum, the index of the layer with this maximum and the raw RMS of the energy profile. On the energy distributions, the same lack of low energy events shows up, it's obviously the same feature as for the total energy deposit. This confirms the idea that this lack of event in the simulations is really a global effect. The BERT model distribution are closer to the data than LHEP ones, but the lack of high energy events is the reason for the 20% discrepancy on the first two moments of the profile RMS distribution. Besides, the index of the layer with the maximum energy, that is linked to the development of the cascade along the calorimeter, is quite well reproduced.

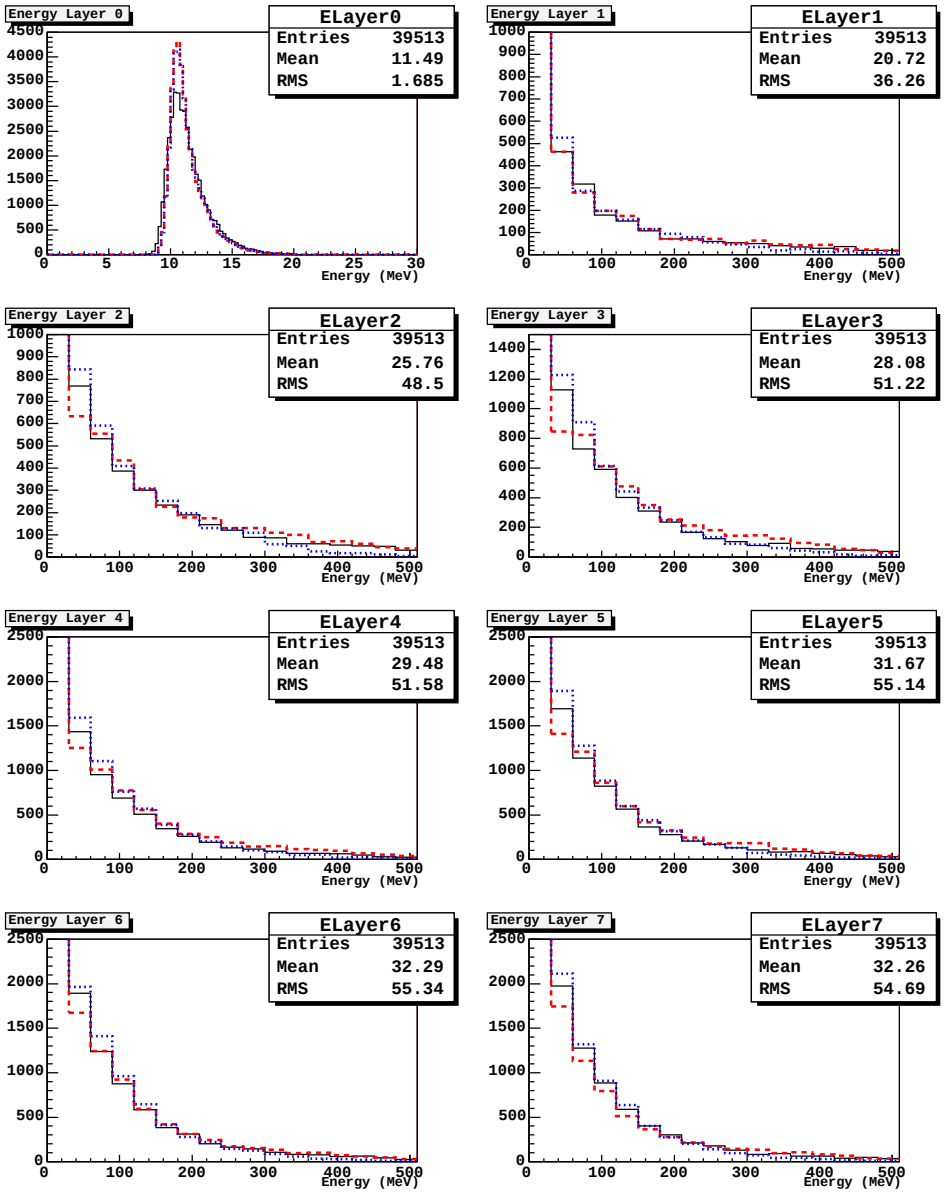


Figure 3.6: Protons 1.7GeV. Energy deposit per layer : plain lines are data, dashed lines are LHEP simulation and dotted lines are BERT simulations. For most of events, data and simulations agree well.

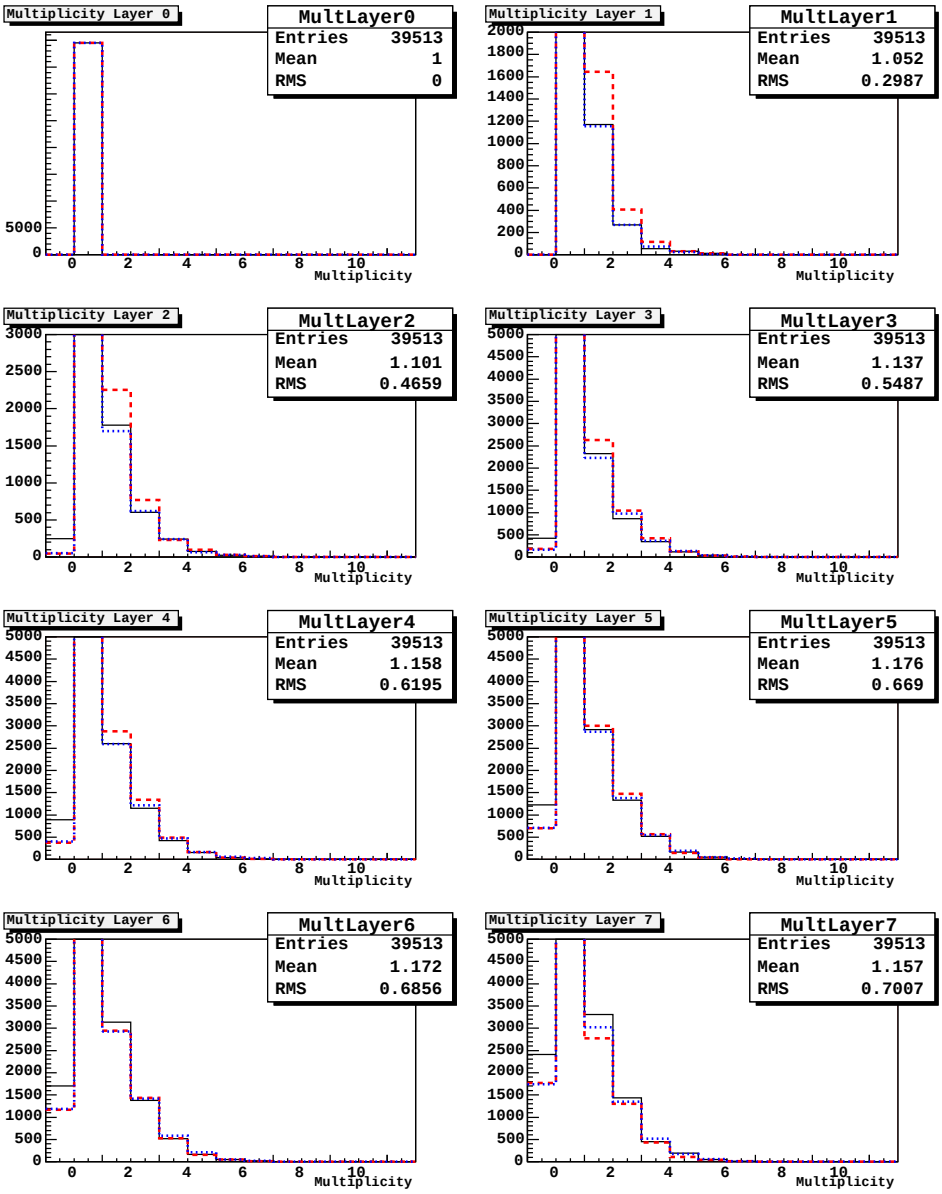


Figure 3.7: Protons 1.7GeV. Multiplicity per layer : plain lines are data, dashed lines are LHEP simulation and dotted lines are BERT simulations. For most of events, data and simulations agree well.

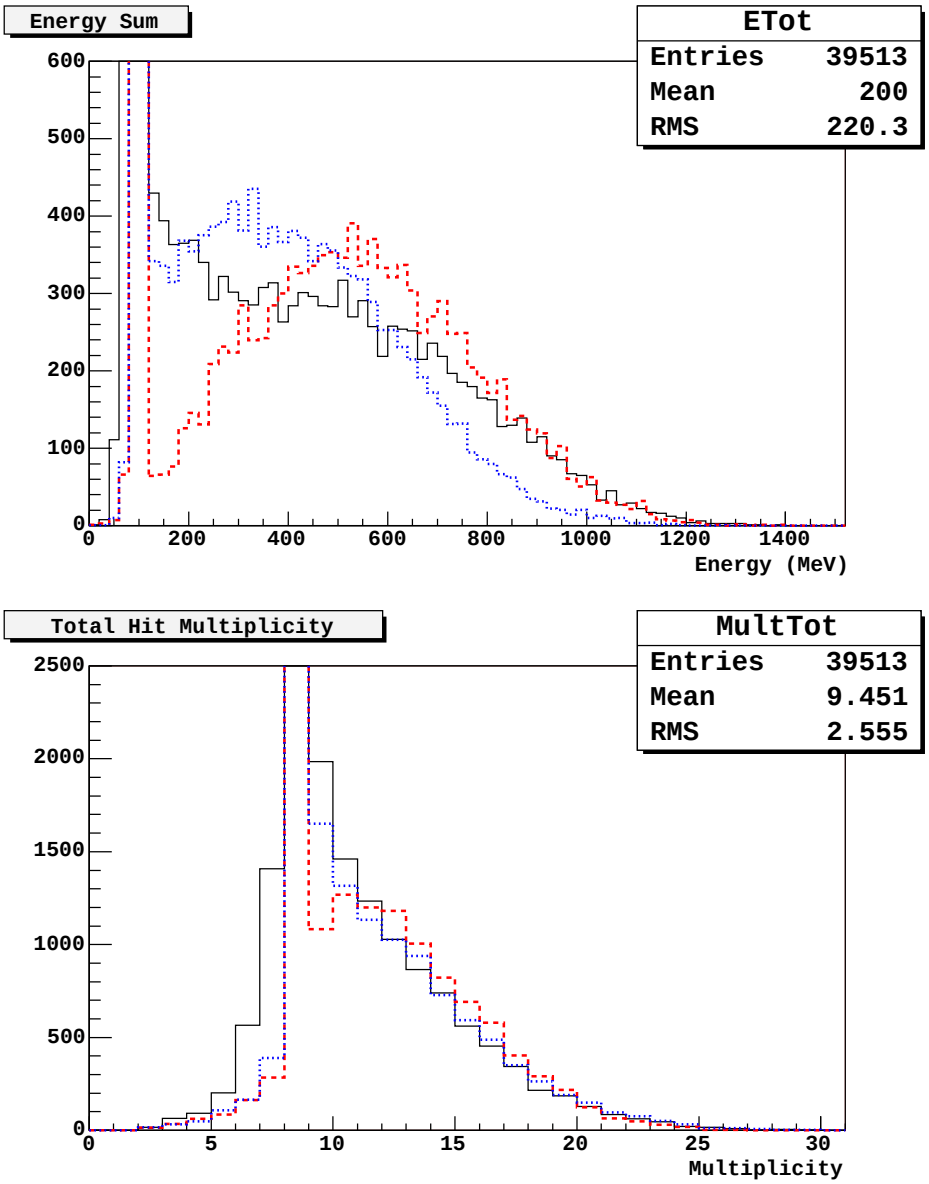


Figure 3.8: Protons 1.7GeV. Total energy deposit and total multiplicity : plain lines are data, dashed lines are LHEP simulation and dotted lines are BERT simulations. Simulated distributions do not reproduce the data for low energy deposit ($E_{Total} \simeq 200MeV$) and for low multiplicities (9 or 10 logs hit).

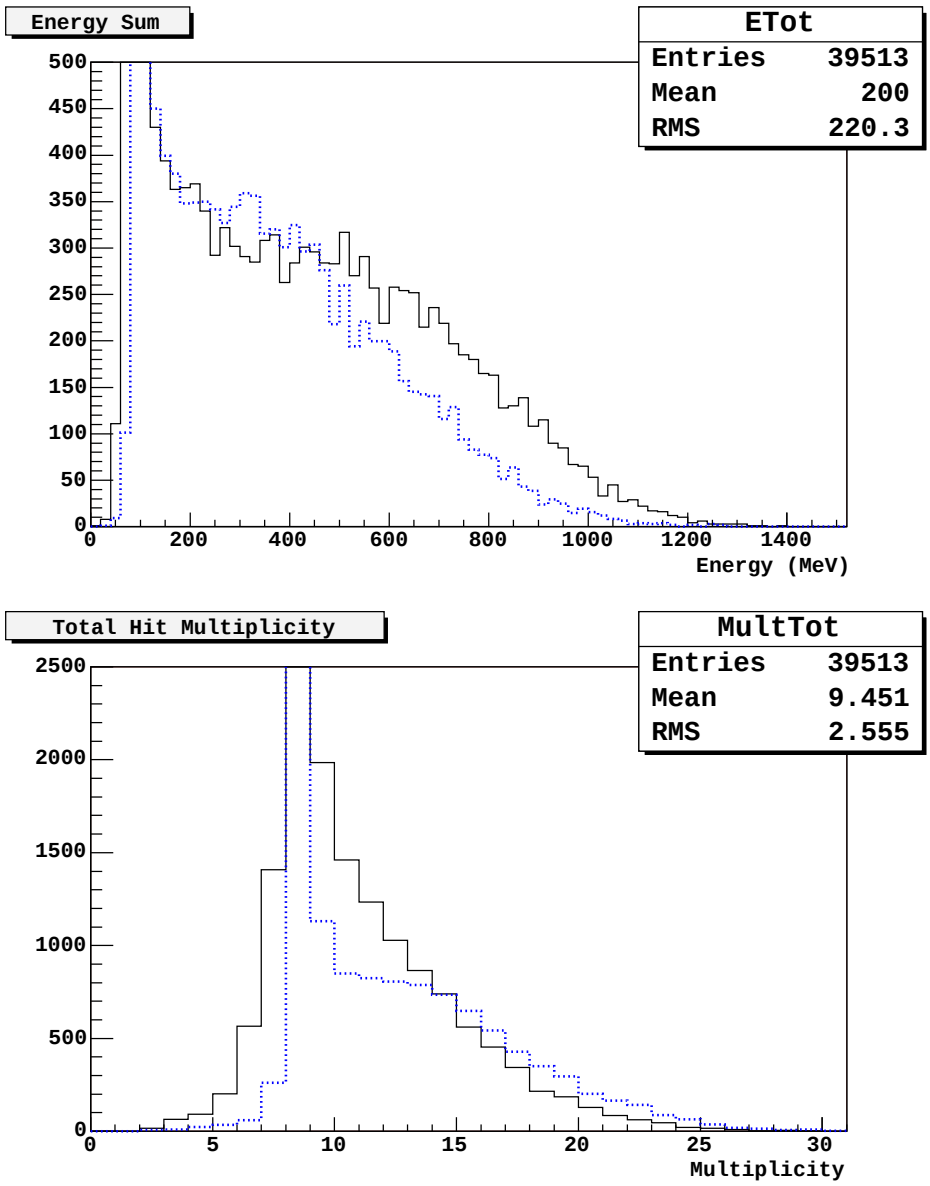


Figure 3.9: Protons 1.7GeV. Total energy deposit and total multiplicity : plain lines are data, dashed lines are LHEP simulation and dotted lines are BIC simulations. The BIC model presents a better energy deposit distribution at low energy but the associated multiplicities are too big.

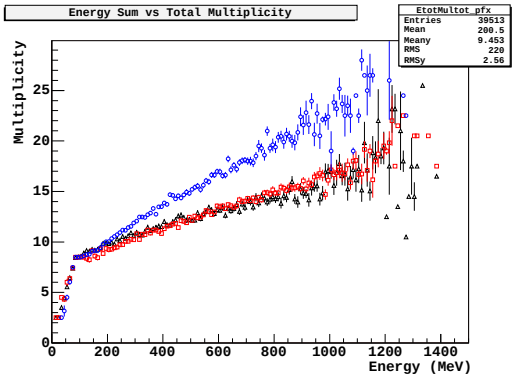


Figure 3.10: Protons 1.7GeV. Correlation between the total multiplicity and the total energy deposit for data (triangles), LHEP model (squares) and the BIC model (circles). The correlation shown by the BIC model is different from the one observed for the data.

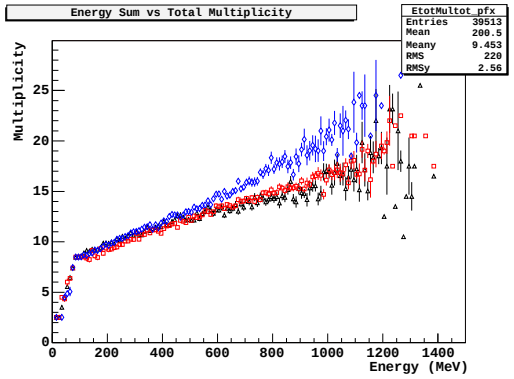


Figure 3.11: Protons 1.7GeV. Correlation between the total multiplicity and the total energy deposit for data (triangles), LHEP model (squares) and the BERT model (diamonds). The simulated correlation is fine from 0 to 800MeV where almost all events are.

### Maximum energy deposit per layer and associated multiplicity

For a deeper study of hadronic cascades, we use the maximum energy deposit to tag the layer where it happens. LHEP simulations show that for 80% of nuclear reactions, the index of the energy profile maximum corresponds to the layer where the reaction took place (this rate is 63% for the BERT model). Maximum energy deposit are to be compared layer by layer : for each event, the histogram of the layer with the maximum energy is filled with this energy if it's greater than 20MeV.

Figures 3.13 and 3.14 present the maximum energy deposit per layer and the corresponding multiplicities for the data (plain line), LHEP model (dashed line) and BERT model(dotted line). Here the multiplicities do not show any particular feature, nonetheless the maximum energy deposit distributions change as we go deeper in the calorimeter. The main feature seen on the data, is that the last two layers distributions have lower energy than the first ones. The effect is strong on the very last layer. The LHEP simulation does not reproduce this feature at all and shows the same distribution in all the layers. The energy distributions from the BERT simulation reproduce quite well this feature even if one could argue that the width of the simulated distribution is too low.

An explanation might be that if the nuclear reaction happens in the last layer then the maximum energy deposit will automatically be in the last layer, which is not the case for a hadronic cascade that develops early in the calorimeter and let it's maximum energy deposit in one of the following layer. This would mean that the Bertini model offers a better simulation of the development of hadronic cascade in the calorimeter.

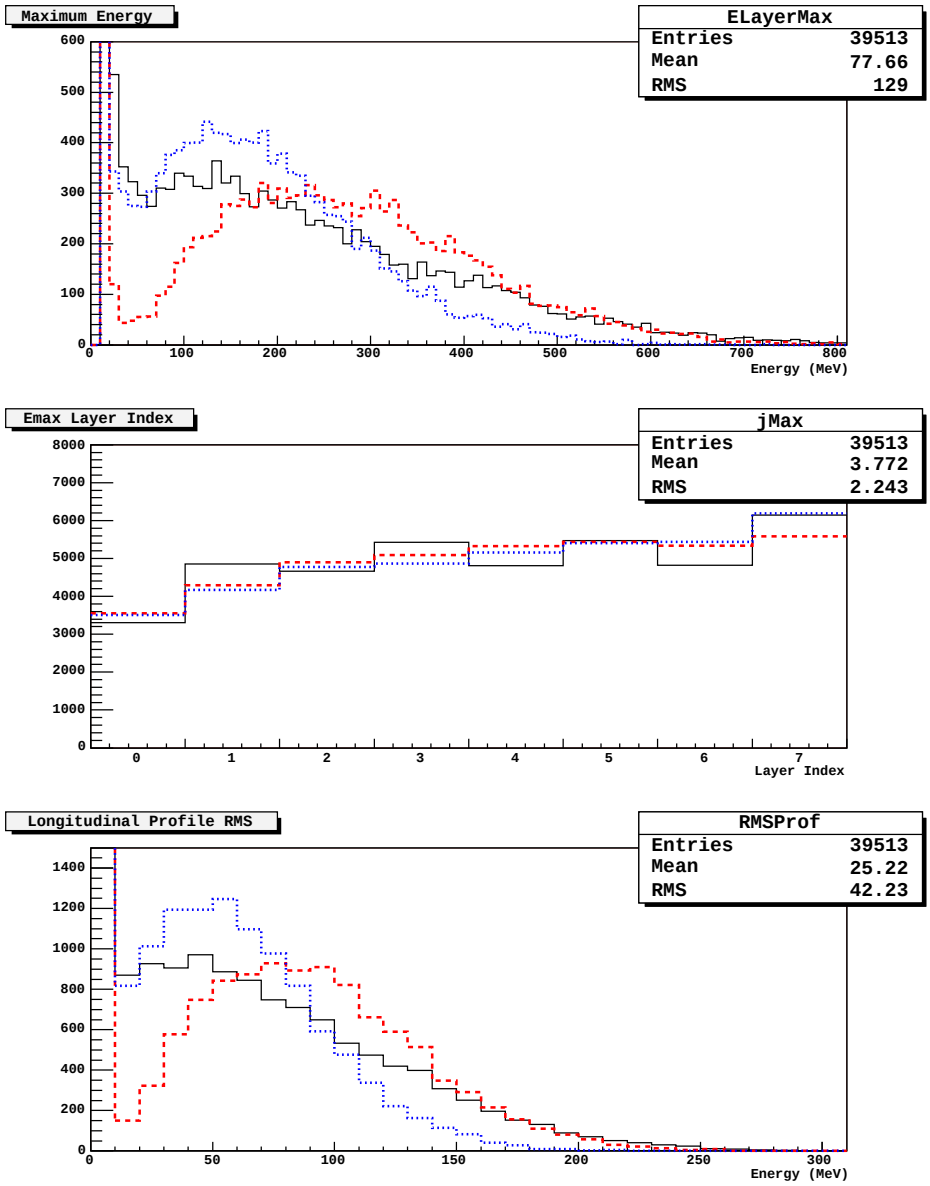


Figure 3.12: Protons 1.7GeV. Energy profile maximum, index of the layer with this maximum and RMS of the energy profile for data (plain line), LHEP model (dashed line) and BERT model(dotted line).

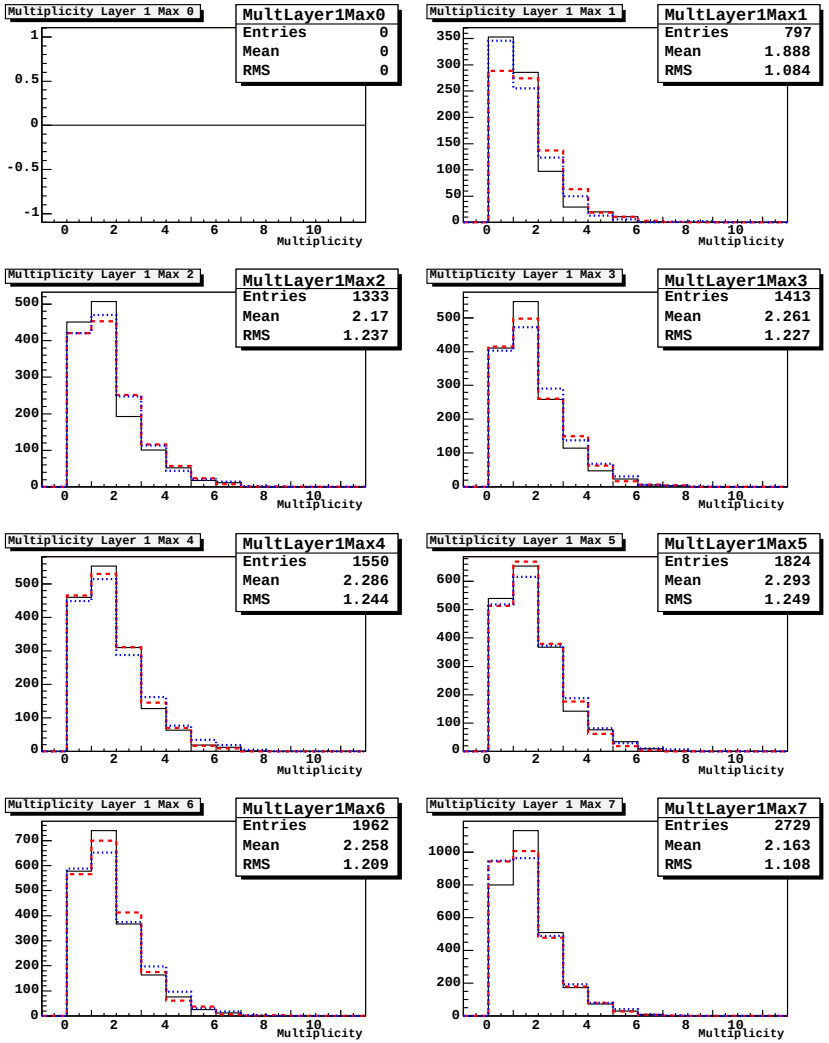


Figure 3.14: Emax multiplicity per layer

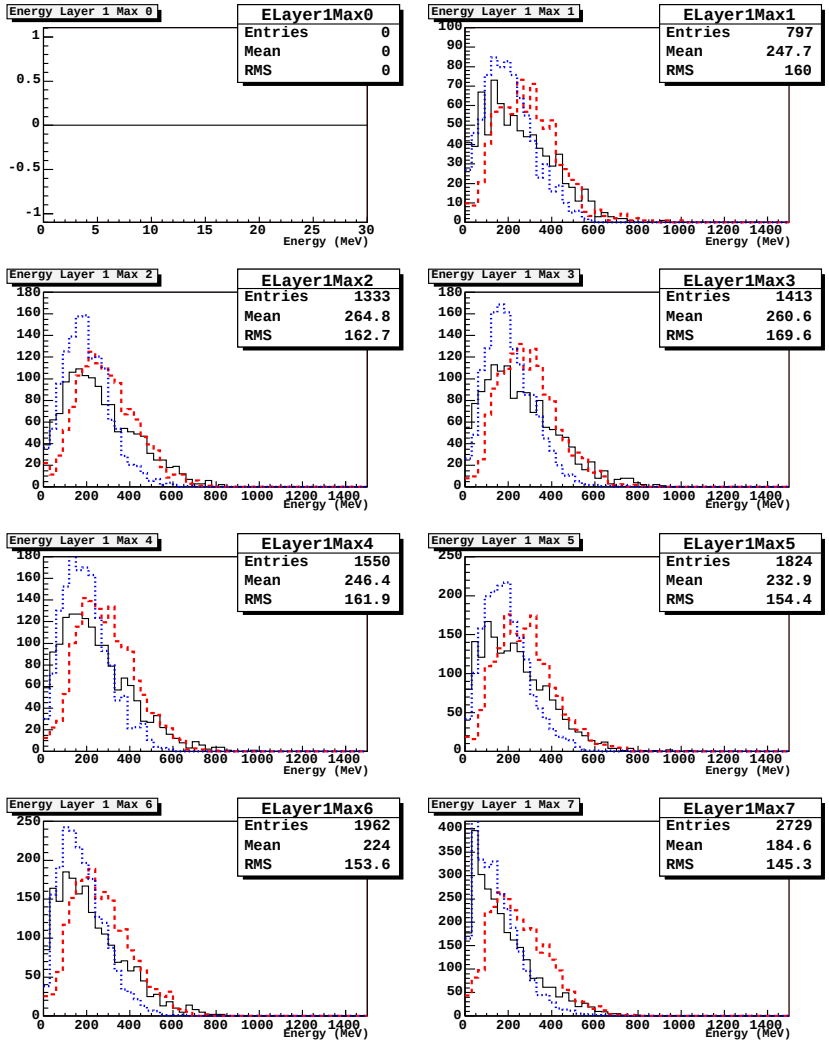


Figure 3.13: Maximum energy deposit per layer

## 3.4 Simulations and results for 3.4GeV deuterons

### 3.4.1 3.4GeV protons simulations

None of the hadronic cascade models available in GEANT4 is able to generate nuclear reaction for deuterons. However, this is not really a problem as it's been shown experimentally that at a few GeV proton and deuteron hadronic cascades have the same properties, what is far more complex to explain theoretically. So, we will compare 3.4GeV deuteron beam test data with proton simulations at 3.4GeV of kinetic energy.

### 3.4.2 Data and simulation comparisons

The same method as the one previously used is followed for the comparisons and table 3.2 reports the first two moments of the distributions for data and LHEP and BERT simulations.

| **Mean** of distributions for data and LHEP and BERT models | | | | | | | |
|---|---|---|---|---|---|---|---|
| Variables | $E_{layer}$ | $M_{layer}$ | $E_{Sum}$ | $M_{Sum}$ | $E_{Max}$ | $J_{Emax}$ | $RMS$ |
| unit | $MeV$ | logs | $MeV$ | logs | $MeV$ | logs | $MeV$ |
| data | 45 | 1.3 | 273 | 10.0 | 32 | 4.0 | 39 |
| LHEP | 37 | 1.2 | 244 | 9.6 | 30 | 3.8 | 29 |
| $\Delta_{LHEP}$ | -8 | -0.1 | -29 | -0.4 | -2 | -0.2 | -10 |
| BERT | 37 | 1.3 | 241 | 9.9 | 31 | 3.9 | 27 |
| $\Delta_{BERT}$ | -9 | - | -32 | -0.1 | -1 | -0.1 | -12 |
| **RMS** of distributions for data and LHEP and BERT models | | | | | | | |
| Variables | $E_{layer}$ | $M_{layer}$ | $E_{Sum}$ | $M_{Sum}$ | $E_{Max}$ | $J_{Emax}$ | $RMS$ |
| unit | $MeV$ | logs | $MeV$ | logs | $MeV$ | logs | $MeV$ |
| data | 109 | 0.9 | 328 | 4.1 | 59 | 2.2 | 68 |
| LHEP | 86 | 0.8 | 310 | 3.7 | 51 | 2.2 | 56 |
| $\Delta_{LHEP}$ | -23 | -0.1 | -18 | -0.4 | -8 | - | -12 |
| BERT | 82 | 0.9 | 306 | 4.2 | 54 | 2.2 | 51 |
| $\Delta_{BERT}$ | -27 | - | -22 | 0.1 | -5 | - | -17 |

Table 3.2: $3.4GeV$ deuterons from GSI data. Differences between the first two moments of both the real and simulated distributions : for a variable $X$, $\Delta_{LHEP} = X_{LHEP} - X_{data}$ et $\Delta_{BERT} = X_{BERT} - X_{data}$

#### Energy deposit and hit multiplicity per layer

Figures 3.15 and 3.16 display the comparisons between data and simulation for energy deposit and multiplicity per layer : plain lines are data, dashed lines are LHEP simulation and dotted lines are BERT simulations. From a global point of view, the energy deposit distributions present a nice agreement between data and both simulation, however one can notice a small lack of events in the simulations around

$100MeV$ energy deposit per layer. Moreover, the difference on the first two moments of these distributions reaches 25% and is that high because the simulated distributions also lack a few high energy events. The multiplicity per layer distributions present the same kind of features with a lack of events with 2 or 3 logs hit but with no consequence on the mean and RMS as shown on table 3.2. Besides a quick look to figure 3.6 is sufficient to see that the gap between LHEP and BERT simulations is smaller at $3.4GeV$ than at $1.7GeV$.

### Energy sum and total hit multiplicity

Figure 3.17 displays the comparisons between data and simulations for the total energy deposit and the total multiplicity . For both distributions, the same feature seen for $1.7GeV$ protons is observed : there is an important lack of events with low energy deposit (around $200MeV$) and low multiplicity (9 or 10 logs hit) , in the simulated distributions compared to beam test data. Again, the BERT model is better than LHEP even if the difference between both model at $3.4GeV$ is smaller than at $1.7GeV$ .

### Energy profile maximum and RMS, index of the layer with the maximum energy deposit

Figure 3.18 displays the distributions for the energy profile maximum, the index of the layer with this maximum and the raw RMS of the energy profile. On the energy distributions, the same lack of low energy events shows up, it's obviously the same feature as for the total energy deposit. The same scenario is played here as for $1.7GeV$ protons. However, again, the discrepancies between the LHEP and the BERT model are smaller at $3.4GeV$ than at $1.7GeV$.

### Maximum energy deposit per layer and associated multiplicity

Figures 3.19 and 3.20 present the maximum energy deposit per layer and the corresponding multiplicities for the data (plain line), LHEP model (dashed line) and BERT model(dotted line). Maximum energy deposit distributions are not well reproduced by both simulations, even the BERT model distributions are not good as they were at $1.7GeV$. But the most striking discrepancy comes from the multiplicities : in all the layers, the main peak is at one log hit in the data and at two logs hit in the simulations. The maximum energy deposit often corresponds to the layer of the nuclear reaction and we have to keep in mind that the bullets we use in the simulation are protons and not deuterons as in the data. The conclusion is that we might see here the limit of comparing deuteron hadronic cascade data with proton hadronic cascade simulations for our specific variables.

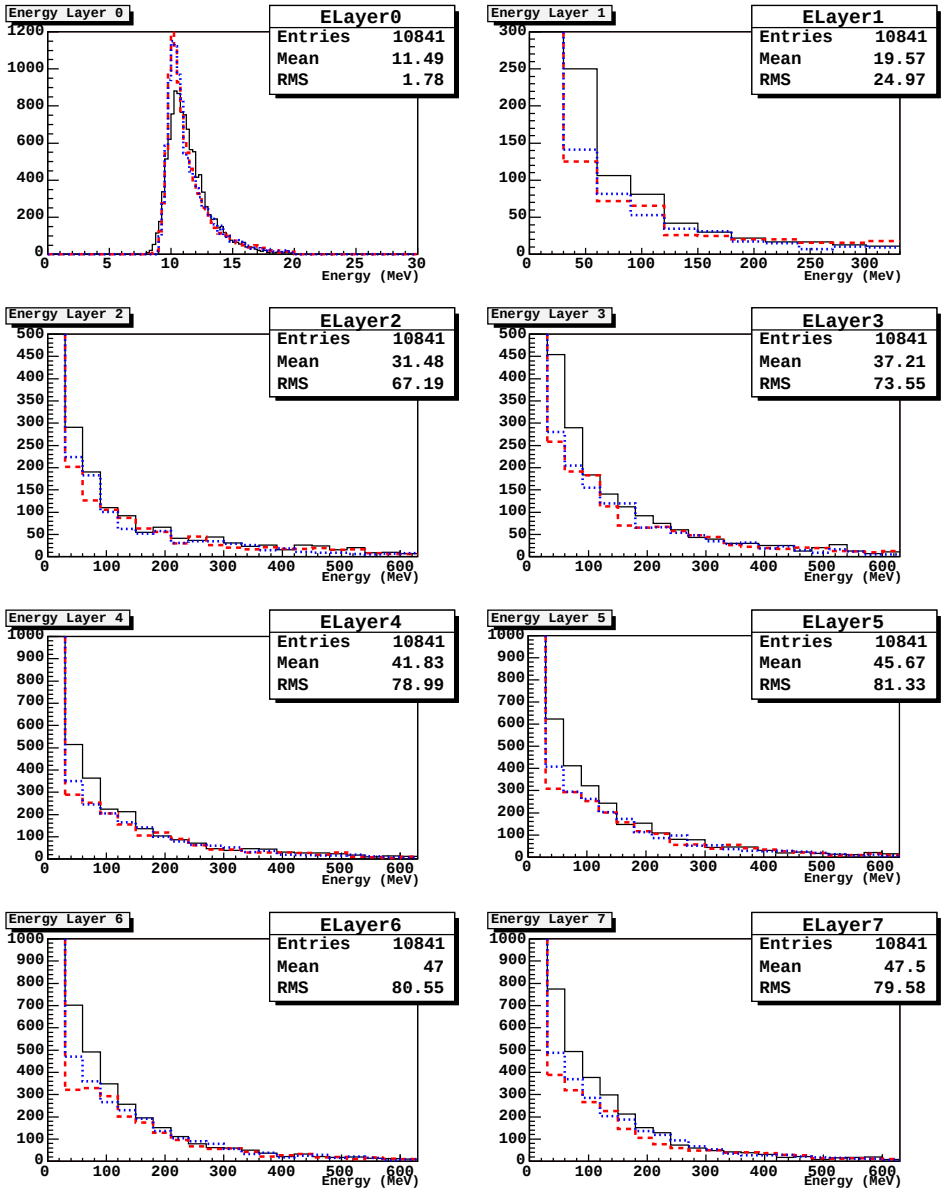


Figure 3.15: Deuterons 3.4GeV. Energy deposit per layer : plain lines are data, dashed lines are LHEP simulation and dotted lines are BERT simulations. Please note that histograms are in log scale to show the full distributions. For most of events, data and simulations agree well. Data are from 3.4GeV deuterons and simulations from 3.4GeV protons.

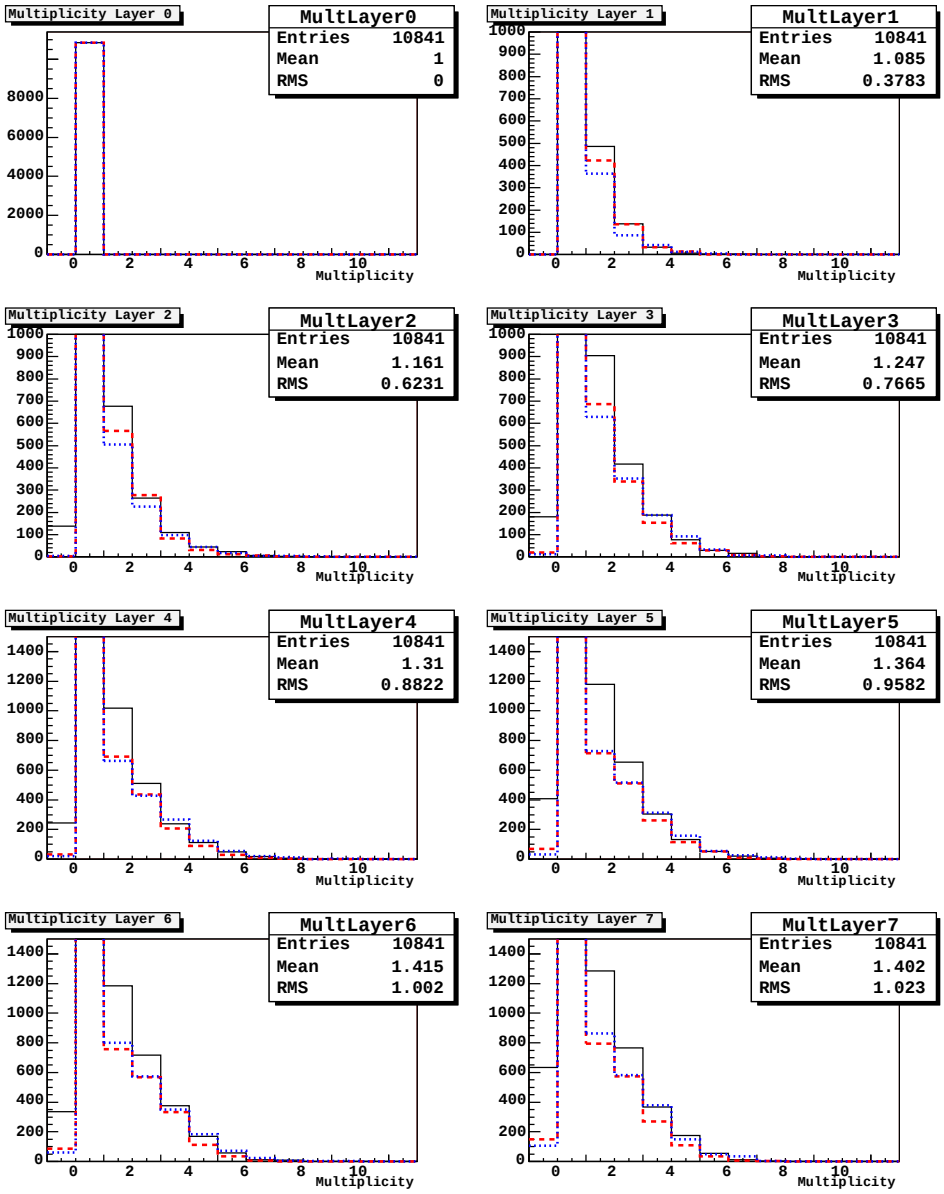


Figure 3.16: Deuterons 3.4GeV. Multiplicity per layer : plain lines are data, dashed lines are LHEP simulation and dotted lines are BERT simulations. For most of events, data and simulations agree well. Data are from 3.4GeV deuterons and simulations from 3.4GeV protons.

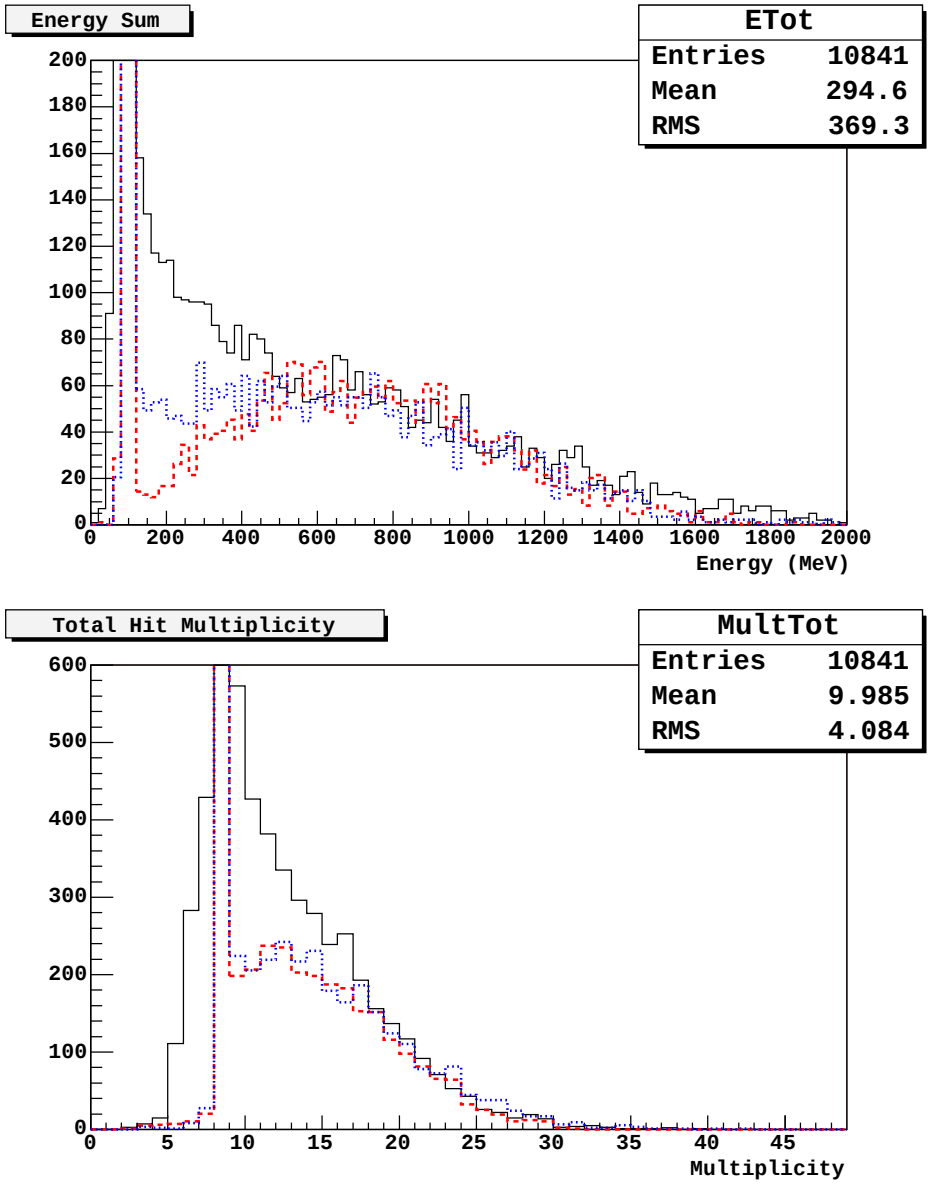


Figure 3.17: Deuterons 3.4GeV. Total energy deposit and total multiplicity for data (plain lines), LHEP simulation (dashed lines) and BERT simulations (dotted lines). Data are from 3.4GeV deuterons and simulations from 3.4GeV protons.

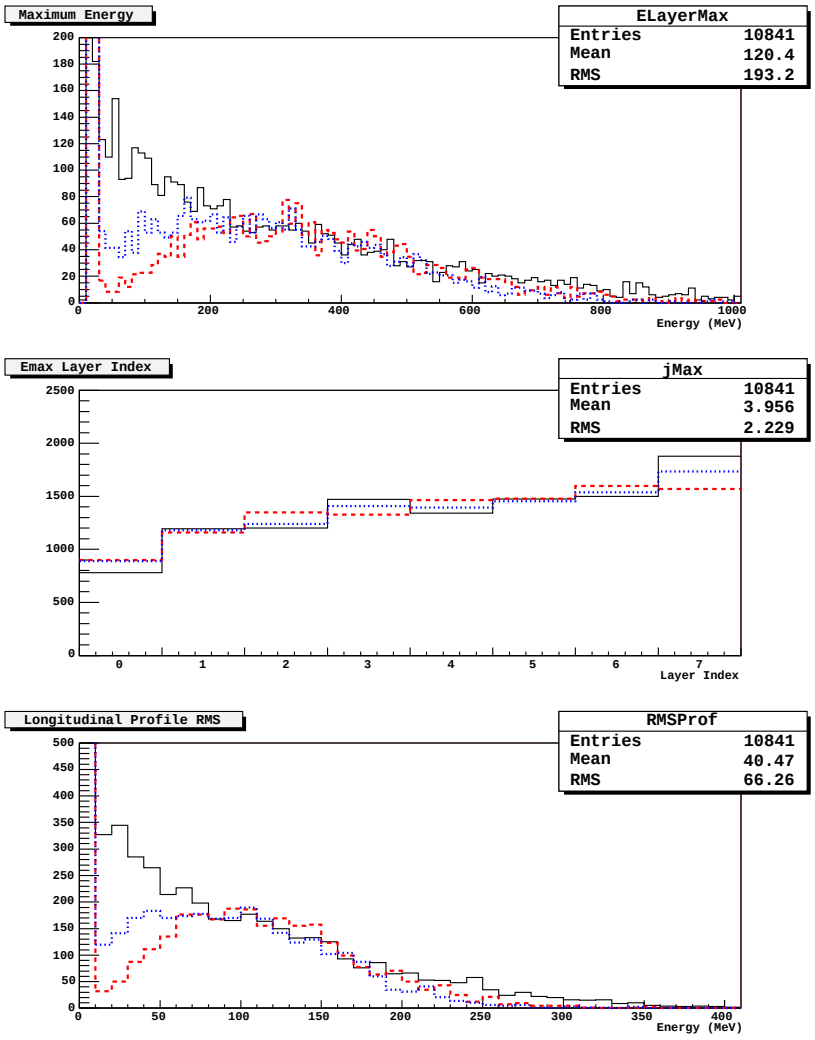


Figure 3.18: Deuterons 3.4GeV. Energy profile maximum, index of the layer with this maximum and RMS of the energy profile for data (plain line), LHEP model (dashed line) and BERT model(dotted line). Data are from 3.4GeV deuterons and simulations from 3.4GeV protons.

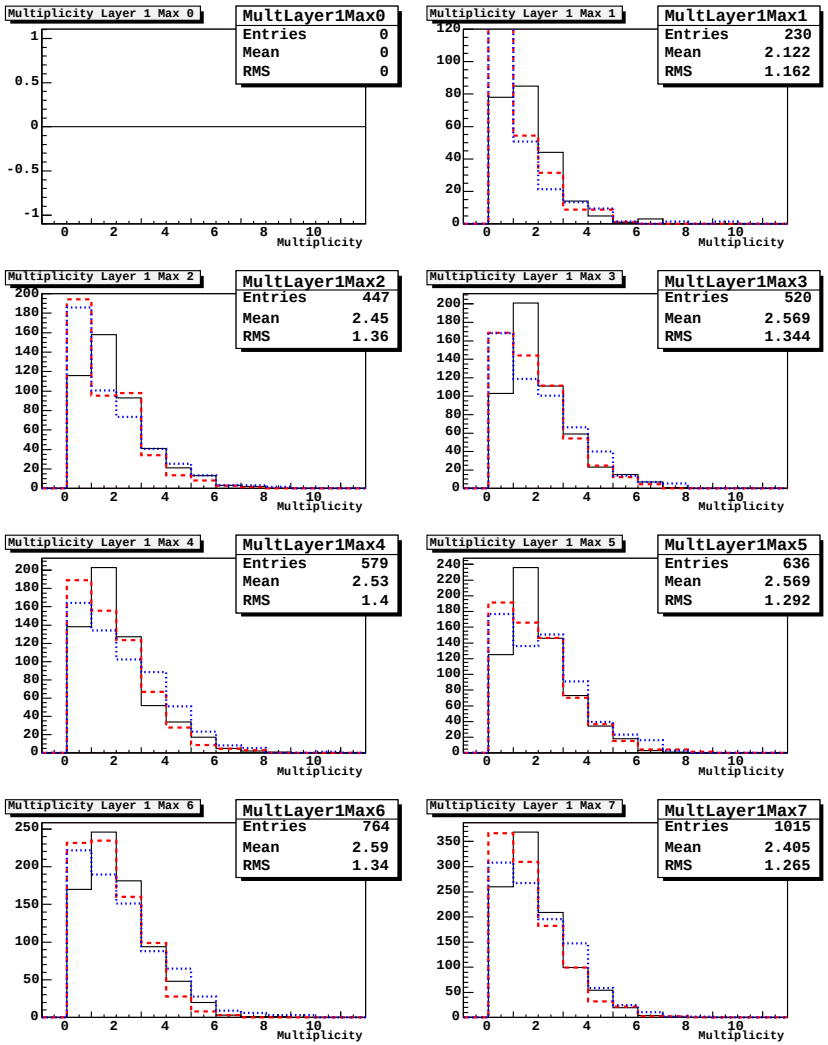


Figure 3.20: Emax multiplicity per layer

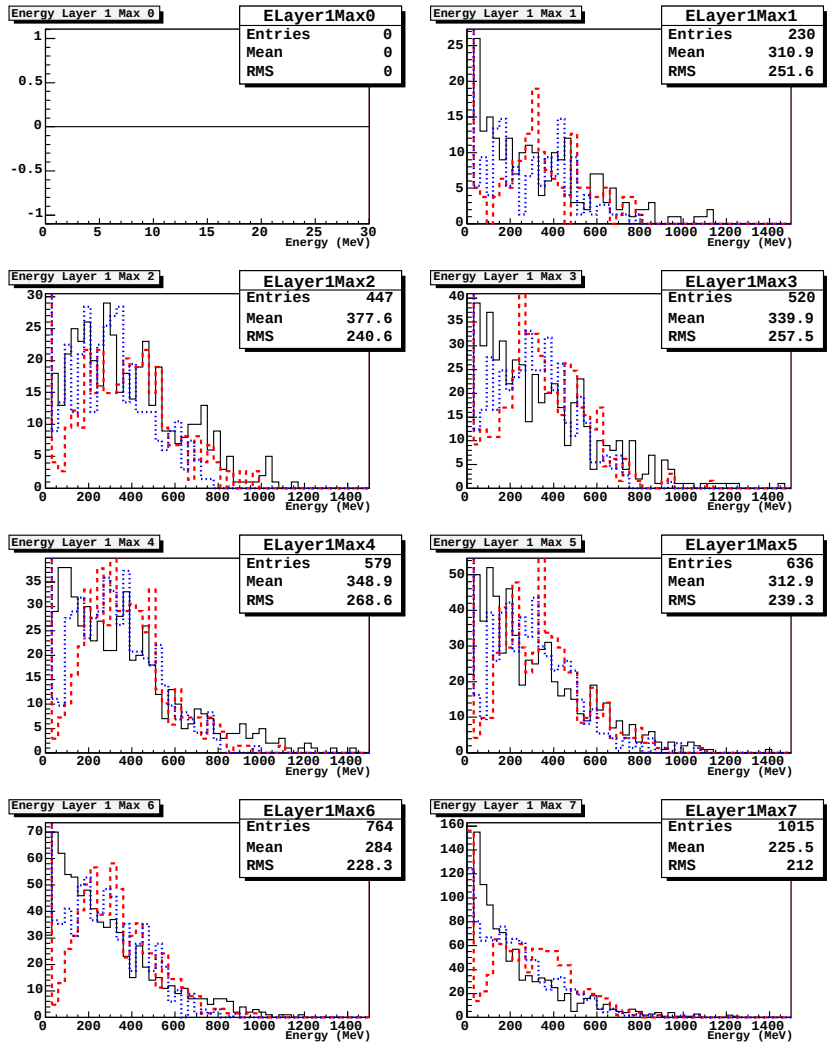


Figure 3.19: Maximum energy deposit per layer

# 4 GLAST CERN beam test

## 4.1 The beam test

### 4.1.1 Experimental setup

The beam test took place at CERN in august 2003 on the H6 line. As shown on figure 4.1, the experiment was set up as follow :

- Plastic scintillators (S1 and S2) : S1 measures $4cm \times 4cm$ and S2 should measure $2cm \times 2cm$ but more likely $2cm \times 2.5cm$ from tracker data. S1 and S2 are used in coincidence to trigger the DAQ only on beam particles.
- Tracker (T1 and T2) : the tracker, brought to us by Italian collaborators [20], consists in two modules with two $410\mu m$ thick silicon XY planes each. The active window measures $9.5 \times 9.5\ cm^2$.
- Lead plate : we had the possibility to add a lead plate of known thickness upstream from the calorimeter in order to be able to sample the longitudinal profile of electromagnetic showers. It was also useful to emulate the thickness of GLAST tracker that is equivalent to 1.4 radiation length.
- Calorimeter (C1 and C2) : the calorimeter is split into two modules : C1 is composed of 8 layers of 6 horizontal flight CDEs and C2 is composed of 3 layers of 5 horizontal small CsI logs with only one diode at each side, lent by the NRL* . The calorimeter was placed on a rotating plate on a moving table. As of now, the calorimeter will only refer to C1, the main calorimeter, also known as the *minical*.

Let's follow a beam particle through our experiment : it first goes through both scintillators that trigger the DAQ, and then goes through the tracker that measures its position on both silicon planes. The particle then goes through the lead plate and finally enters the calorimeter where it can, depending on its nature, make a simple ionization energy deposit or generate an electromagnetic shower, or generate a hadronic cascade.

### 4.1.2 Beams and electronic

During the experiment, we could have 10 full days of beam from the H6 line on the SPS. The primary beam was a $450GeV/c$ proton beam from which we had several high energy primary positron beams from $50GeV/c$ up to $200GeV/c$ and secondary beams at $10GeV/c$ and $20GeV/c$ with a mixture of electrons, muons, pions and other particles. Hadrons from $10GeV/c$ and $20GeV/c$ runs will be used to test hadronic cascade simulations. We also had some $20GeV/c$ muon beam for calibration and localization tests purposes.

A few words about the calorimeter electronic may be useful. The CsI logs are true flight CDEs with the same wrapping, diodes and bonding, but the main part of

*Naval Research Laboratory

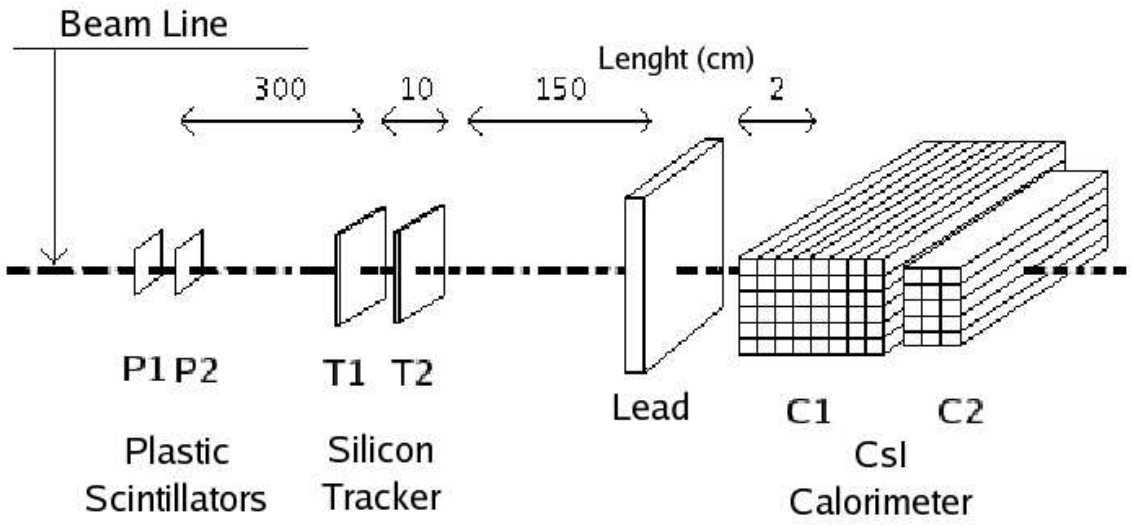


Figure 4.1: Main elements on the beam line.

the electronic chain was designed in Bordeaux and is specific. First, the big diodes have a high gain preamplifier and the small diodes, a low gain preamplifier. Second, we have two sets of amplifiers : one with a gain $\times 1$, that is the muon gain, and another with gain $\times 1/20$ for a general purpose. We had also attenuators to be used for the high energy beam runs. Besides, 7 CAEN V785 VME modules were used to code the $192 + 30$ channels of the calorimeters : each module has 32 channels able to code 4000mV over 4096 bins.

## 4.2 Data analysis

### 4.2.1 Calibrating the tracker

The tracker has two original features : on-line zero suppression so that only hit strips are recorded, and floating strips that are not connected to the ASIC but that increase the detector sensitivity [14].

The tracker data reduction is done by a program written by the Italian team ([20], [1]) and follow this procedure :

- pedestal subtraction : dedicated pedestal runs are done by forcing the trigger when there is no particle in the detector.
- common mode subtraction consists in subtracting the mean value of the number of bins read for each strips on one ASIC.
- particle position reconstruction in each silicon plane using full analogical information from all the hit strips.

The expected position resolution with respect to the center of the tracker plane is around $40\mu m$ using the analogical information [1]. As the distance between T1 and T2 is about $10cm$ and the distance between T2 and the front of the calorimeter is about $150cm$, one can deduce that the position resolution on the entry point of particles in the calorimeter is less than 1mm. This means that the position resolution is good enough so that we will be able to select events entering the calorimeter in a chosen log. For instance, figure 4.2 displays the beam profile limited to the width of the smallest plastic scintillator, in both tracker modules.

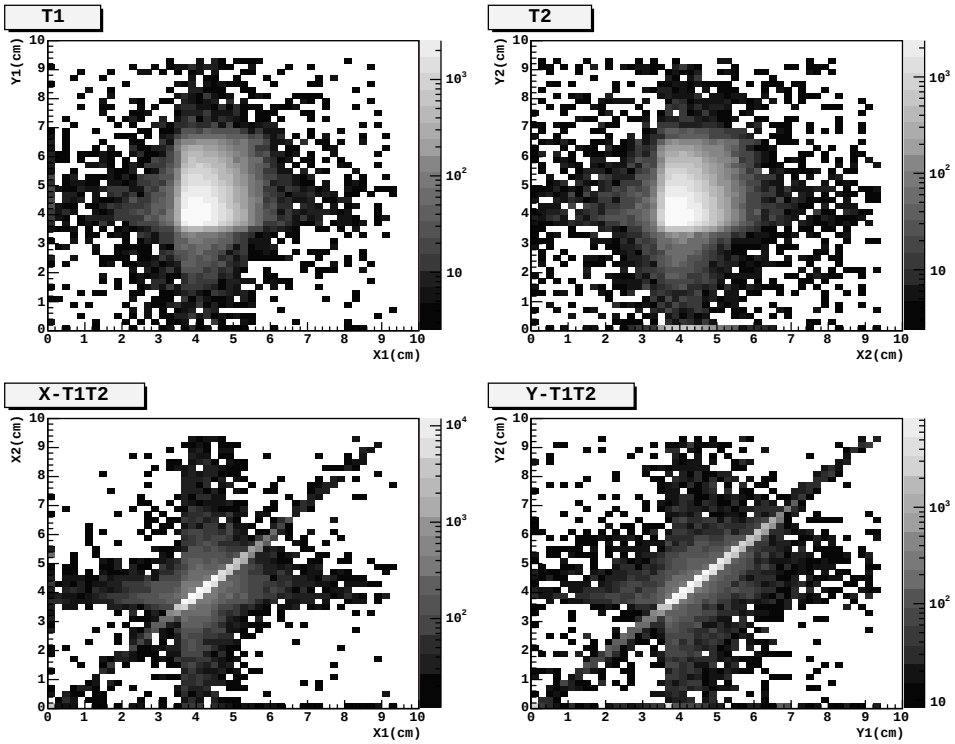


Figure 4.2: Beam profile for $20GeV/c$ particles in both tracker modules : upper left, X vs Y in T1 and upper right, X vs Y in T2. The two lower plots show the correlation between X1 and X2, lower left, and between Y1 and Y2, lower right.Good events are on the diagonal.

### 4.2.2 Calibrating the calorimeter

Picture 4.3 shows the calorimeter made of 8 layers of 6 horizontal flight CDEs. The calibration has been done by B. Lott and then controlled and improved by S. Svensson, a Swedish student during an internship in Bordeaux. A $20GeV/c$ monocinetic muon beam is used for calibration purpose as the ionization energy deposit of muons in CsI is very well known. Equation (4.1) summarizes the energy calibration for each channel of the calorimeter :

$$E_i = (C_i - C_{i_0} + b_i \times e^{-(C_i - C_{i_0})a_i}) \times \alpha_i \times att_i \times gain_i \times gdpd_i \qquad (4.1)$$

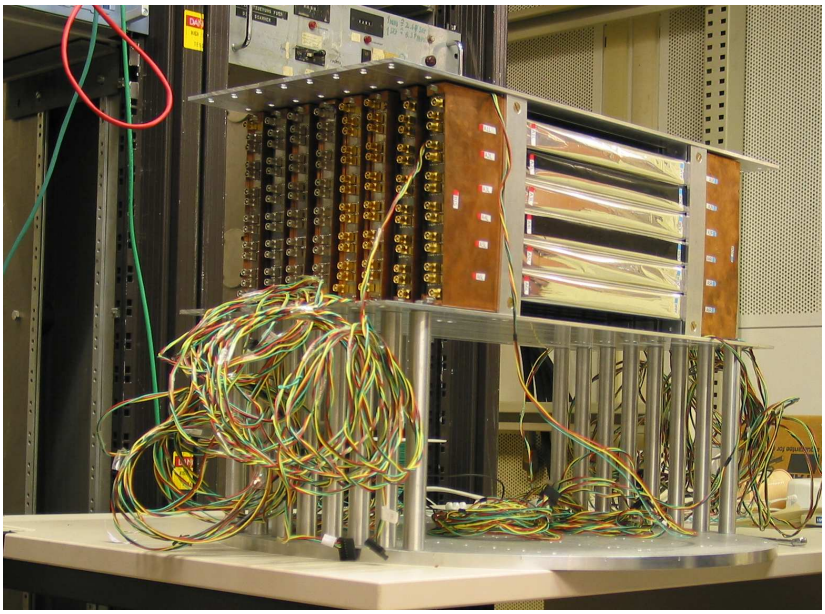

Figure 4.3: The calorimeter waiting to see the CERN SPS beam.

where • $E_i$ is the energy measured in MeV for channel i.

• $C_i$ is the number of bins read by the ADC for channel i.

• $C_{i_0}$ is the pedestal in bins for channel i

• $a_i, b_i$ are two factors used to take account for non linearities observed for low ADC values .

• $\alpha_i$ is the energy conversion factor from bins to MeV, deduced from muon beam data. For each big diode, the energy deposit spectrum of muons is fitted to the same spectrum simulated with GEANT4 to get the conversion factor.

• $gain_i$ is the inter-calibration factor between muon gain amplifiers and beam gain amplifiers.

• $att_i$ is the gain of the attenuator added on channel i to prevent saturation during high energy runs, i.e. over 50GeV/c.

• $gdpd_i$ is the inter-calibration factor between big diodes and small diodes for channel i.

The calibration procedure now goes as follow : each big diode channel is directly calibrated using the muon energy deposit and a fit to simulation, then inter-calibration of muon gain amplifier over beam gain amplifier is done using charge injection runs, eventually small diodes are inter-calibrated over big diodes using beam data.

The final conversion factors have a distribution peaked around 1MeV per bin for the big diode and 7MeV per bin for small diodes. The energy calibration resolution for each log is around 3% if one uses big diodes up to 2GeV and small diodes over 2GeV to avoid saturation and non-linearities.

### 4.2.3 Cuts

#### Tracking cuts

The beam is quite wide but is already cut by the scintillators, the smallest one measures $\sim 2cm \times 2.5cm$ according to figure 4.2. However, the beam entering the calorimeter covers the two central logs so that some particles go through the 1.5mm gap between them. The events concerned are very hard to reproduce by the simulation so that it's far better to remove them using tracker information, before the analysis.

What we need is to map at least the two central logs of the calorimeter in the tracker, in order to be able to select particles not going through gaps. The idea is to use the muon runs again as the position of the calorimeter was the same as for the data runs we are interested in. With muon runs, the two central CDEs are mapped using the correlation between the energy deposit and the position reported by each module of the tracker, as shown on figure 4.4. If the particle hit the log properly then the energy deposit is to be around 12MeV. On the upper left plot on figure 4.4 for instance, the energy is around 12MeV when the position is between $4cm$ and $4.6cm$ that defines the intersection of the beam, the smallest scintillator and the CsI log. Taking into account all the correlations, the two central logs are located in the vertical direction.

For $20GeV/c$ runs, the statistic is great so that a cut is applied to select only events that enter properly the third log of the first layer. For $10GeV/c$ runs, there are less events so that the cut is less restrictive and keeps events entering properly the third and the fourth logs, without the gap between both of course.

#### Cuts on minimum ionizing particles

The tertiary beams at 10 and $20GeV/c$ contain at least electrons, muons and pions, but maybe also anti-protons or other hadrons. For the calorimeter, all the minimum ionizing particles (MIPS) look like the same when they are of charge 1. As we cannot reproduce the unknown composition of the beam with the simulation, it's better to cut all the MIPS before the analysis in order to focus on hadronic cascades only.

All the MIPS let around 12MeV per layer, that is around 100MeV for the 8 layers of the calorimeter. The problem is that we need the cut to be efficient on beam data taken with the low gain amplifiers, remember that with these, even the big diode channels do not show the muon peaks. The idea is to use the muon runs again to adjust a cut on the total energy deposit in the calorimeter. The threshold on the total energy deposit has to be high enough to cut all the MIPS and to be efficient with small gain amplifiers, but not too high not to cut on too many hadronic cascades.

The right threshold is 200MeV of total energy deposit in the calorimeter. Simulations show that no MIPS can let more than 200MeV and the same number of MIPS is kept as the cut is applied on the energy sum processed from big diodes with muon gain amplifiers, or with small diodes for which the electronic gain is equivalent to the big diodes with low gain amplifiers. For the hadronic cascades study, all the minimum ionizing events will be removed by applying a threshold of $200MeV$ on

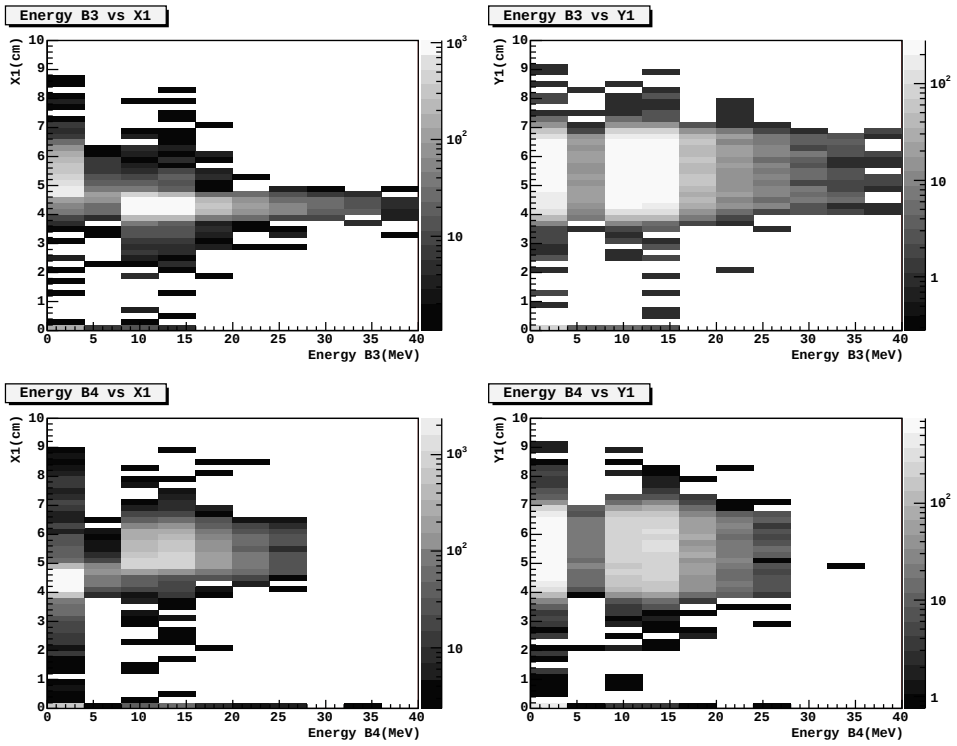


Figure 4.4: Energy deposit in logs 3 and 4 of the first layer as a function of the position given by T1 on both axis. For the log B3, the muon peak at 12MeV is located between $4cm$ and $4.6cm$ along X1 and between $4cm$ and $7cm$ along Y1. For the log B4, the muon peak at 12MeV is located between $4.8cm$ and $5.4cm$ along X1 and between $4cm$ and $7cm$ along Y1.

the calorimeter energy sum.

### Separating hadronic and electromagnetic showers

After the MIPS have been removed from the data, two categories of events are left : hadronic cascades and electromagnetic showers. Of course, the first step of the analysis is to separate them into two well defined sets of events. Electromagnetic showers are well known and well simulated, so that will use them as a reference to benchmark some features of our simulation before going on to a deep analysis of hadronic cascades.

One of the official method to reconstruct an electromagnetic shower energy consists in using the correlation between the energy deposit in the last layer and the total energy deposit in the calorimeter. Plotting this correlation for our $20GeV/c$ beam data gives figure 4.5 where one can see two distinct populations.

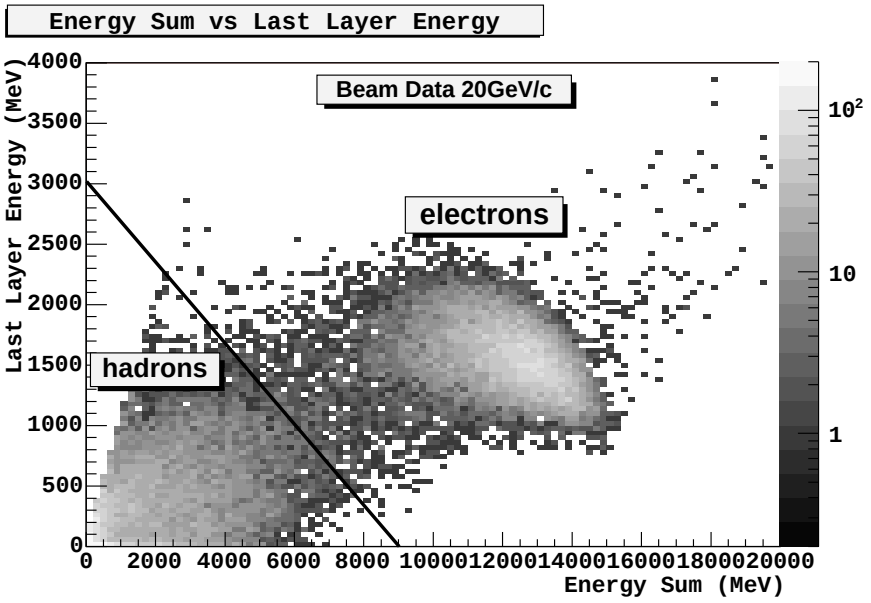


Figure 4.5: Total energy deposit in the calorimeter as a function of the energy deposit in the last layer. Hadronic cascades and electromagnetic shower are well separated.

Simulations of the same correlation for pions (figure 4.6) and electrons (figure 4.7) are used to confirm that high energy deposit events are electrons and low energy deposit events are hadronic cascades. We have also used simulations to optimize the cut, shown on figure 4.5, to separate hadrons and electrons, so as to remove as many electromagnetic showers as possible without removing too many hadronic cascades. However, it's interesting to notice that both populations are well separated so that the cut efficiency is high and stable when tuning parameters. We will refer to this cut using the last layer correlation as the LLC cut : LLC is true for electrons and false for hadrons.

Table 4.1 displays the efficiency of the cuts according to the simulation realized with monocinetic beams with different momenta and different particle types. Cuts efficiencies are high and are the same at $10GeV/c$ and $20GeV/c$.

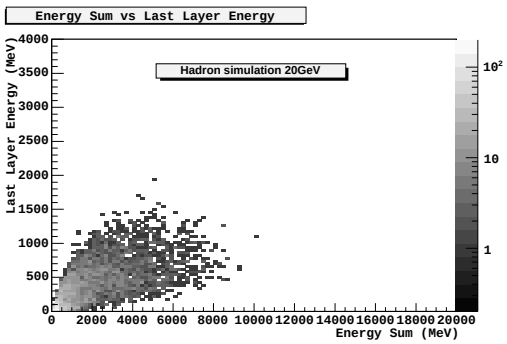


Figure 4.6: Total energy deposit in the calorimeter as a function of the energy deposit in the last layer : $20GeV/c$ hadrons.

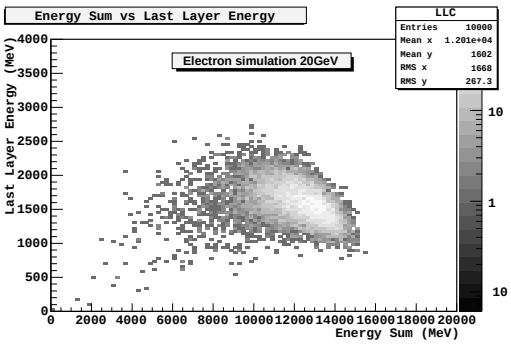


Figure 4.7: Total energy deposit in the calorimeter as a function of the energy deposit in the last layer : $20GeV/c$ $e^-$.

| name<br>cut | simulated<br>particle | MIPS<br>rejection | Cascade selection<br>hadronic | <br>electromagnetic |
|---|---|---|---|---|
| Etotal>200MeV | pion | 100% | 72% | none |
| not LLC | pion | 0% | 99.5% | none |
| LLC | electron | none | none | 99.5% |

Table 4.1: Summary of the cuts applied on CERN beam test data, and their efficiency

## 4.3 Simulations

The GEANT4 simulation calls the LHEP model which is somewhat the only one available in this energy range. The geometry takes account for : the tracker, simulated by a silicon plane $0.04X_0$ thick[†], a lead plate $1.5X_0$ thick and a calorimeter built with 11 layers of 6 horizontal CDEs. The last three layers are simulated because of possible back-splash effects, but actually none has been observed for these energies. Moreover, the length between layers is 15mm and the gap between logs within a layer is $1.5mm$. The thickness of the lead plate and the gap length have been adjusted using electromagnetic showers data, as we expect their longitudinal profile to be reproduced by the simulation within a few percents, as shown on figure 4.8.

The beam profile is Gaussian as suggest the profile shown in the tracker, and cuts to select only events entering the calorimeter properly by one log are applied as for the data. Choosing a particle type is more problematic as we do not really know their nature in data. Actually, the fact is that we are interested in benchmarking proton simulation as GLAST will be mostly hit by protons. Moreover, simulations show that pions and protons give the same results in our calorimeter, the main change is for the inelastic interaction cross section but we do not care. So we will simulate hadronic cascades from $10GeV/c$ and $20GeV/c$ pions.

[†]X0 is the radiation length, 1.85cm in CsI, about the thickness of a CDE.

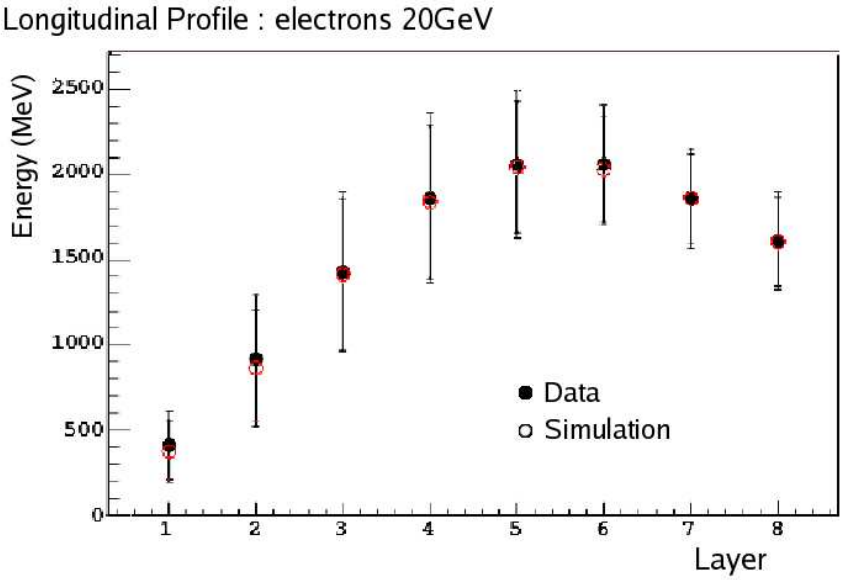


Figure 4.8: Mean energy longitudinal profile of electromagnetic showers at $20GeV/c$ : comparison between data and simulation. Error bars show the width of the energy deposit per layer distributions.

## 4.4 Electrons versus hadrons at $20GeV/c$

The very first interesting study is to compare electromagnetic showers and hadronic cascades at $20GeV/c$ in our calorimeter.

Figure 4.9 displays the energy deposit per layer, for hadronic cascades (dashed line) and electromagnetic showers (plain line). The first bin peak has been knowingly cut for the display, and corresponds to the hadrons that have not yet generated a nuclear interaction. It's interesting to notice that this peak is getting smaller and smaller as particles goes deeper in the calorimeter. Besides, electromagnetic showers globally develop earlier in the calorimeter and have their maximum energy deposit in the $6^{th}$ layer.

For $20GeV/c$ events, a log is said to be hit when its energy is greater than $50MeV$ and the thresholds has been lowered to $30MeV$ for $10GeV/c$ events. When a log is hit, its energy is summed into the layer energy deposit. Figure 4.10 presents the distribution of the number of logs hit per layer, for hadronic cascades (dashed line) and electromagnetic showers (plain line). On this plot, electromagnetic showers show a higher number of logs hit than hadronic showers but with much less dispersion. The number of hadrons hitting one log only, decreases layer after layer as nuclear reactions happen.

Figure 4.11 displays the total energy deposit and the total number of logs hit (total multiplicity) for the whole calorimeter for hadronic cascades (dashed line) and electromagnetic showers (plain line). What is most striking is that hadrons and electrons with the same impulsion have very different total energy deposits and multiplicities : electromagnetic showers develop more rapidly and leave a lot of

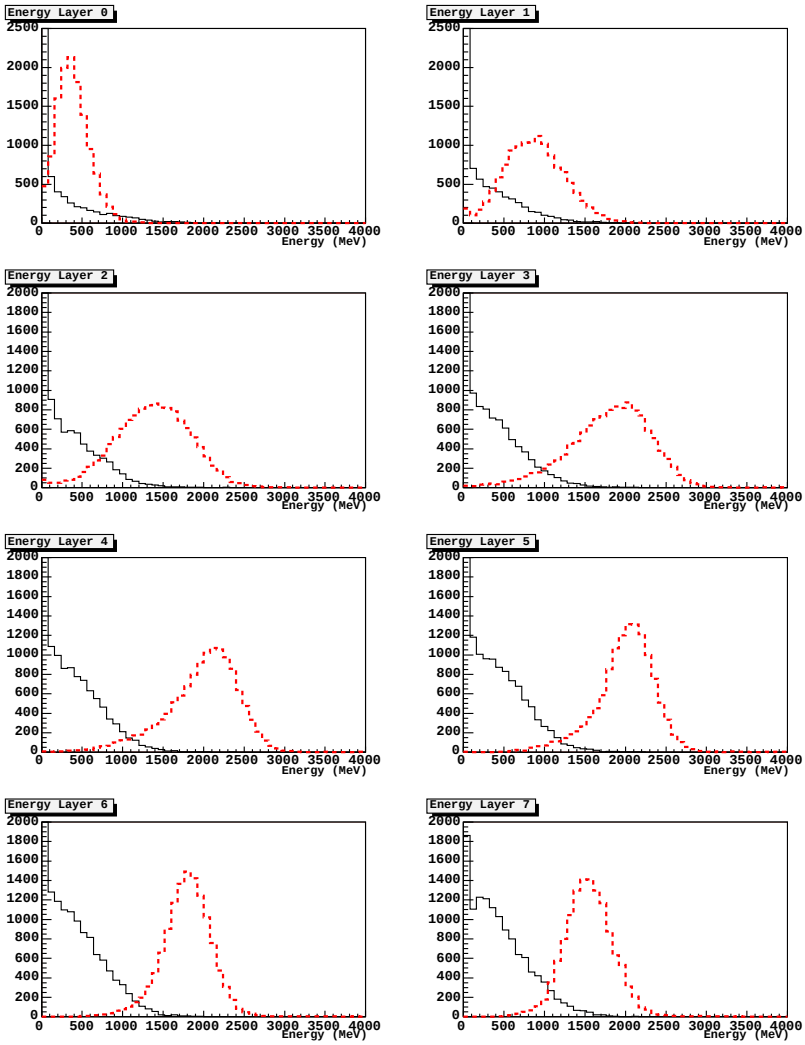


Figure 4.9: $20GeV/c$ beam data. Energy deposit per layer, for hadronic cascades (dashed line) and electromagnetic showers (plain line).

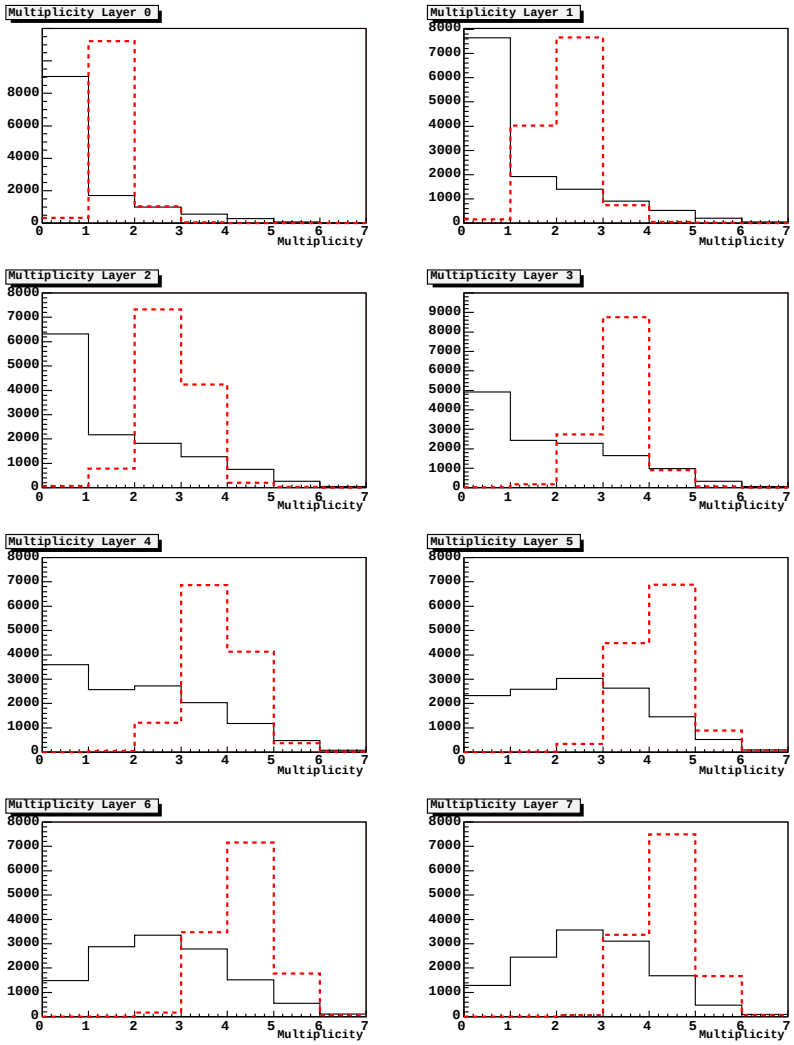


Figure 4.10: 20$GeV/c$ beam data. Number of logs hit per layer, for hadronic cascades (dashed line) and electromagnetic showers (plain line).

energy compared to hadronic cascades. However, it's as easy to check with simulations that $20GeV/c$ hadronic cascades leave about the same energy as a $5GeV/c$ electromagnetic shower.

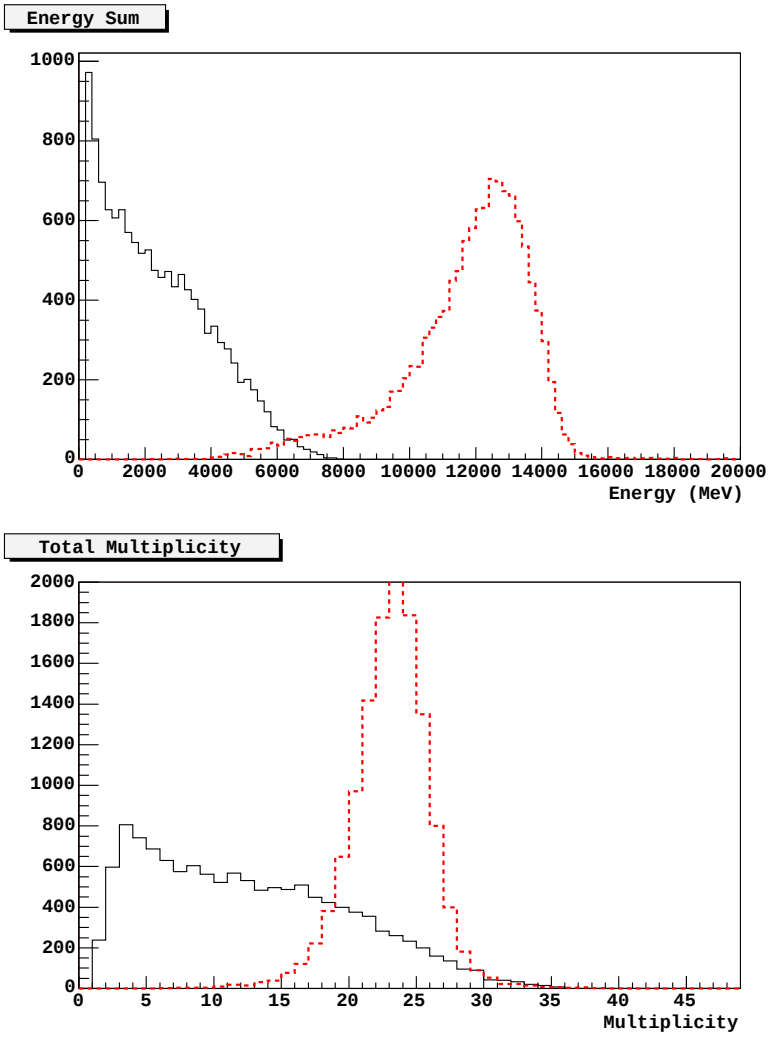


Figure 4.11: $20GeV/c$ beam data. Total energy deposit and total multiplicity for hadronic cascades (dashed line) and electromagnetic showers (plain line).

Figure 4.12 displays the results from the longitudinal energy profile fitting by a $\Gamma$ function as described in section 1.2.2. The upper plot shows the reconstructed energy : the distribution is quite thin and peaked around $20GeV$ for electromagnetic cascades (plain line), but is broad and peaked around $5GeV$ for hadronic cascades (dashed line). The middle plot shows the reconstructed starting point of the shower : again, the distribution for electrons is peaked around 0 and the distribution for hadrons has a strong dispersion. The lower plot shows the fit $\chi^2$ distributions : the distribution is narrower and closer to 0 for electromagnetic showers than for hadronic cascades, however, the overlap between both distributions is quite broad. Actually, many hadronic cascades really look like electromagnetic showers of another energy

and their identification as part of the background will be hard to achieve.

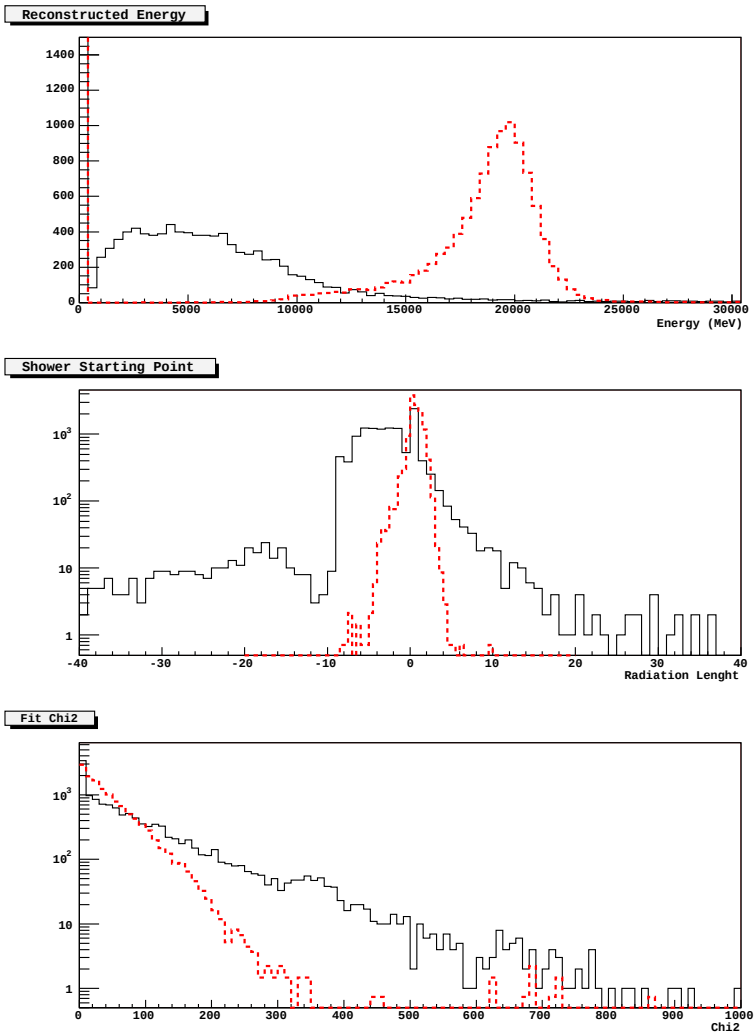


Figure 4.12: $20GeV/c$ beam data. Results from the longitudinal energy profile fitting by a $\Gamma$ function for hadronic cascades (dashed line) and electromagnetic showers (plain line).

## 4.5 $20GeV/c$ pions hadronic cascades

$20GeV/c$ data will be presented first, as the statistic is greater than for $10GeV/c$ data, it's easier to see and understand the distribution properties. The comparisons between data and the LHEP simulation are lead the same way as it has been done for the GSI data. Table 4.2 reports the values of the first two moments (mean and RMS) of all the simulated and real distributions for $20GeV/c$ incident particles. Only histograms of data and simulated pions hadronic cascades will be shown in the following, however table 4.2 also show the values for simulated proton induced hadronic cascades to demonstrate that results do not depend upon the bullet choice for our variables.

| **Mean** of distributions for data and the LHEP model | | | | | | | |
|---|---|---|---|---|---|---|---|
| Variables | $E_{layer}$ | $M_{layer}$ | $E_{Sum}$ | $M_{Sum}$ | $E_{Max}$ | $J_{Emax}$ | $RMS$ |
| unit | $MeV$ | logs | $MeV$ | logs | $MeV$ | logs | $MeV$ |
| data | 333 | 1.7 | 2404 | 12.1 | 786 | 4.7 | 258 |
| pions | 318 | 1.8 | 2237 | 12.4 | 630 | 5.2 | 205 |
| $\Delta_{pion}$ | -15 | 0.1 | -167 | 0.3 | -156 | 0.5 | -53 |
| proton | 304 | 1.6 | 2109 | 12.0 | 589 | 5.1 | 191 |
| $\Delta_{proton}$ | -29 | -0.1 | -295 | -0.1 | -197 | 0.4 | -67 |
| **RMS** of distributions for data and the LHEP model | | | | | | | |
| Variables | $E_{layer}$ | $M_{layer}$ | $E_{Sum}$ | $M_{Sum}$ | $E_{Max}$ | $J_{Emax}$ | $RMS$ |
| unit | $MeV$ | logs | $MeV$ | logs | $MeV$ | logs | $MeV$ |
| data | 352 | 1.5 | 1614 | 7.4 | 416 | 2.3 | 138 |
| pion | 310 | 1.4 | 1604 | 7.8 | 334 | 2.0 | 113 |
| $\Delta_{pion}$ | -42 | -0.1 | -10 | 0.4 | -82 | -0.3 | -25 |
| proton | 309 | 1.5 | 1626 | 7.9 | 327 | 2.0 | 109 |
| $\Delta_{proton}$ | -43 | -0.1 | 12 | 0.4 | -89 | -0.3 | -29 |

Table 4.2: $20GeV/c$ CERN data. Differences between the first two moments of both the real and simulated distributions : for a variable $X$, $\Delta_{pion} = X_{pion} - X_{data}$ et $\Delta_{proton} = X_{proton} - X_{data}$.

### Energy deposit and hit multiplicity per layer

Figures 4.13 and 4.14 show the energy deposit and hit multiplicity per layer for data (plain line) and LHEP simulation (dashed line). The global shape of the distributions ( and the main parameters (mean, RMS) ) are quite well reproduced by the simulation, for both the energy deposit and the multiplicity. According to table 4.2, the difference on the mean of the simulated and real distributions is only around $15MeV$ on $300MeV$. The difference on the RMS reaches $40MeV$, what is a consequence of a lack of a few high energy events ($E_{Layer} > 1500MeV$) in association with a slight excess of low energy events ($E_{Layer} < 200MeV$) in the simulation.

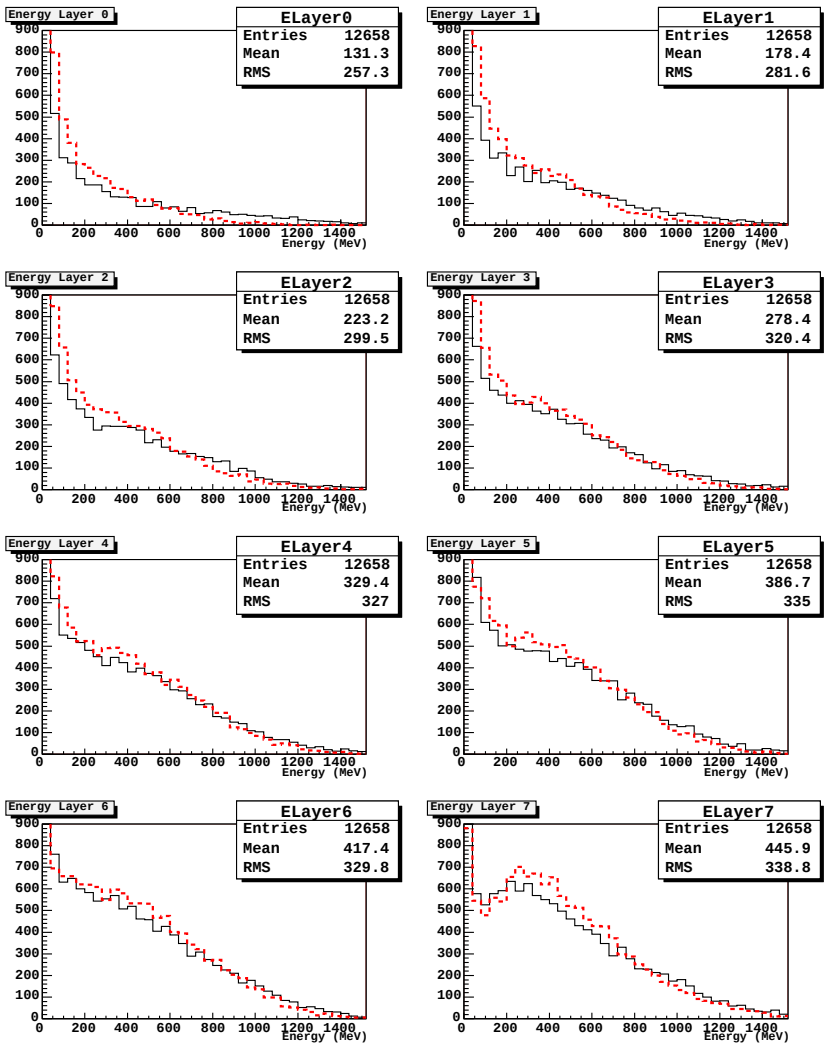


Figure 4.13: $20 GeV/c$ hadrons. Hadronic cascades energy deposit per layer for data (plain line) and LHEP simulation (dashed line).

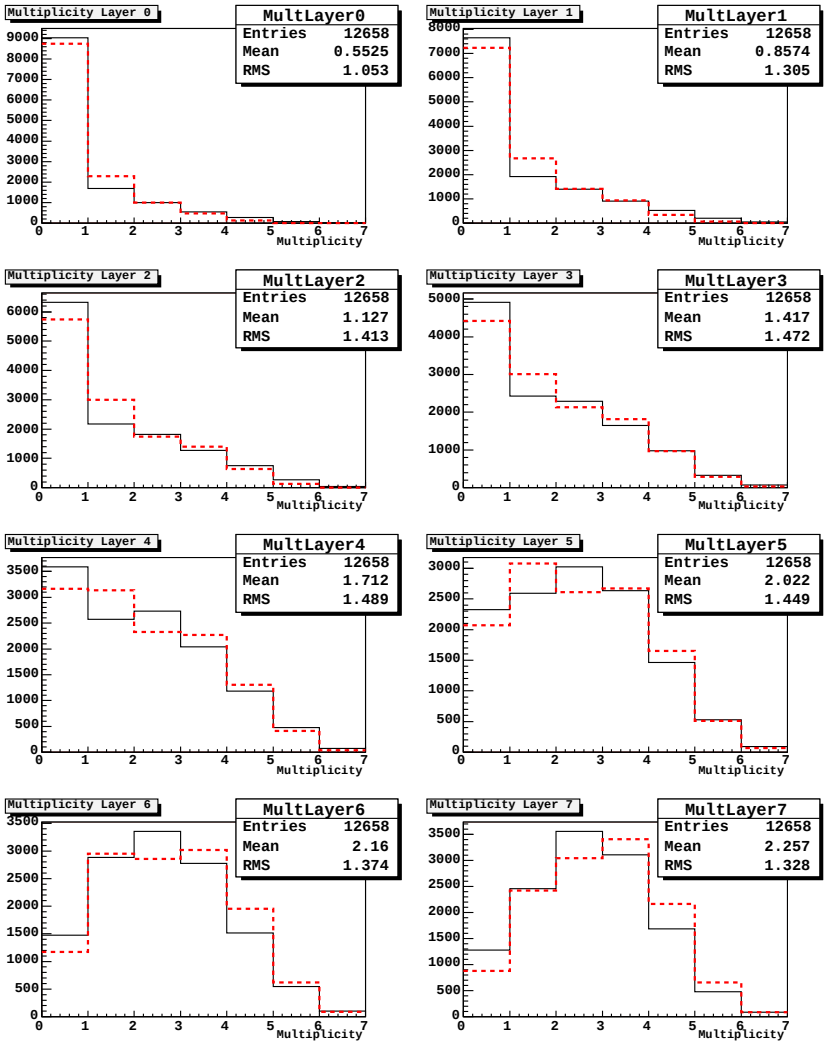


Figure 4.14: $20 GeV/c$ hadrons. Multiplicity per layer of hadronic cascades for data (plain line) and LHEP simulation (dashed line).

### Energy sum and total hit multiplicity

Figure 4.15 presents the calorimeter energy sum and the total hit multiplicity for data and the LHEP model. The agreement between data and simulation is good for the full energy and multiplicity ranges. In particular, no lack of high energy or high multiplicity events shows up. In details, for three bins around $E_{Sum} \sim 500MeV$, there are less event in the data than in the simulation, the difference reaching about 25%. This slight discrepancy has no consequence on the very good agreement over the mean and RMS of the distributions shown on table 4.2.

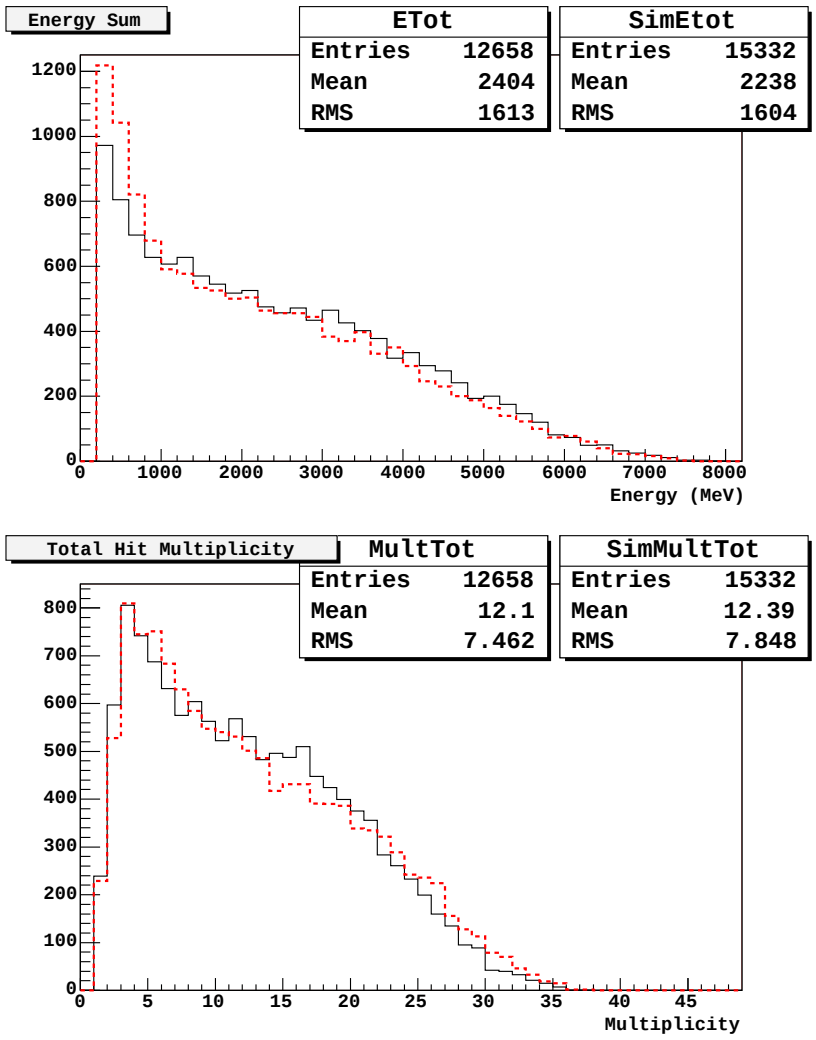


Figure 4.15: $20GeV/c$ hadrons. Total energy deposit and total multiplicity of hadronic cascades for data (plain line) and LHEP simulation (dashed line).

### $\Gamma$ profile fitting

Comparisons for the profile fitting variables are more surprising at first sight though, as shown on figure 4.16. Both the reconstructed energy and the shower starting point

distributions are well reproduced by the simulation as they present the same shape and features, meanwhile the $\chi^2$ distributions are obviously different. The simulated and real $\chi^2$ distributions have the same (and expected) exponential shape but with two different slopes, the slope from the simulation being steeper.

Looking into a couple of those low $\chi^2$ events, I could found a significant difference on the energy of the longitudinal profile maximum. Actually, this discrepancy exists for all kind of events, as shown on figure 4.17, the mean and RMS of the simulated distribution of the energy profile maximum are 20% smaller than in the data. To go further, one need to notice that here the reconstruction $\chi^2$ is a measure of dispersion on the energy deposit per layer. Then, comparing the distribution of raw longitudinal energy profile RMS presented on figure 4.18, shows that the dispersion is greater for data than for simulations. This would not be surprising if the same plot done for electromagnetic showers does not show such a discrepancy (the agreement is better than 5%) , so that we can deduce that the observation is a feature of hadronic cascades only and not of the whole experiment. The idea is finally to calculate again the energy profile RMS without taking account for the layer with the maximum energy as displayed on figure 4.19. The agreement between real and simulated RMS distributions is then really good.

The conclusion is that the energy profile maximum of hadronic cascades is not well reproduced by the simulation and a consequence is that the reconstruction $\chi^2$ is smaller in the simulation than in the data. Besides, one can infer that central collisions with a very high energy deposit in one layer are specifically not well simulated, and that's probably why there is a lack of events at high energy deposit per layer in the simulation.

From a global point of view, the LHEP simulation reproduces well the shape of our variables for $20GeV/c$ hadronic cascades. The energy profile maximum is underestimated by more than 20% and a direct consequence is that the $\chi^2$ of the profile fitting reconstruction is also underestimated as the exponential distribution is steeper with nearly a factor of 2 on the slope. However, this feature does not appear to be an issue as far as rejection algorithms are concerned : if algorithms are efficient on simulations they have to be at least as efficient on real data with a greater dispersion.

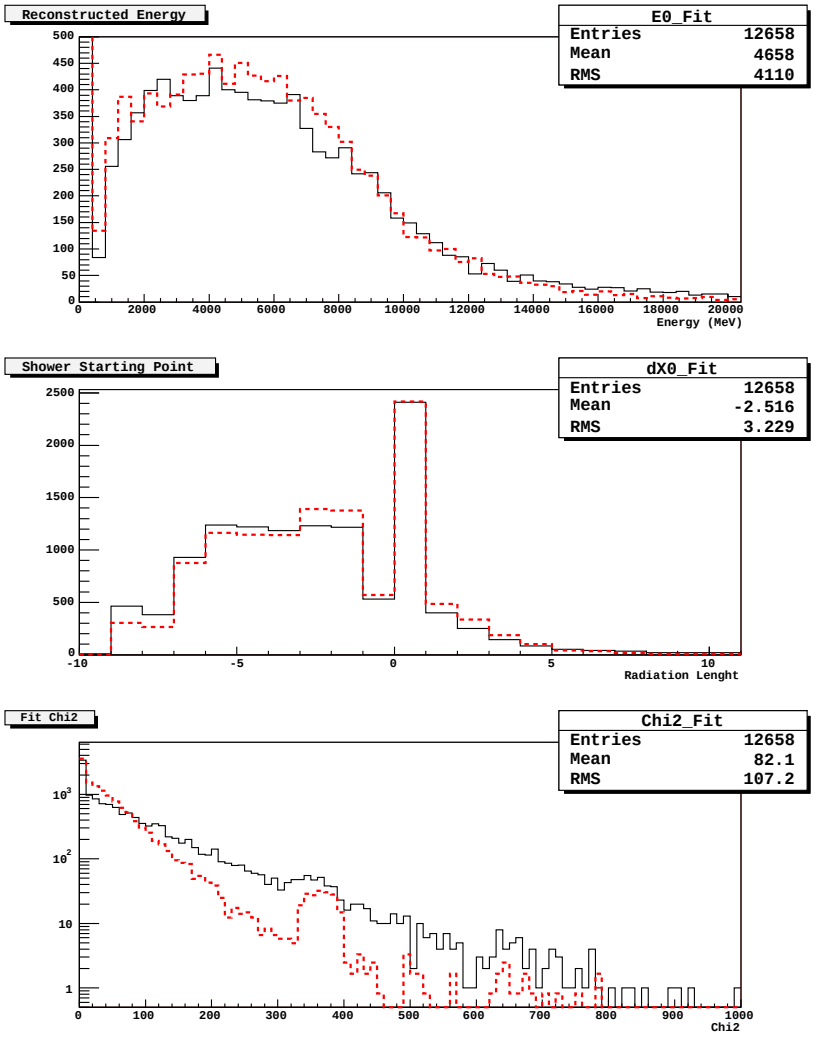


Figure 4.16: $20GeV/c$ hadrons. Results from the longitudinal energy profile fitting by a $\Gamma$ function of hadronic cascades for data (plain line) and simulation (dashed line).

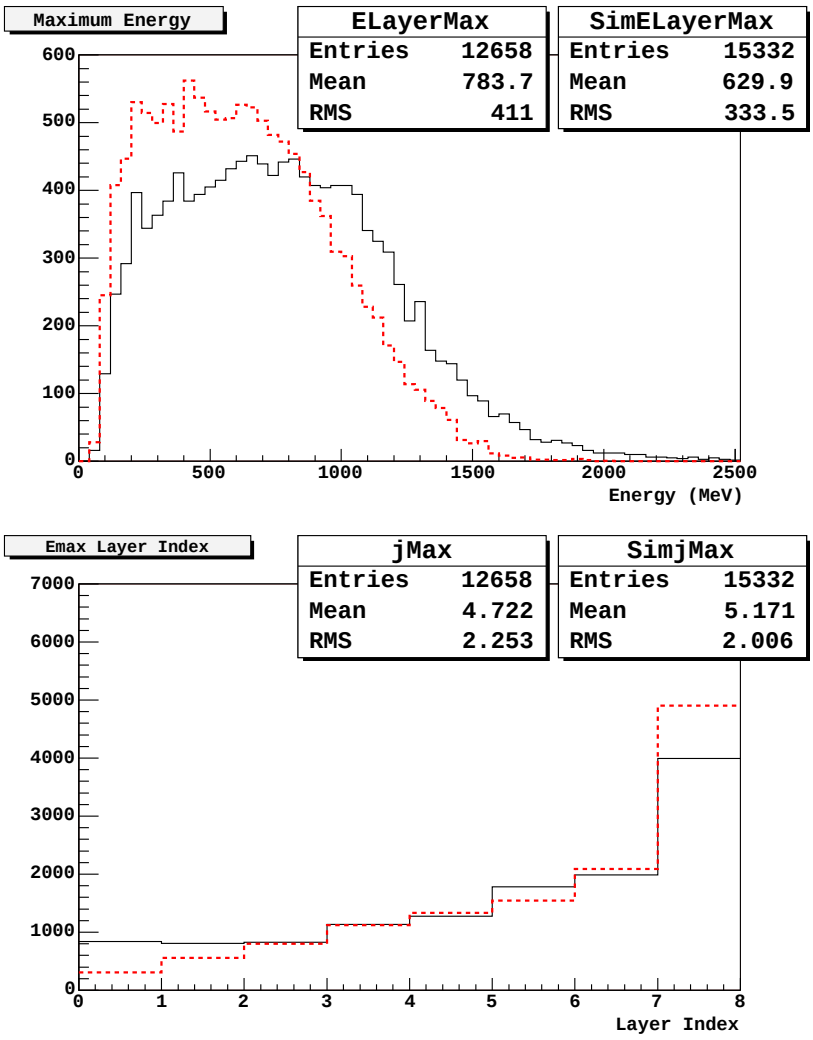


Figure 4.17: $20 GeV/c$ hadrons. Energy profile maximum and index of the layer with this maximum of hadronic cascades for data (plain line) and simulation (dashed line).

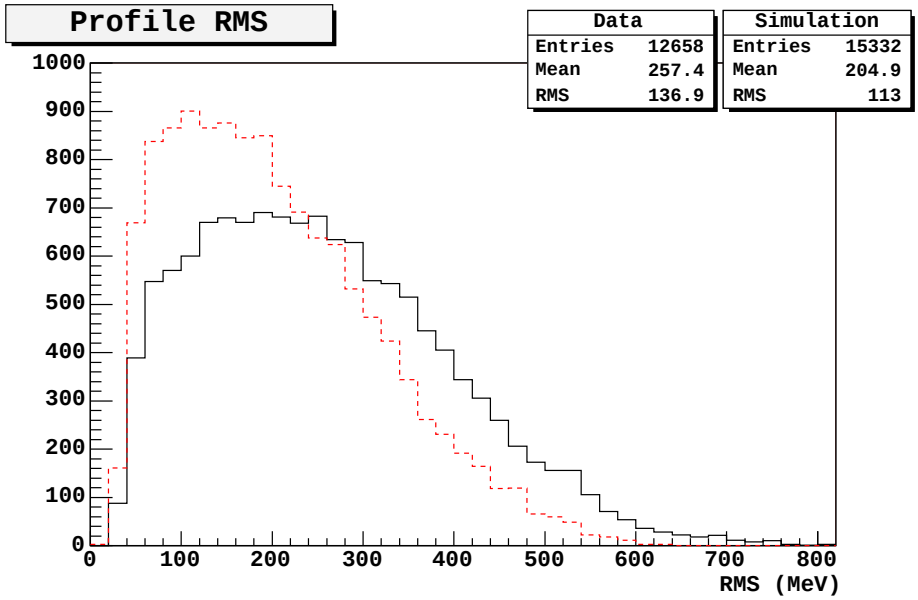


Figure 4.18: $20GeV/c$ hadrons. RMS of the energy profile of hadronic cascades for data (plain line) and simulation (dashed line). RMS from the simulations are smaller than data RMS.

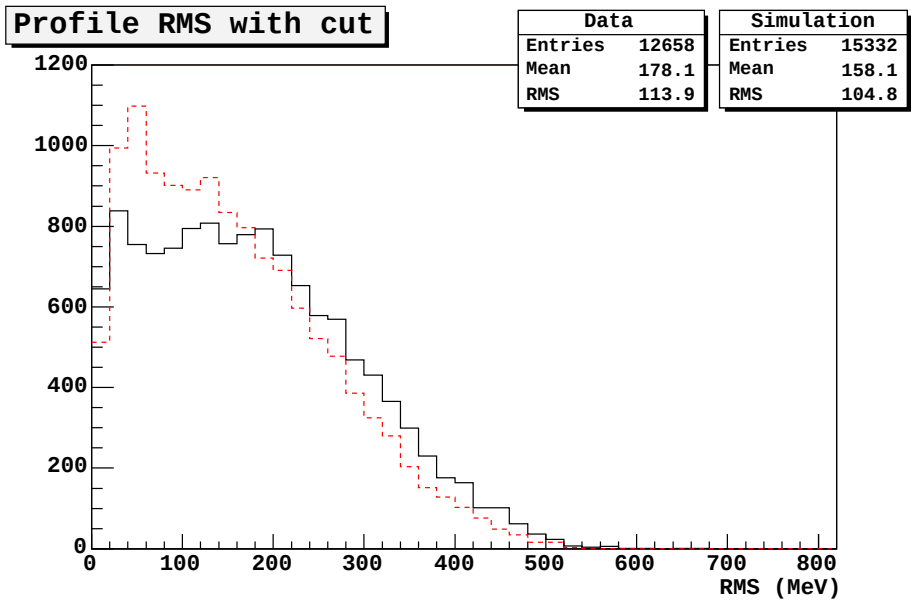


Figure 4.19: $20GeV/c$ hadrons. RMS of the energy profile removing the energy profile maximum for data (plain line) and simulation (dashed line). The agreement is far better now between data and simulation.

## 4.6 $10GeV/c$ pions hadronic cascades

For $10GeV/c$ hadronic cascades, the threshold per log has been lowered down to $30MeV$ in order to obtain a slightly better agreement on electromagnetic showers. Moreover, our statistic is unfortunately down by a factor of three with respect to $20GeV/c$ data, despite looser cuts on the particle position in the tracker.

Table 4.3 reports the values of the first two moments (mean and RMS) of all the simulated and real distributions for $10GeV/c$ incident particles. Only histograms of data and simulated pions hadronic cascades will be shown in the following, however table 4.2 also show the values for simulated antiproton induced hadronic cascades to demonstrate that a possible contamination of the beam by antiprotons is not an issue.

| **Mean** of distributions for data and the LHEP model | | | | | | | |
|---|---|---|---|---|---|---|---|
| Variables | $E_{layer}$ | $M_{layer}$ | $E_{Sum}$ | $M_{Sum}$ | $E_{Max}$ | $J_{Emax}$ | $RMS$ |
| unit | $MeV$ | logs | $MeV$ | logs | $MeV$ | logs | $MeV$ |
| data | 228 | 1.7 | 1606 | 12.2 | 572 | 4.1 | 186 |
| pion | 185 | 1.9 | 1294 | 12.8 | 382 | 4.7 | 125 |
| $\Delta_{pion}$ | -43 | 0.2 | -312 | 0.6 | -190 | 0.6 | -61 |
| antiproton | 193 | 1.9 | 1337 | 13.2 | 404 | 4.6 | 132 |
| $\Delta_{antiproton}$ | -35 | 0.2 | -269 | 1.0 | -167 | 0.5 | -54 |
| **RMS** of distributions for data and the LHEP model | | | | | | | |
| Variables | $E_{layer}$ | $M_{layer}$ | $E_{Sum}$ | $M_{Sum}$ | $E_{Max}$ | $J_{Emax}$ | $RMS$ |
| unit | $MeV$ | logs | $MeV$ | logs | $MeV$ | logs | $MeV$ |
| data | 241 | 1.4 | 900 | 6.2 | 311 | 2.4 | 101 |
| pion | 175 | 1.5 | 818 | 7.1 | 182 | 2.2 | 61 |
| $\Delta_{pion}$ | -66 | 0.1 | -82 | 0.9 | -129 | -0.2 | -40 |
| antiproton | 184 | 1.5 | 843 | 7.2 | 200 | 2.2 | 64 |
| $\Delta_{antiproton}$ | -57 | 0.1 | -57 | 1.0 | -111 | -0.2 | -37 |

Table 4.3: $10GeV/c$ CERN data. Differences between the first two moments of both the real and simulated distributions : for a variable $X$, $\Delta_{pion} = X_{pion} - X_{data}$ et $\Delta_{antiproton} = X_{antiproton} - X_{data}$.

The agreement between data and simulation for the energy deposit and the multiplicity per layer displayed on figures 4.20 and 4.21 is quite good with only a slight lack of high energy deposit event in the simulation. However, the agreement is not as good as it was at $20GeV/c$ and this shows up again when comparing the total energy deposit and the total multiplicity as presented on figure 4.22. On this figure, one can also notice that some electrons probably survived the cuts for $E_{Sum} \sim 2200MeV$ and $M_{Sum} \sim 17$.

For the reconstruction, see figure 4.24, both the energy and the shower starting point are well reproduced and the discrepancy on the $\chi^2$ distribution has the same origin as the one noticed at $20GeV/c$. The maximum energy deposit distribution, shown on figure 4.23, is not reproduced by the simulation very well with a

discrepancy reaching 40% on the first two moments.

From a global point of view, the study at $10GeV/c$ confirms what has been seen at $20GeV/c$, the agreement being a little worse though. However it's difficult to really conclude definitely as the statistic is low and so are the energy deposit in the calorimeter what is another cause of errors.

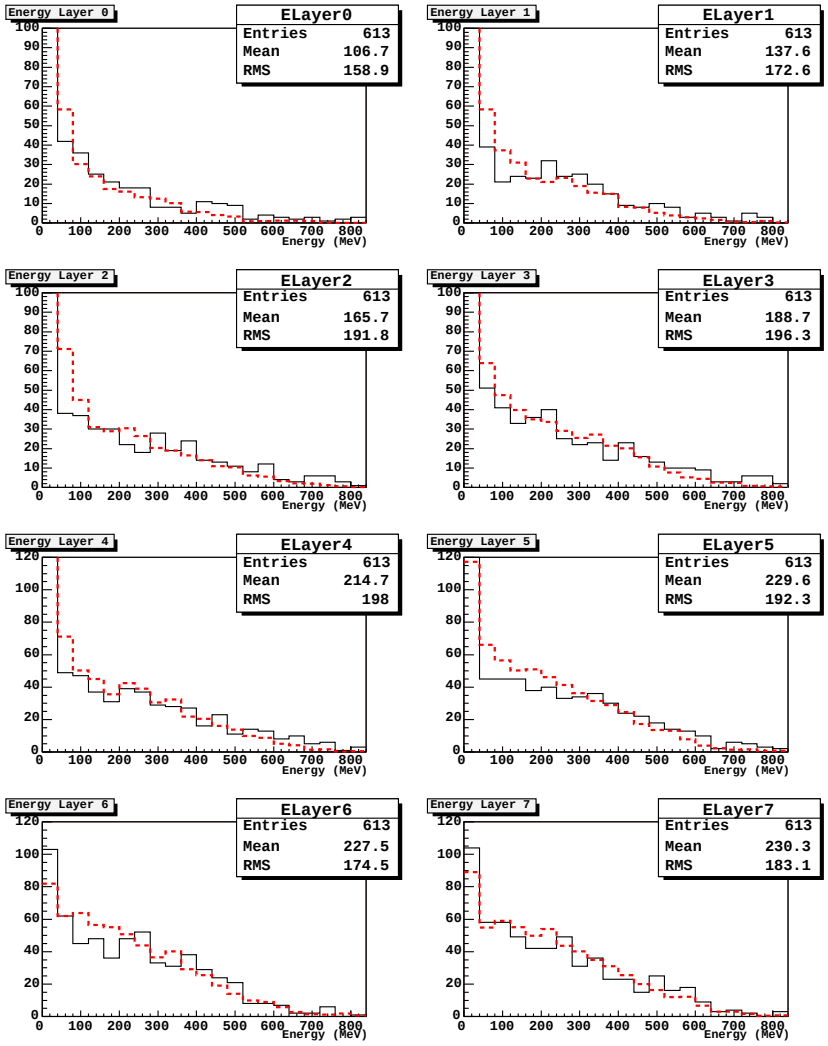


Figure 4.20: $10GeV/c$ hadrons. Energy deposit per layer of hadronic cascades for data (plain line) and LHEP simulation (dashed line).

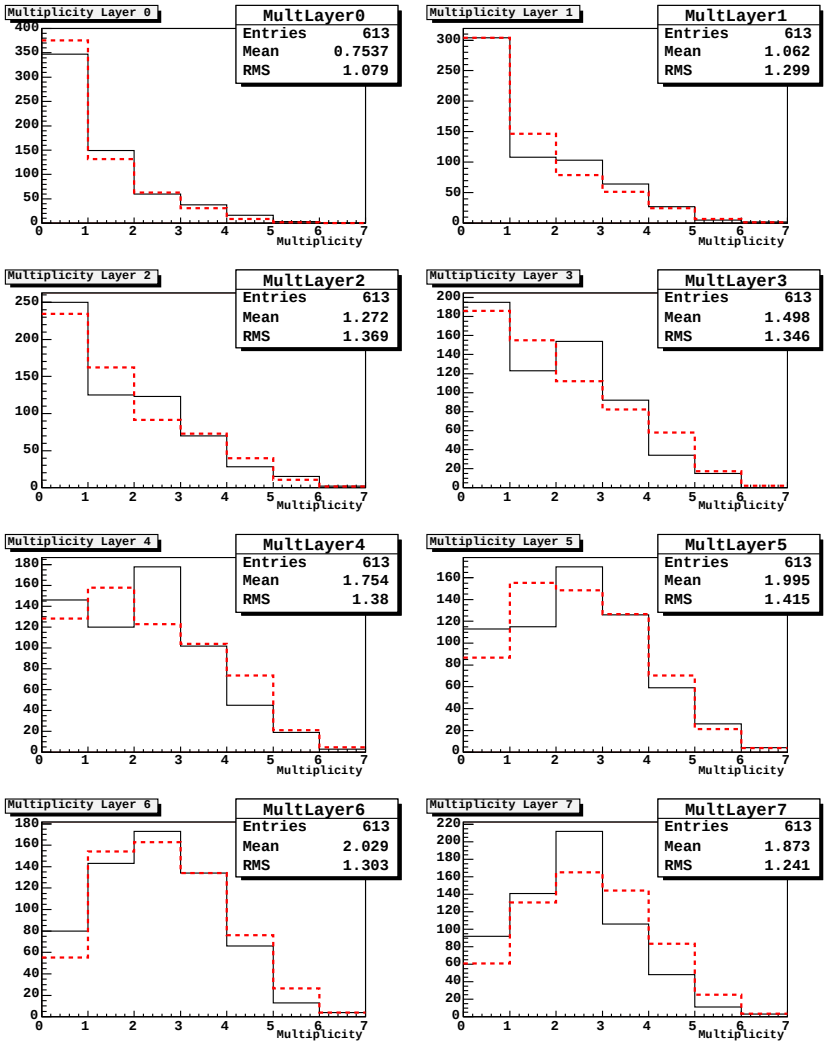


Figure 4.21: $10 GeV/c$ hadrons. Multiplicity per layer of hadronic cascades for data (plain line) and LHEP simulation (dashed line).

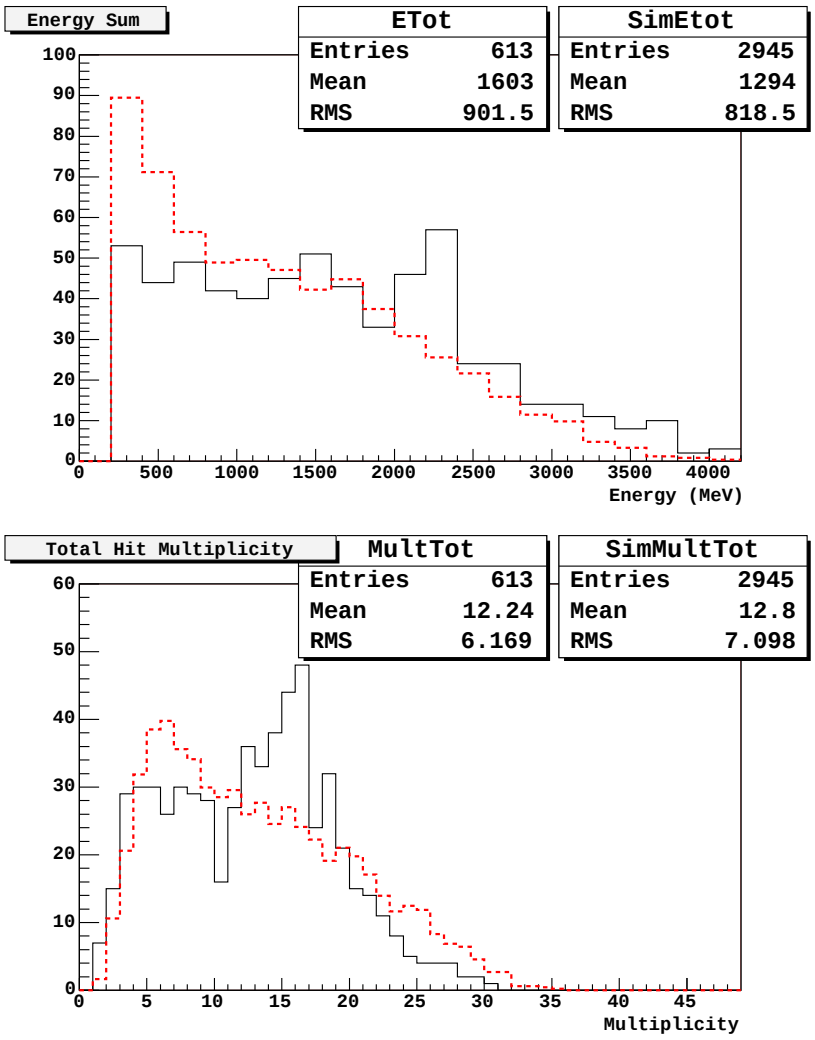


Figure 4.22: $10GeV/c$ hadrons. Total energy deposit and total multiplicity of hadronic cascades for data (plain line) and LHEP simulation (dashed line).

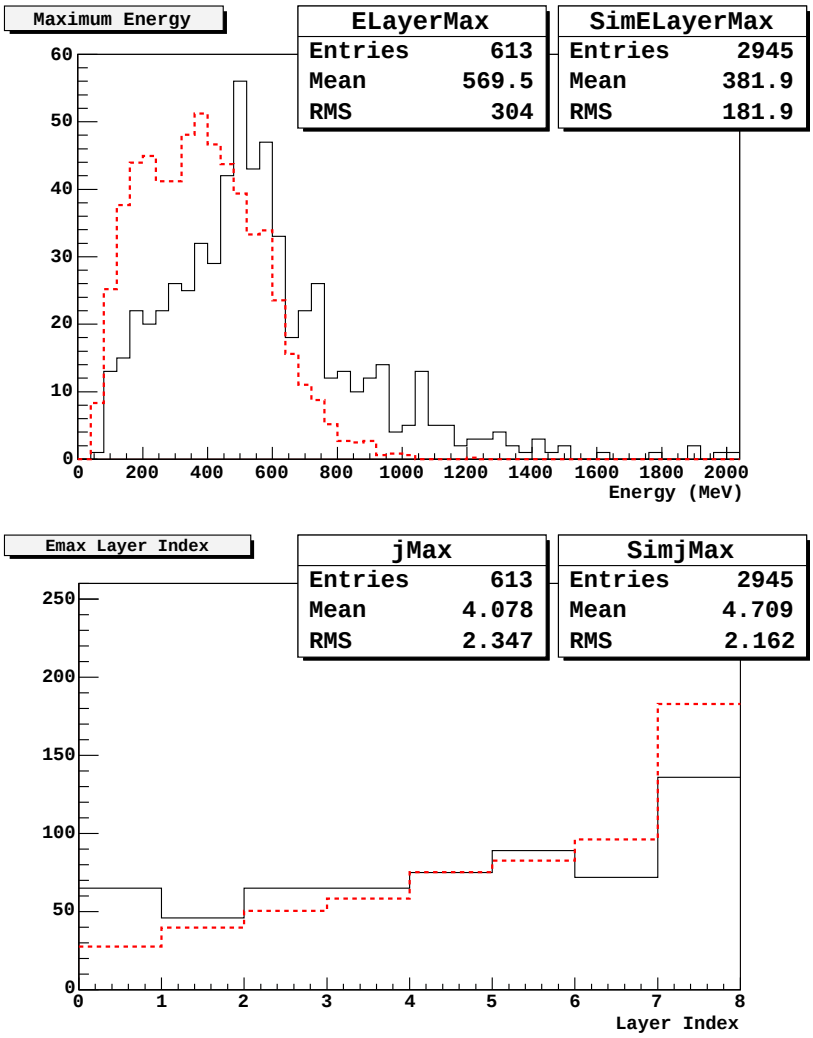


Figure 4.23: $10 GeV/c$ hadrons. Energy profile maximum and index of the layer with this maximum of hadronic cascades for data (plain line) and LHEP simulation (dashed line).

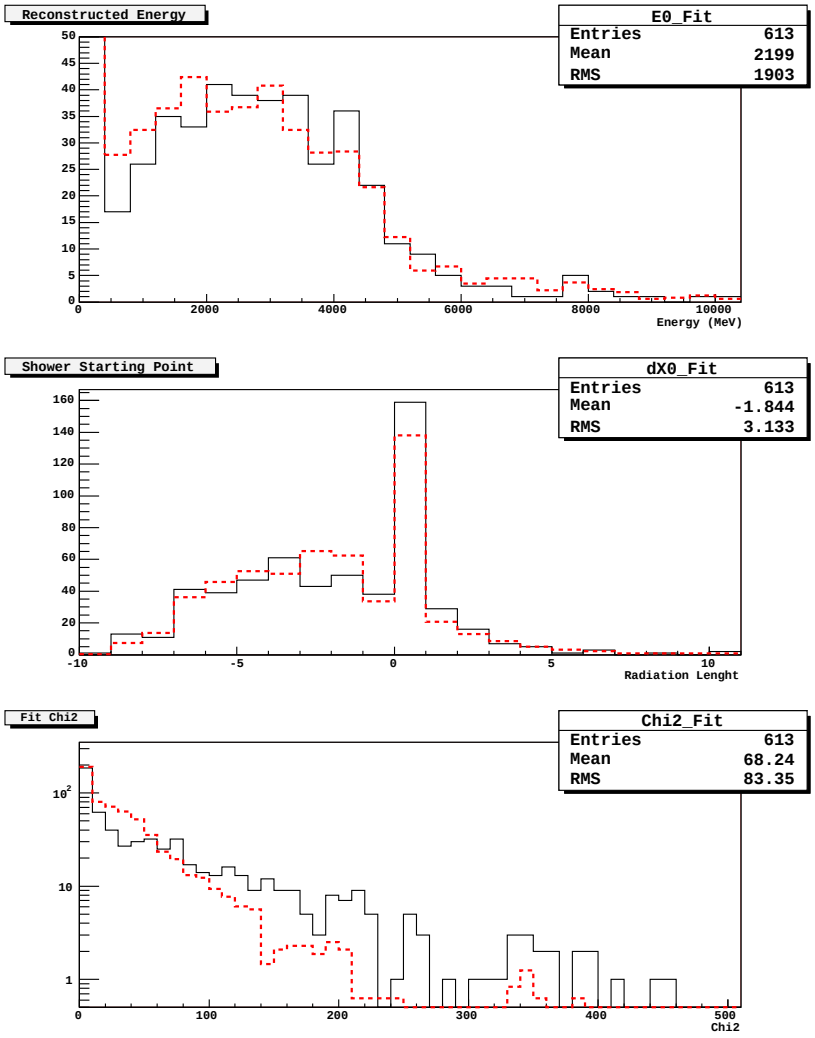


Figure 4.24: $10GeV/c$ hadrons. Results from the longitudinal energy profile fitting by a $\Gamma$ function of hadronic cascades for data (plain line) and LHEP simulation (dashed line).

# Conclusion

Hadronic background rejection algorithms are developed and tuned over Monte-Carlo simulations based on Geant4. Different hadronic cascade models are available within Geant4, the default one being LHEP coming from the GHEISHA code. We have benchmarked the different hadronic cascade models at different energies over data from GSI and CERN beam tests.

At low energy, comparisons with 1.7GeV protons and 3.4GeV deuterons from GSI show a good agreement between data and simulations for the energy deposit and the multiplicity per layer for both the LHEP and the Bertini models. On the opposite, the calorimeter energy sum distribution is not well reproduced by the simulations that present a lack of low energy deposit events ($E_{Tot} < 200MeV$). The Binary Cascade model shows a very strange feature, with low energy deposits corresponding to high multiplicities, not seen in the data. This feature rules out the Binary Cascade model, at least with respect to the default LHEP model. The Bertini model presents less important discrepancies with the data than the LHEP model : the lack of low energy events is less dramatic but is important though. The main conclusion from the low energy study is that the Bertini intra-nuclear cascade model should be used instead of LHEP to generate the sets of events dedicated to hadronic background rejection.

At high energy, comparisons with 10GeV/c and 20GeV/c hadrons from CERN show a good agreement between data and simulation for almost all the studied variables for the LHEP model. QGS based models do not show a far better agreement and are known to require longer processing time so that it's not recommended to use them. The only discrepancy observed concerns the dispersion on energy deposits that has a consequence on the $\chi^2$ of the profile fitting reconstruction. But, this discrepancy is small and should not have bad effects on the development of rejection algorithms. Actually, at high energy, the LHEP model give satisfying results and should still be used for hadronic cascade simulations.

# Appendix

# A High energy models

## A.1 QGSC model : comparisons for 20GeV/c pions

The QGSC model seems to provide a little bit more energy to nuclear reactions than the other tested models. A consequence is that, as shown on table A.1, all the distributions are slightly better reproduced by the QGSC model compared to the LHEP model.

| **Mean** of distributions for data and the LHEP and QGSC models | | | | | | | |
|---|---|---|---|---|---|---|---|
| Variables | $E_{layer}$ | $M_{layer}$ | $E_{Sum}$ | $M_{Sum}$ | $E_{Max}$ | $J_{Emax}$ | $RMS$ |
| unit | $MeV$ | logs | $MeV$ | logs | $MeV$ | logs | $MeV$ |
| data | 332 | 1.7 | 2404 | 12.1 | 785 | 4.7 | 258 |
| LHEP | 318 | 1.8 | 2237 | 12.4 | 629 | 5.2 | 204 |
| $\Delta_{LHEP}$ | -14 | 0.1 | -167 | 0.3 | -156 | 0.5 | -53 |
| QGSC | 344 | 1.8 | 2489 | 13.0 | 738 | 5.0 | 236 |
| $\Delta_{QGSC}$ | 12 | 0.1 | -85 | 0.9 | -47 | 0.3 | -22 |

| **RMS** of distributions for data and the LHEP and QGSC models | | | | | | | |
|---|---|---|---|---|---|---|---|
| Variables | $E_{layer}$ | $M_{layer}$ | $E_{Sum}$ | $M_{Sum}$ | $E_{Max}$ | $J_{Emax}$ | $RMS$ |
| unit | $MeV$ | logs | $MeV$ | logs | $MeV$ | logs | $MeV$ |
| data | 352 | 1.5 | 1614 | 7.4 | 415 | 2.3 | 137 |
| LHEP | 310 | 1.4 | 1604 | 7.8 | 333 | 2.0 | 113 |
| $\Delta_{LHEP}$ | -42 | -0.1 | -10 | 0.4 | -82 | -0.3 | -24 |
| QGSC | 339 | 1.4 | 1702 | 8.1 | 363.0 | 2.1 | 121 |
| $\Delta_{QGSC}$ | -13 | -0.1 | 88 | 0.7 | -52 | -0.2 | -16 |

Table A.1: $20GeV/c$ CERN data. Differences between the first two moments of both the real and simulated distributions : for a variable $X$, $\Delta_{LHEP} = X_{LHEP} - X_{data}$ et $\Delta_{QGSC} = X_{QGSC} - X_{data}$. Particles used in simulations are pions.

On figures A.1 to A.5, data are in plain lines, results from the LHEP model in dashed lines and results from the QGSC model in dotted lines. The energy sum distribution shown on figure A.3 and the energy profile maximum on figure A.4 are very well reproduced by the QGSC model and are probably the most convincing plots. However, the improvement proposed by the QGSC model is not that great that it succeeds in reproducing the slope of the profile fitting $\chi^2$ distribution, shown on figure A.5. The use of the QGSC model is consequently not really required for the GlastRelease purpose. Moreover the computation time is increased by 45% comparing to the default LHEP model.

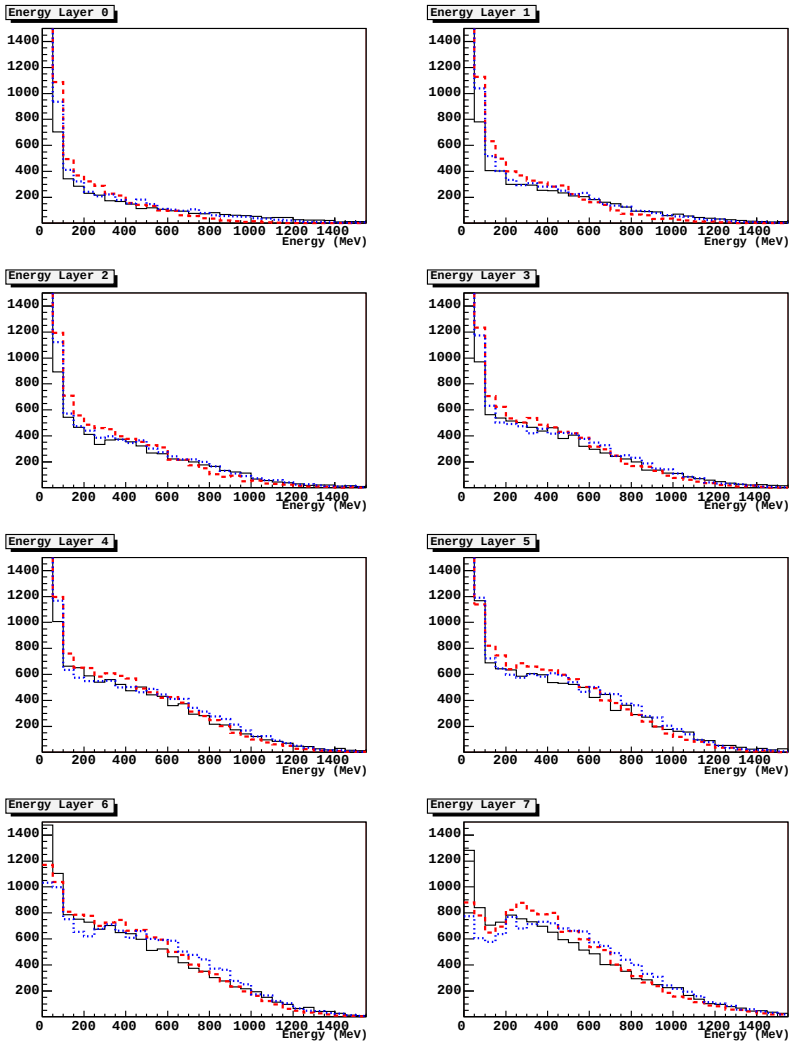


Figure A.1: 20GeV/c hadrons. Energy deposit per layer of hadronic cascades for data (plain line), LHEP simulation (dashed line) and QGSC simulation (dotted line).

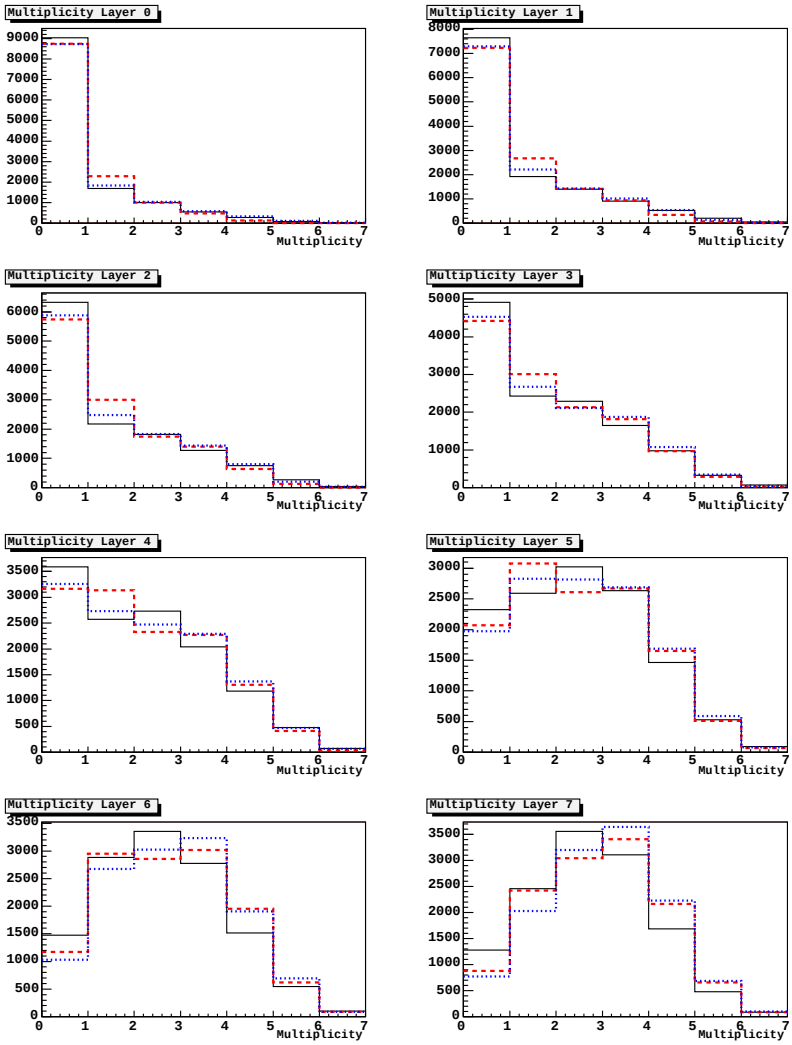


Figure A.2: 20GeV/c hadrons. Multiplicity per layer of hadronic cascades for data (plain line), LHEP simulation (dashed line) and QGSC simulation (dotted line).

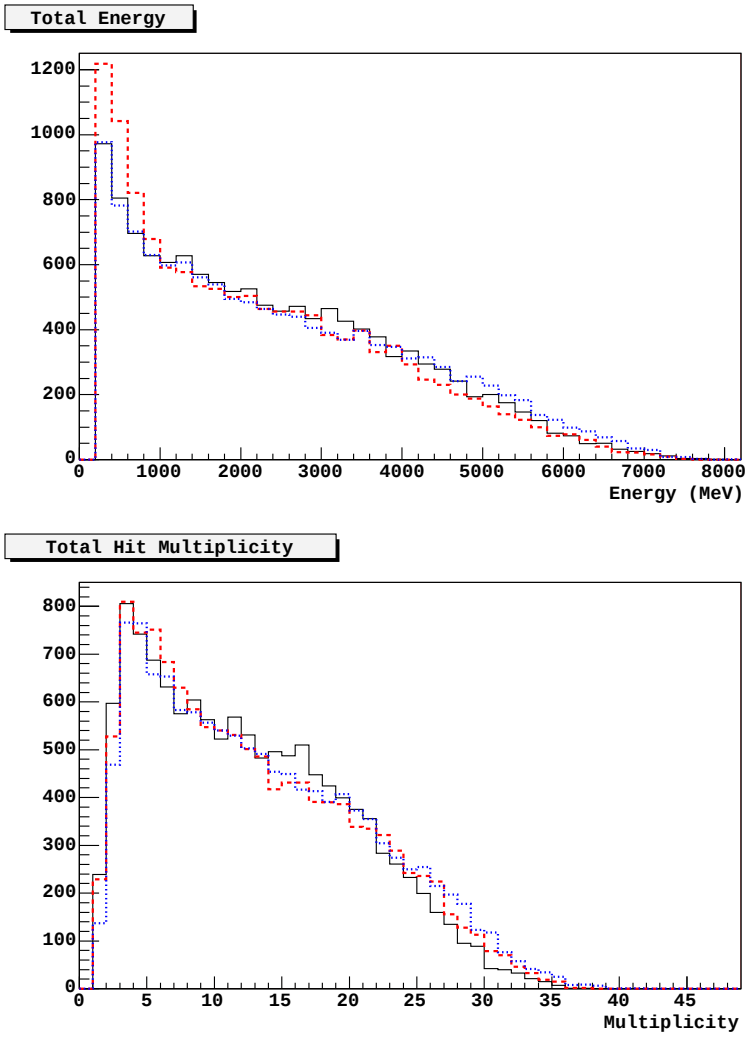


Figure A.3: 20GeV/c hadrons. Total energy deposit and total multiplicity of hadronic cascades for data (plain line), LHEP simulation (dashed line) and QGSC simulation (dotted line). These distributions look significantly better for the QGSC model than for the LHEP model.

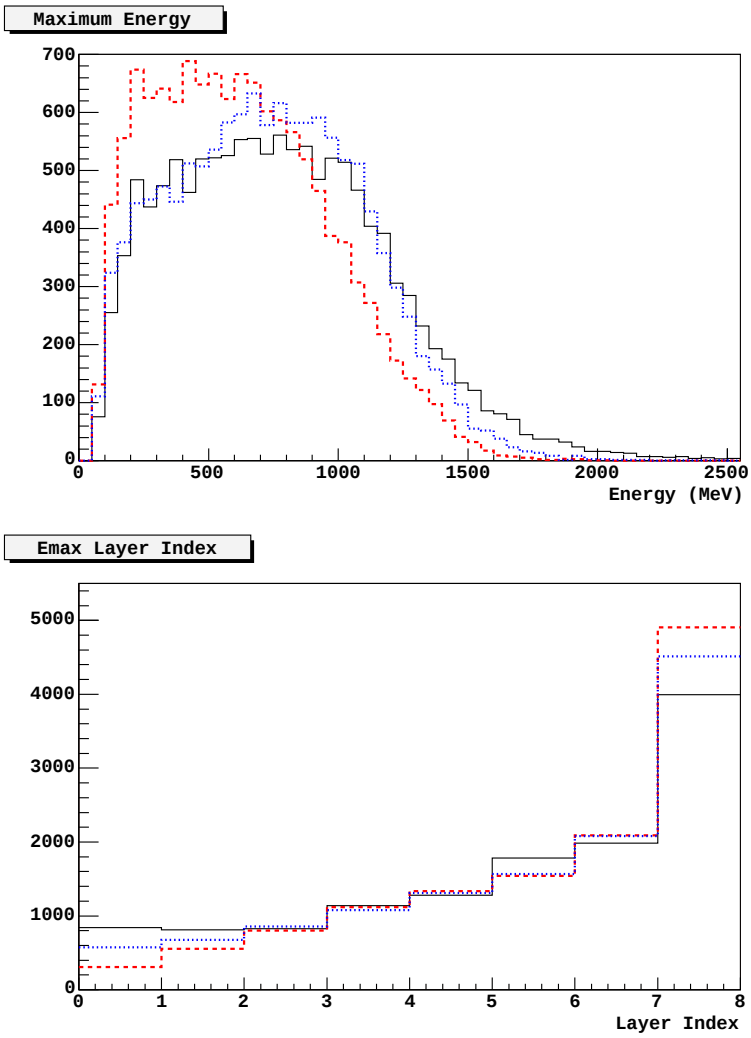


Figure A.4: 20GeV/c hadrons. Energy profile maximum, index of the corresponding layer and energy profile RMS of hadronic cascades for data (plain line), LHEP simulation (dashed line) and QGSC simulation (dotted line).

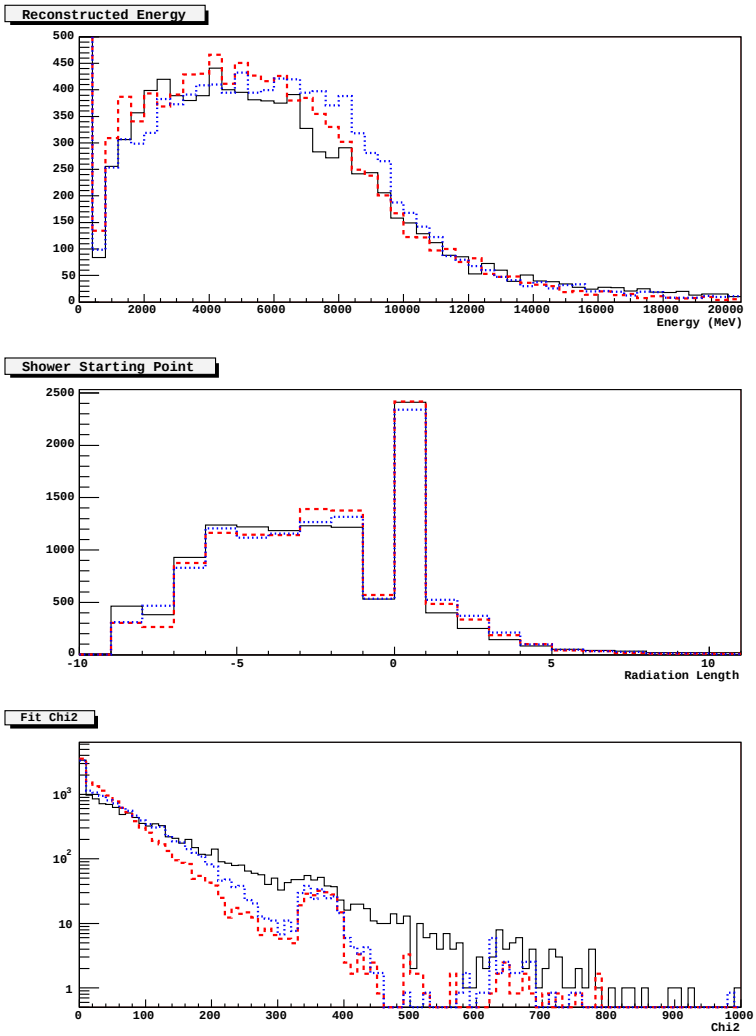


Figure A.5: 20GeV/c hadrons. Results from the longitudinal energy profile fitting by a $\Gamma$ function of hadronic cascades for data (plain line), LHEP simulation (dashed line) and QGSC simulation (dotted line).

# B GlastRelease

## B.1 GlastRelease v5r0p2 with BERT model

Following Francesco Longo advice, I was able to turn on the Bertini intranuclear cascade model in GlastRelease v5r0p2 : modifications are into the `G4GENERATOR` package so it could actually be done on any newer version of GlastRelease without any problems. The aim is first to check that the BERT model is really used instead of the default LHEP model, and second to check if the results would be comparable to the GSI data despite all the differences in the geometry. So, we compare here results from GlastRelease v5r0p2 with BERT model and $1.7GeV$ proton induced hadronic cascades from GSI data.

Tests have been quite successful. Results presented on the following plots from B.1 to B.4, show that the agreement between the GlastRelease simulation with the BERT hadronic cascade model and the GSI data is about as good as it was with GEANT4 standalone.

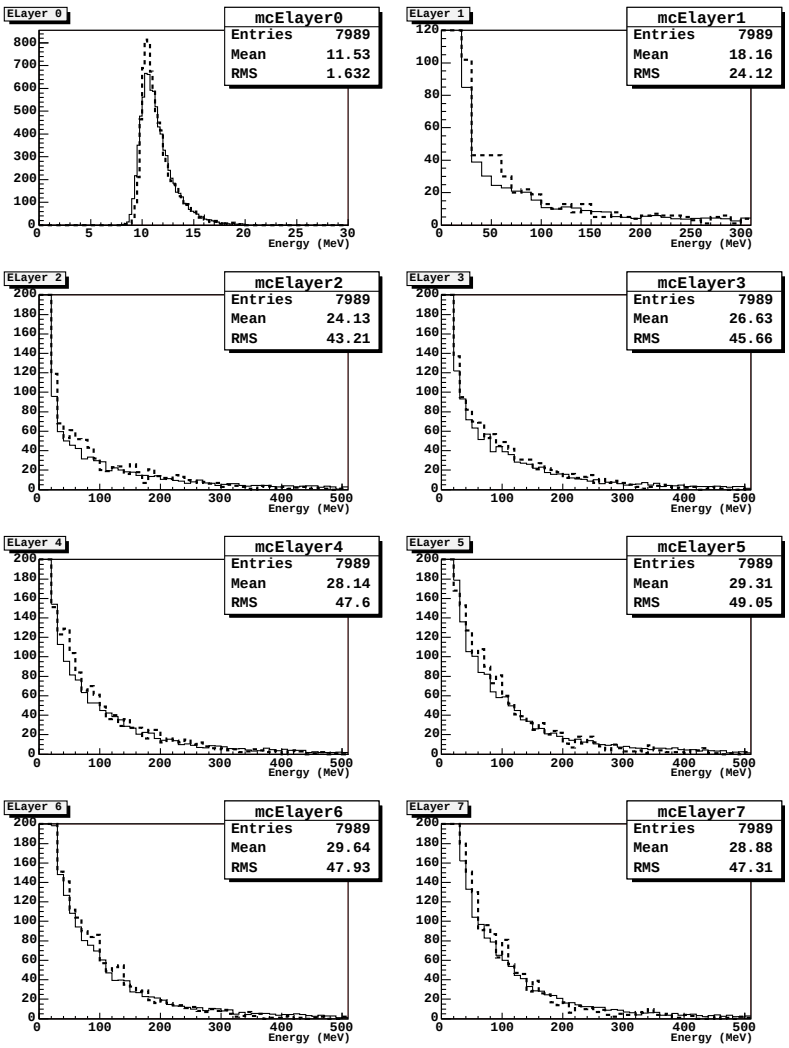


Figure B.1: $1.7GeV$ protons. Energy deposit per layer of hadronic cascades for data (plain line), GRv5r0p2 with BERT model (dashed line).

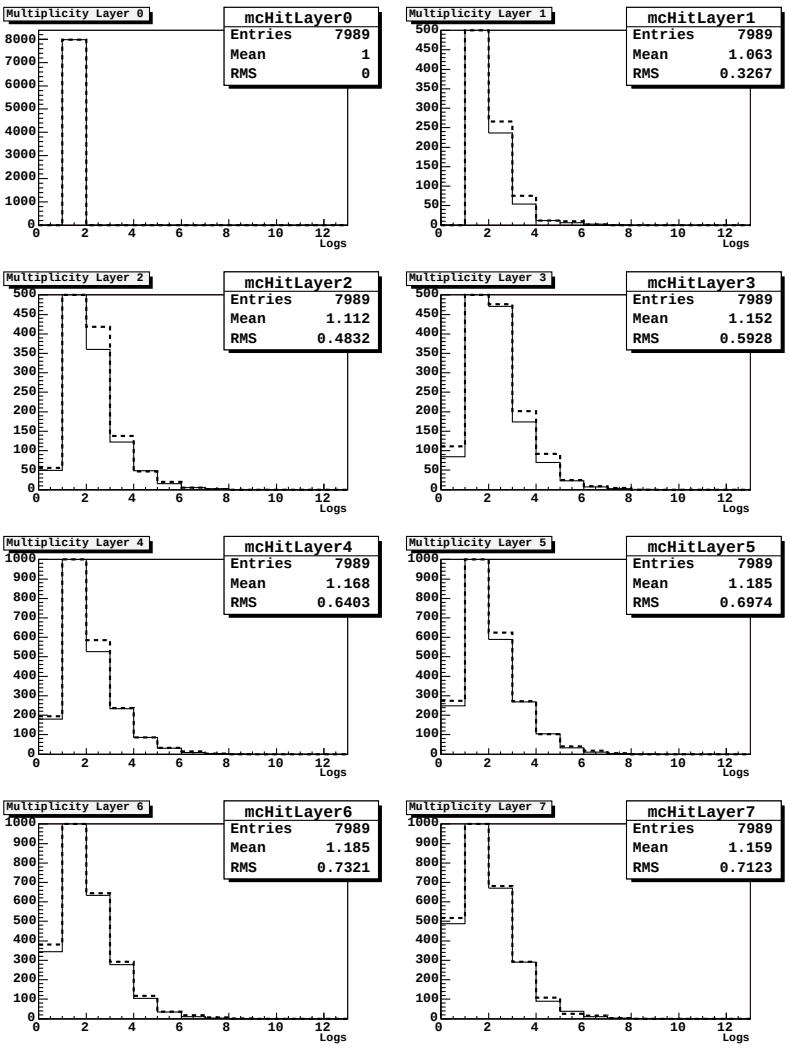


Figure B.2: $1.7GeV$ protons. Multiplicity per layer of hadronic cascades for data (plain line), GRv5r0p2 with BERT model (dashed line).

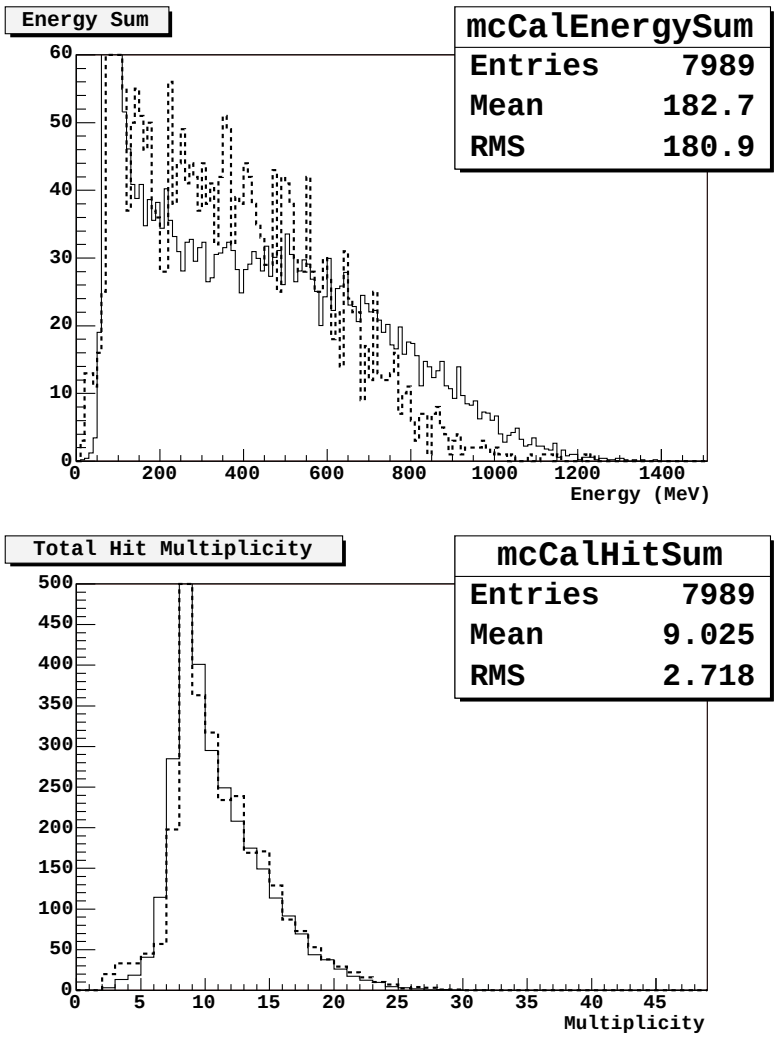


Figure B.3: $1.7GeV$ protons. Total energy deposit and total multiplicity of hadronic cascades for data (plain line),GRv5r0p2 with BERT model (dashed line).

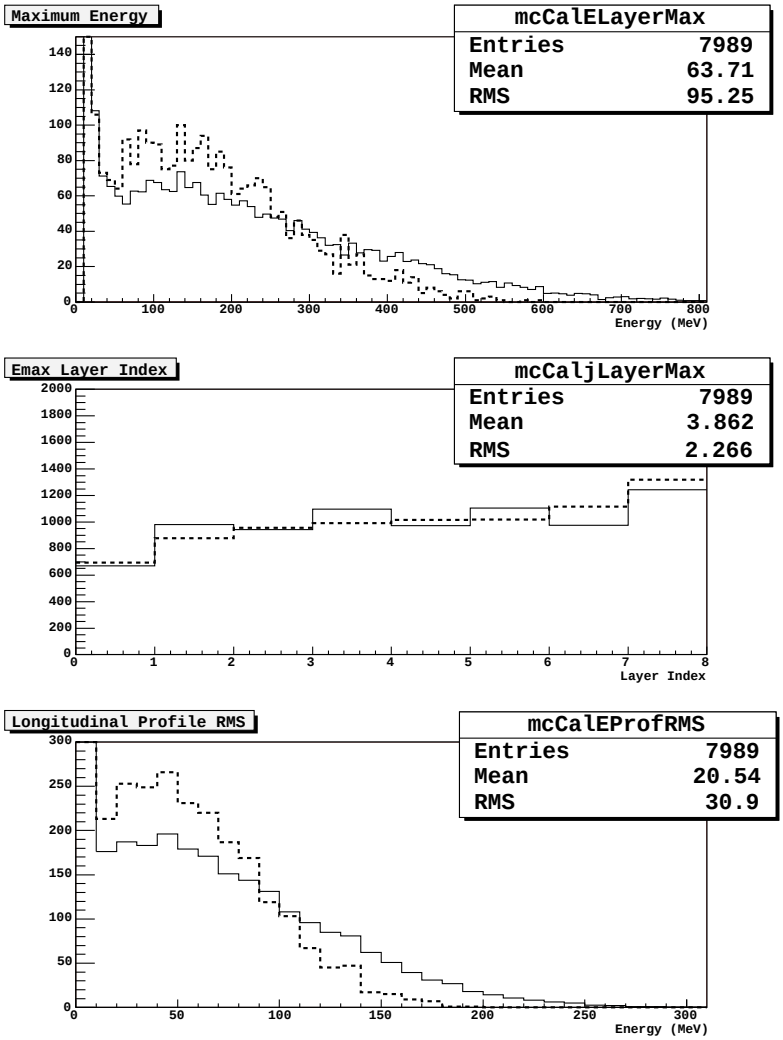


Figure B.4: $1.7GeV$ protons. Energy profile maximum, index of the corresponding layer and energy profile RMS of hadronic cascades for data (plain line), , GRv5r0p2 with BERT model (dashed line).

# Bibliography

[1] Barbiellini, G. et al., *The Agile Silicon Tracker : testbeam results of the prototype silicon detector.*, N.I.M. in Physics Research, A490 (2002) 146-158

[2] Bertini H. W., *Low Energy Intranuclear-Cascade Calculation*, Phys. Rev. 131, Nb. 4, (1963)

[3] Bertini H. W., *Intranuclear-Cascade Calculation of the Secondary Nucleon Spectra from Nucleon-Nucleus Interactions in the Energy Range 340 to 2900MeV and Comparisons with Experiment*, Phys. Rev. 188, Nb. 4, (1969)

[4] Bertini H. W. and Guthrie P , *Results from Medium-Energy Intranuclear-Cascade Calculation*, Nucl. Phys. A169, (1971)

[5] Fesefeldt H., *The GHEISHA program*, RWTH Aachen Report PITHA 85/02 (1985)

[6] Folger G., Wellisch J.P., *The Binary Cascade*, Computing in High Energy and Nuclear Physics (CHEP) conference, Interlaken, Switzerland, September 2004

[7] Agostinelli S. et al, *Geant4 - A Simulation Toolkit.*, N.I.M. in Physics Research, A506 (2003) 250-303

[8] Geant4 Physics Reference Manual, Chapter IV. Hadronic Interactions

[9] Geissel H. et al., *The GSI projectile fragment separator (FRS) : a versatile magnetic system for relativistic heavy ions.*, NIM in Physics Research B70, 286-297 (1992)

[10] Griffin J. J., *Statistical Model of Intermediate Structure*, Physical Review Letters 17, (1966), 478-481.

[11] Griffin J. J., *Statistical Model of Intermediate Structure*, Physics Letters 24B, 1 (1967), 5-7.

[12] Johnson W. Neil, *GLAST Large Array Telescope : Calorimeter Subsystem WBS 4.1.5*, LAT-PR-00871-00

[13] Johnson W. Neil and Ampe J., *Calorimeter Front End ASIC - GCFEv9 Design Description*, LAT-SS-01972-01, 2003

[14] Krammer M. and Pernegger H. *Signal collection and position reconstruction of silicon strip detectors with* $200\mu m$ *readout pitch.*, N.I.M. in Physics Research, A397 (1997) 232-242

[15] Lott B. et Piron F., *Probing the quenching effect in CsI for high-energy particles*, 17 septembre 2004

[16] Mizuno T. et al, *Cosmic-Ray Background Flux Model Based on a Gamma-Ray Large Area Space Telescope Balloon Flight Engineering Model*, The Astrophysical Journal, Volume 614, Issue 2, pp. 1113-1123 (2004)

[17] Parlog M. et al for the INDRA collaboration, *Response of CsI(Tl) scintillators over a large range in energy and atomic number of ions (Part I): recombination and delta – electrons*, Nucl.Instrum.Meth. A482 (2002) 674-692

[18] Parlog M. et al for the INDRA collaboration, *Response of CsI(Tl) scintillators over a large range in energy and atomic number of ions (Part II): calibration and identification in the INDRA array*, Nucl.Instrum.Meth. A482 (2002) 693-706

[19] Particle Data Group, Review of Particle Physics (2004), Chapitre 27.5

[20] Prest M. et al., *The Agile Silicon Tracker : an inovative* $\gamma$*-ray instrument for space.*, N.I.M. in Physics Research, A501 (2003) 280-287

[21] Ritz S. et al, *GLAST Large Area Telescope Onboard Filter Status*, LAT Collaboration Meeting 15 September 2003

[22] Serber R., *Nuclear Reactions at High Energies*, Phys. Rev. 72, Nb. 11, (1947)

[23] Terrier R. *Calorimetrie et recherche de sources en astronomie gamma spatiale.* Thèse de doctorat (27 septembre 2002), Laboratoire de Physique Corpusculaire et Cosmologie - College de France (IN2P3/CNRS), UNIVERSITE DENIS DIDEROT - PARIS VII.

[24] Weisskopf V. F. et Ewing D. H., *On the Yield of Nuclear Reactions with Heavy Elements*, PhysRev 57, 472-485 (1940)

[25] Wellisch H.P. and Axen D., *Total reaction cross section calculations in proton-nucleus scattering*, Phy. Rev. C, Vol.54 Nb.3 (1996)

---

Web Sites

---

[26] GEANT4 - http://wwwasd.web.cern.ch/wwwasd/geant4/geant4.html

[27] Gesellschaft für Schwerionenforschung - `http://www.gsi.de/`

[28] http://www.physik.rwth-aachen.de/ harm/geant/gheisha/index.html